Spring 2009

# Crustal modification by tectonic events and upper mantle anisotropy beneath the Midcontinent Rift and New Madrid Seismic Zone: insights from receiver function studies and teleseismic shear wave splitting

Moikwathai Moidaki



Department: Geosciences and Geological and Petroleum Engineering

# CRUSTAL MODIFICATION BY TECTONIC EVENTS AND UPPER MANTLE ANISOTROPY BENEATH THE MIDCONTINENT RIFT AND NEW MADRID SEISMIC ZONE: INSIGHTS FROM RECEIVER FUNCTION STUDIES AND TELESEISMIC SHEAR WAVE SPLITTING

by

MOIKWATHAI MOIDAKI

A DISSERTATION

Presented to the Faculty of the Graduate School of the

MISSOURI UNIVERSITY OF SCIENCE & TECHNOLOGY

In Partial Fulfillment of the Requirements for the Degree

DOCTOR OF PHILOSOPHY

in

GEOLOGY AND GEOPHYSICS

2009

Approved by

DR. STEPHEN GAO (ADVISOR)

DR. ESTELLA ATEKWANA (ADVISOR)

DR. JOHN HOGAN

DR. KEVIN MICKUS

DR. DAVID ROGERS

# ABSTRACT

The earth's crust and upper mantle have been continually modified by tectonic processes such as rifting, earthquake activity. In this dissertation, shear wave splitting and receiver function techniques were employed to study the extent of crustal and upper mantle modifications beneath the New Madrid Seismic Zone (NMSZ) and the Midcontinent Rift (MCR). Shear wave splitting analysis in the MCR reveals the presence of fossilised anisotropy along the rift axis. Beyond the 1.1 Ga MCR, the polarization angle (φ) observations are mostly parallel to the absolute plate motion direction. The most likely cause for the intriguing observation in the MCR is azimuthal anisotropy related to sub-vertical magmatic dykes along the strike of the rift. Receiver function results show an over-thickened crust (45km) with high Vp/Vs ratios beneath the MCR.

In the NMSZ, anticipated rift-parallel fast directions associated with vertical magmatic dikes or along-rift flow, rift-orthogonal fast directions from small-scale convection, or reduction in splitting times as a result of vertical asthenospheric flow are not observed, suggesting that the NMSZ is a shallow feature. Shear-wave splitting parameters for the NMSZ suggest complex anisotropy which fit well with a double layer model with the lower layer fixed at APM direction. Receiver function results in the NMSZ show average crustal thickness of about 33.4±0.28 km for stations within the Mississippi embayment and variable crustal thicknesses in the Mazatazal Belt (30.2±0.14 to 53.1±0.29 km thick).

# ACKNOWLEDGEMENTS

My appreciation goes to Dr. S. Gao who contributed tremendously and tirelessly to make this work a success. Dr. Gao and Dr. Kelly Liu restored my hope and ultimately my energy. My appreciation goes to Dr. Estella Atekwana for her support and encouragement in my studies in the USA. She has been very helpful in making this work a success, her comments and suggestions were very constructive. I did not have a good background in geology but Dr. J. P. Hogan made sure I understood a bit about rocks from the surface to the inner core and a bit of structural geology.

I would also like to thank Dr. Obo-Ikuenobe Franca for her kind heart. My appreciation goes to the Head of the Department of Geological Sciences and Engineering Dr. Laudon. Mrs. Katherine Mattison and Paula Cochran were always willing to assist. The input from my committee members (Dr. Gao, Dr. Hogan, Dr. Estella, Dr. Rogers and Dr. Mickus) were very helpful. Even though the road to the finishing line was bumpy, I finally made it to the end through the encouragement and support of my fellow schoolmates (Tom Jerris, Oleg Kovin, Hesham, Ali, Sattam and Dr. K. Baraka). I would also like to extend my appreciation to Miss Dimpho Motshabi, Tefo (T4), Bokang (BK) and Daphney (Daf), Rev. B.E Lekganyane and all the members of my family especially my mother, Miss Kereng Moidaki and my brother, Kepaletswe. I thank the Almighty God for making 'plates' which diverge, converge and subduct and, hence, creating earthquakes which generate elastic waves which I used to study the earth's interior.

# TABLE OF CONTENTS

# LIST OF FIGURES

# LIST OF TABLES

Table Page

# 1. INTRODUCTION

## 1.1 CONTINENTAL RIFT ZONES

Shear wave splitting and receiver function analysis are widely used methods for studying crustal modification in various tectonic environments (Silver, 1996; Savage, 1999; Dugda et al., 2005). The earth's crust and mantle have undergone constant modifications through time as a result of tectonic activities. These modifications are well pronounced in continental rift zones, subduction zones and in transcurrent fault systems. Continental rift zones are complex features defined by several large-scale structural components including faulted margins, the border faults of the faulted margins, the uplifted flanks of the faulted margins, and large scale transfer zones (Van Schmus and Hinze 1989; Walker et al., 2004). Other small-scale structures also develop within rift basins. These include: strike-slip and reverse faults, extensional fault-displacement, fault-propagation, and fault-bend folds.

Knowledge on crustal modification and upper mantle anisotropy substantially increased during the past several decades. It is generally accepted that rifting episodes are associated with magmatic activities that originated in the lithospheric upper mantle or in the asthenosphere (Van Schmus and Hinze, 1985). These tectonic activities have profound effects on crustal structure in terms of crustal composition (felsic or mafic crust). Previous geophysical studies in continental rift zones have demonstrated large gravity and heat flow anomalies, indicating the presence of anomalous mantle material or partial melt beneath the rift axis. A close relationship has been suggested between

asthenospheric upwelling and penetrative magmatism as driving forces for lithospheric rifting (Bhattacharji and Koide 1987).

Current understanding of crustal modification has been derived from a wide range of geophysical methods, including potential field methods (gravity and magnetic methods), seismic reflection/refraction, and analysis of teleseismic earthquake data (e.g., receiver function studies and shear wave splitting analysis). Most rift basins are dissected by large-scale intra-basin faults (i.e., faults with displacements of more than several hundred meters and lengths of tens of kilometers). These intra-basin faults can strike parallel or obliquely to the trend of the border faults and can have normal and/or strike-slip components of displacement. The depth extent of these faults could range from few meters to the brittle-ductile transition. Orientation and displacement on these intra-basin faults is controlled, in part, by the obliquity of the maximum extension direction relative to the rift-basin trend (Withjack and Jamison, 1986; Tron and Brun, 1991). For orthogonal extension, intra-basin faults are likely to strike parallel to the rift trend and perpendicular to the maximum extension direction and have normal displacements. For oblique extension, intra-basin faults are likely to strike obliquely to the rift trend and sub-perpendicular to the maximum extension direction and have mostly normal displacement.

Seismic anisotropy in the form of shear wave splitting has been observed in nearly all settings, such as subduction zones, oceanic basins and continental interiors (Fouch et al., 2000). Shear-wave splitting measurements on the continents showed that in compressive regions, anisotropy is caused by vertically coherent deformation of the mantle with fast directions parallel to the strike of

compressive features (Silver, 1996). Seismic tomography and geodynamic modeling by Forte et al (2007) suggest a vertical asthenospheric flow induced by the subducting Farallon plate beneath the Central United States. This study suggests complex anisotropy in North America is caused by lateral mantle flow induced by the subducting Farallon slab during the Cenozoic. Shear wave splitting measurements have been obtained in different geological/tectonic environments, such as Baikal rift (Gao et al., 1997), Rio Grande Rift (Sandvol et al., 1992), Afar rift (Ewenet et al., 2004), Archean shields (Vinnik et al., 1996), and mountain belts (McNamara et al., 1994). Sandvol et al (1992) found fast axes along the axis of the Rio Grande Rift to be subparallel to the rift axis. Although significant process has been made, no single tectonic process can account for all of the observations and hence contribution of various processes is required (Silver, 1996).

Several receiver function-based studies have been conducted using PmS-P and PPmS-P differential travel times (Clarke and Silver, 1991). Zandt and Ammon, (1995) made measurements of $\Phi$ (Vp/Vs ratio) and observed that Precambrian shields have a mean $\Phi$ of (1.84 ± 0.06), Archaean-early Proterozoic platforms have an average $\Phi$ of (1.75), late Proterozoic have a $\Phi$ of 1.78, early Proterozoic have a $\Phi$ of 1.76, Mid-late Proterozoic have an average $\Phi$ of 1.81, and Palaeozoic have an average $\Phi$ of 1.73. Cenozoic and Mesozoic crust has the lowest $\Phi$ of (1.73 ± 0.09) (Musacchio et al., 1997), suggesting a relationship between $\Phi$ and the age of the crust.

Studies of the relation between P and S wave velocities using seismic refraction data by Musacchio et al. (1997) in the Grenville and Applachian

provinces of North America revealed that the crust exhibits increasing Φ with depth, from 1.64 to 1.84. The high Φ is an indication of a crust with an average mafic composition. Dugda et al. (2005) observed Φ values of 1.78 to 2.9 in the Afar region and Main Ethiopian Rift. The high values of Φ were attributed to magma intrusion beneath the crust. The Rio Grande Rift was also studied by Wilson et al. (2005). Their results show that crustal thickness averages 44.1 ± 2.3 km beneath the Great Plains and 45.6 ± 1.1 km beneath the Colorado Plateau. Crustal thinning beneath the Rio Grande Rift is broadly symmetric about the rift axis, with the thinnest crust (35 km) located directly beneath the rift axis, suggesting a pure shear stretched lithosphere beneath the RGR.

In this dissertation, the Mesoproterozoic Midcontinent rift and the New Madrid Seismic Zone are investigated by quantifying the effects of rifting and associated volcanic eruptions on the structure and composition of the crust and mantle beneath the MCR and NMSZ by measuring the crustal thickness (H), crustal mean $V_p/V_s$, and the sharpness of the Moho (R) at portable and permanent broad band by stacking P-to-S converted waves (PmS) and their multiples (PPmS and PSmS). These measurements will shed new lights on how the crust was modified beneath these rifts.

Mantle anisotropy is believed to result from strain-induced, preferred orientation of mantle minerals (mainly olivine), and thus shear wave splitting measurements can characterize the orientation and depth extent of mantle strain fields. This allows us to examine the structural geology within the mantle. The seismic community is in the initial stages of determining the relation between strain and anisotropy and of mapping the strain and determining how much of it

is caused by past and present lithospheric deformation and how much of it is caused by crustal, asthenospheric, and lower mantle sources.

Observed shear wave splitting parameters are used to provide insights on stress generation and accommodation of deformation and evidence for melt migration in the upper mantle, establish a relationship between the shear wave splitting parameters with main faults trending directions, and to determine whether there is a relationship between the North American Plate motion and the direction of the fast axes of the olivine in the upper mantle. Understanding the distribution of seismic anisotropy can address these issues. Shear wave splitting measurements on the NMSZ will constrain better the temporal and spatial variation of anisotropy and quantify the orientation, magnitude beneath the New Madrid Seismic Zone and to investigate the existence of two layer model as suggested by Marone and Romamowicz (2007) (Figure 1.1). The alignment of the fast axis within the NMSZ with respect to the direction of the Reelfoot rifts will enable us to elucidate the depth extent of the Reelfoot fault system. Understanding of the deformation mechanism on the upper mantle in continental interiors using shear wave splitting is an ongoing research and therefore, the complex geology of the NMSZ with abundant granitic intrusions (Jodi et al., 1998) with its intricate pattern of faulting makes this area ideal for studying upper mantle anisotropy at intra-continental settings. In this study, data from both permanent and temporary stations within the NMSZ and MCR area were incorporated. The increased number of shear wave splitting observations from previously studied permanent stations will provide clearer picture of seismic anisotropy in the upper mantle beneath NMSZ.

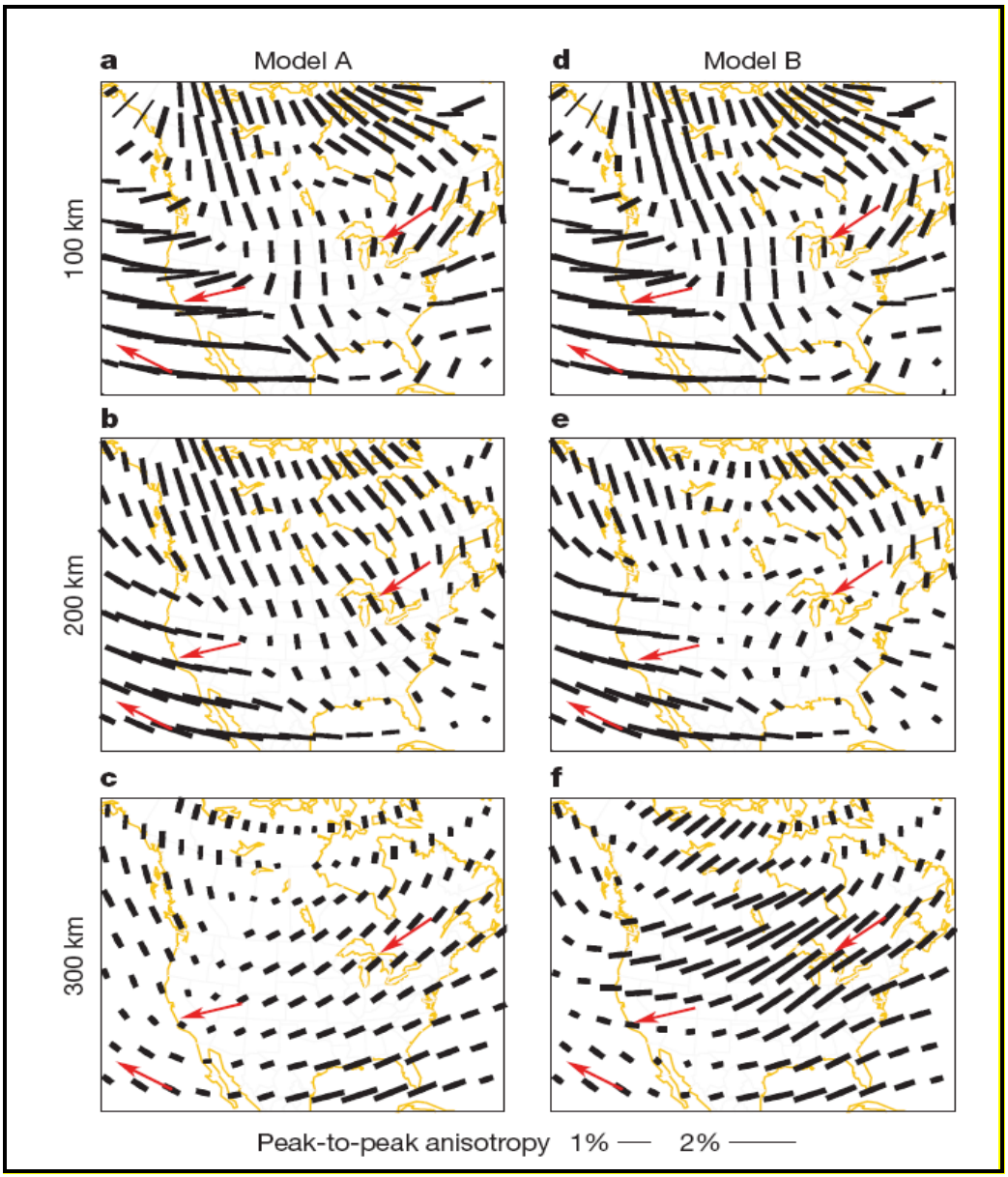


Figure 1.1: Horizontal slices at three different depths showing azimuthal anisotropy in the North American upper mantle. Model A (a–c) was derived using uniquely fundamental mode and overtone surface waveforms. Model B (d–f) was obtained by joint inversion of surface waveforms and SKS splitting measurements. The length of the black bars is proportional to the maximum amplitude of azimuthal anisotropy, and their azimuth is parallel to the axis of fast propagation. Red arrows indicate the APM direction in a hotspot reference frame. The sharp transition in the fast-axis direction of anisotropy at 100 km depth across the Rocky Mountain Front is observed and is in agreement with APM at 300 km everywhere (Marone and Romanowicz 2007).

**1.1.1 Tectonic History of the Midcontinent Rift.** The Midcontinent Rift (MCR) or Keweenawan Rift (Figure 1.2), identified as intense, curvilinear gravity and magnetic anomalies, is a 2,000 km long geological rift in the center of the North American continent and south-central part of the North American plate (Van Schmus and Bickford, 1981; Hinze et al., 1990). It formed when the North American craton began to split apart during the Mesoproterozoic era about 1.1 billion years ago. The rift failed, leaving behind thick layers of igneous rocks that are exposed in its northern reaches, but buried beneath later sedimentary formations along most of its western and eastern arms. The arms meet at Lake Superior, which is contained within the rift valley. The lake's north shore in Ontario and Minnesota defines the northern arc of the rift. From the lake, the rift's eastern arm trends south to central lower Michigan. The western arm runs from Lake Superior southwest through portions of Wisconsin, Minnesota, Iowa, and Nebraska to northeastern Kansas. Investigation by Thiel (1956) and Hinze et al. (1982) showed that rocks produced during the formation of the MCR are exposed in the Lake Superior area, along the lake shore from Duluth north into Canada and east into Michigan, including Wisconsin's Bayfield and Michigan's Keweenawan peninsulas comprise the classical association of bimodal volcanic rocks, plutonic and clastic sedimentary units of the 1.0-1.2 Ga old Keweenawan group (Van Schmus and Hinze, 1985).

A few outcrops of mafic volcanic and overlying clastic sedimentary units of the 1100 Ma Keweenawan Supergroup around Lake Superior provide evidence of a major crustal structure whose origin is related to an extensional regime (Hinze et al., 1990). The rocks exposed in this area are dominated by basaltic lavas, a

pre-volcanics, early clastic sequence and a post-volcanics, late clastic sequence. The Keweenawan magmatic rocks were deposited in a rift environment in the time span centered from 1109 – 1094 Ma (Behrendt et al., 1988, 1990). Several large Keweenawan intrusive complexes occur along the margin of the Midcontinent rift (e.g. the Duluh Gabbro along the northwest shore of Lake Superior). These rock units continue southward beneath a cover of younger sedimentary rocks. In Iowa and Minnesota, the elongate mafic suture is up to 80 km wide and has been reactivated to form a fault bounded horst with uplift displacement of as much as 10km (Carmichael and Black, 1986).

The dense basaltic lavas and sedimentary rocks produce a series of linear gravity anomalies that follow the trend of the MCR (Figure 1.2) and produce the most dramatic gravity anomaly in North America. Regional geophysical information has indicated a profoundly disturbed underlying crust and continuation of the MCR in the subsurface beneath relatively flat-lying Phanerozoic sedimentary rock units which overlie the basement of the Midcontinent (Hinze et al., 1992).

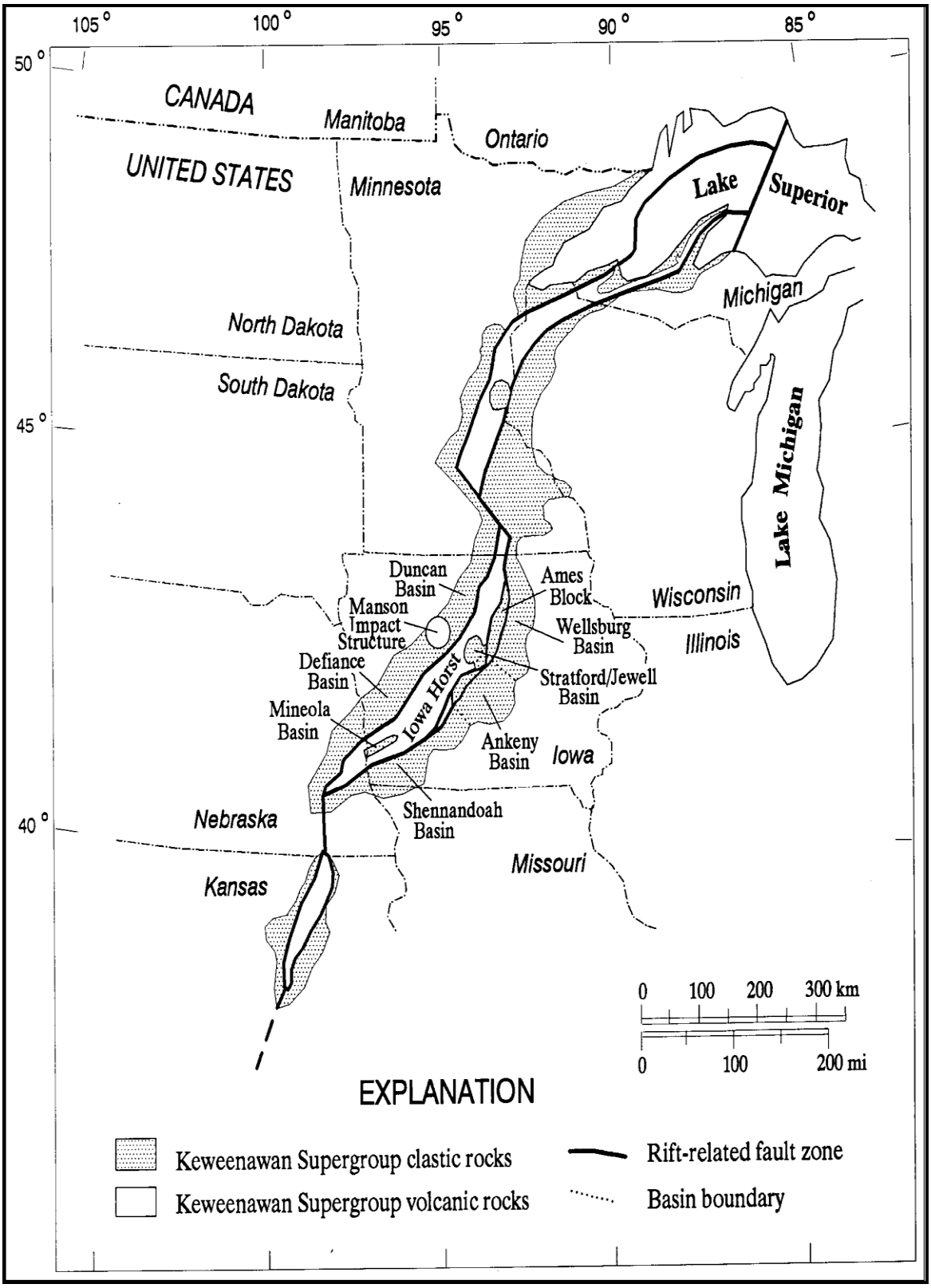


Figure 1.2: Midcontinent rift system and its major lithologies (after Anderson and McKay 1989)

**1.1.2 Tectonic History of the New Madrid Seismic Zone.** The New Madrid Seismic Zone in the North American craton is made up of reactivated faults that formed when North America began to split during the breakup of the supercontinent Rodinia in the Neoproterozoic Era (Bexfield et al., 2006; McBride et al., 2003). The rift failed but remained as an aulacogen. The area was then flooded by an ancient ocean, depositing layers of sediment on the rift. During the Mesozoic Era, as the Atlantic Ocean was opening in the east, rifting was once again re-activated and intrusive igneous rocks were emplaced (Van Schmus and Hinze, 1985). The rifting failed and the continent remained intact, although with a significant zone of weakness. This rift is known as the Reelfoot Rift and coincides with the northernmost portion of the Mississippi embayment. Most of the seismicity is located from 3 to 15 mi (5 to 25 km) beneath the Earth's surface. After formation of the rift during continental breakup (Figure 1.2), the rift underwent subsidence during the times of regional compression associated with either subduction or collision along the eastern and southern margins of North American craton (Braile et al., 1986). During early Mesozoic, the craton was undergoing uplift and erosion resulting in the broad unconformity which is observed in the cratonic basins of North America. Mesozoic reactivation of faults associated with the NMSZ caused structural uplifts and intrusion of plutons near the margins of the rift complex (Figure 1.3). Since the Cretaceous time, the eastern margin of the North American craton has been under a regional compressive stress, reactivating the rift faults in a reverse and strike slip sense resulting in the observed present day seismicity.

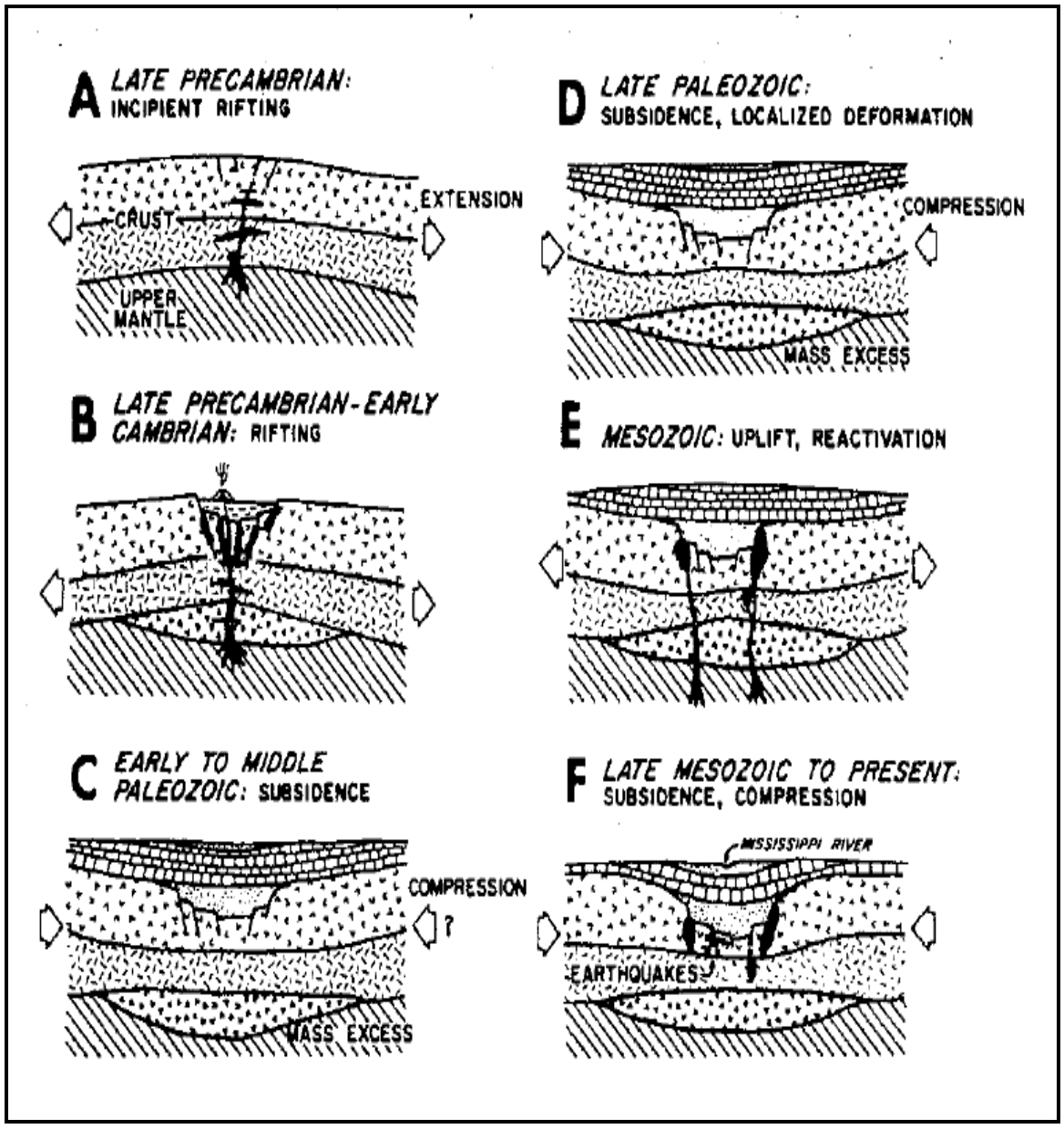


Figure 1.3. Schematic cross section across the New Madrid seismic Zone illustrating the evolution of the rift complex and associated cratonic basins through time (After Braile et al., 1986).

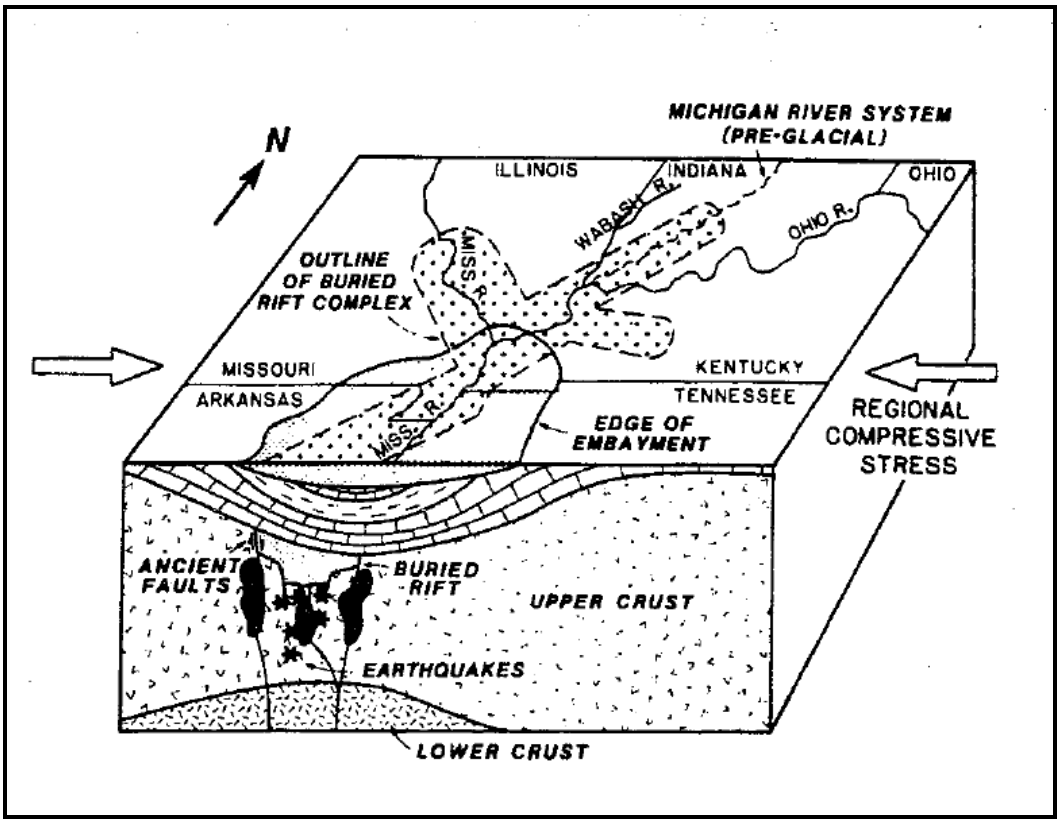


Figure 1.4. Schematic bloc diagram illustrating the present configuration of the buried New Madrid Rift Complex. Dark areas indicate intrusions near the edge of the buried rift. An uplifted and an anomalously dense lower crust is suggested as the cause of the linear positive gravity anomaly associated with the upper Mississippi Embayment, (After Braile et al., 1986)

## 1.2 PROJECT SIGNIFICANCE

The receiver function results from this study will contribute to the understanding of how tectonism modifies the crust. The variation of crustal thickness across continental rift zones will show the extent of deformation the crust has undergone as a result of regional tensional and compression forces. As a result of extension, asthenospheric material intrudes the lithosphere and hence modifies its composition. Measurements of Poisson's ratio (Vp/Vs ratio) will show the extent of modification in the crust. In addition, the Moho sharpness deteriorates as a result of magma intrusion. This deterioration leaves some

continental rift with no or blurred Moho beneath the rift whereas some rifts show preserved Moho. Determinations of these parameters mentioned above have not been conducted at the MCR and NMSZ.

Previous studies have shown the existence of two layer anisotropy beneath North America (Marone and Romanowicz, 2007). This study provides the opportunity to test this two layer model using shear wave splitting. Forte et al. (2007) suggest that complex anisotropy in North America is caused by lateral mantle flow induced by the subducting Farallon slab during the Cenozoic era. Fast polarization directions beneath the NMSZ will provide insights on the flow of the asthenosphere beneath the NMSZ. Shear wave splitting results on the MCR will determine whether there is a difference on the fast axis direction for on-rift and off-rift stations with respect to the absolute plate motion direction.

## 1.3 DISSERTATION OUTLINE

Section 1: This section is the introduction. Section 2 discusses shear wave splitting in NMSZ and section 3 is about shear wave splitting in the MCR whereas sections 4 and 5 are about the receiver function studies on the NMSZ and MCR, respectively. Section 6 summarizes the results and provides recommendations for future studies.

# 2. SHEAR WAVE SPLITTING BENEATH THE NEW MADRID SEISMIC ZONE AND ADJACENT AREAS

## 2.1 ABSTRACT

A total of 93 well-defined PKS, 54 SKKS, and 126 SKS shear-wave splitting parameters were determined at 25 broadband seismic stations in an approximately 1000 by 1000 km$^2$ area centered at the New Madrid seismic zone (NMSZ) in order to map the direction and strength of mantle fabrics and to explore the origin of seismic anisotropy. Unlike most previous shear-wave splitting studies which suggested uniform mean splitting parameters (fast direction and splitting time) in the same area, our results, when presented in the form of individual (instead of mean) splitting parameters using the PKS, SKKS in addition to SKS phases, suggest significant and systematic spatial and azimuthal variations in the splitting parameters. The azimuthal variations at most stations can be best explained as the result of present SW-NE-ward asthenospheric flow and NNE trending lithospheric fabrics formed during past orogenic events. In the NMSZ, anticipated rift-parallel fast directions associated with vertical magmatic dikes or along-rift flow, rift-orthogonal fast directions from small-scale convection, or reduction in splitting times as a result of vertical asthenospheric flow are not observed, suggesting that the NMSZ is a shallow feature which is consistent with results from other geophysical studies such as seismic reflection surveys.

## 2.2. INTRODUCTION

Shear waves propagate through an anisotropic mantle as a pair of orthogonally polarized phases that travel at different speeds (e.g., Savage 1999). Teleseismic shear-wave splitting of PKS, SKKS and SKS phases (hereinafter are collectively referred to as XKS) provides critical information regarding the structure and dynamics of the earth's upper mantle anisotropy (Silver and Chan, 1991; Gao et al 1994; Silver, 1996; Savage, 1999; Mainprice et al., 2005). Splitting measurements are quantified by the delay time (δt) between the two shear waves and the orientation (Φ) of the fast shear wave. The time delay (δt) is proportional to the product of the ray path length and the magnitude of anisotropy along the ray path. Laboratory measurements have shown that the a-axis of olivine align in the direction of maximum finite extension (Karato, 1987), or in the direction of mantle flow (Zhang and Karato, 1995). Lattice preferred orientation (LPO) of anisotropic olivine and orthopyroxene crystals in the upper mantle is generally the primary cause of the observed SKS splitting (Nicolas and Christensen, 1987; Silver and Chan, 1991; Mainprice et al., 2000), and strain-induced LPO is considered to be a valuable indicator of either past or present tectonics (Babuska and Cara 1991).

Numerous shear wave splitting measurements have been carried out in different tectonic settings (Savage, 1999), however the debate between strain and anisotropy, amount of deformation caused by past and present lithospheric deformation is ongoing (Kaminski and Ribe, 2002; Savage, 1999). Anisotropy in the form of shear wave splitting has been observed in nearly all settings, such as

subduction zones, oceanic basins and continental interiors (Fouch et al., 2000). Studies of anisotropy measurements on the continents show that in compressive regions, anisotropy is caused by vertically coherent deformation of the mantle with fast directions parallel to compressive features (Silver, 1996). In contrast measurements of splitting parameters in continental rift environments show fast directions orthogonal to the extension (e.g., Gao et al., 1994, 1997). This observation is believed to be caused by the abundance of magma filled oriented cracks.

The main objectives of this study are to (1) constrain the spatial variation of anisotropy, (2) quantify the orientation and strength of mantle fabrics beneath the NMSZ, (3) determine if a double layer anisotropy exists in the vicinity of the NMSZ as suggested by Marone and Romamowicz (2007), (4) determine if vertical asthenospheric flow exists beneath the NMSZ as proposed by Forte et al. (2007), (5) provide important insights into the dependence of fast axis direction on faulting, (6) determine whether magma filled cracks play a vital role in shear wave splitting in the NMSZ and the surrounding area, and (7) determine the depth extent of the Reelfoot fault system.

## 2.3. GEOLOGIC SETTING OF THE NMSZ AND ADJACENT AREAS

The New Madrid rift system (Figure 2.1) also known as the Reel Foot Rift, is a Precambrian to Middle Cambrian failed rift system, underlying the Illinois basin extending from southern Illinois and western Kentucky southwestward to central Arkansas (Ervin and McGinnis, 1975; Braile et al., 1986). The NMSZ is

made up of reactivated faults that formed when North America began to split or rift apart during the breakup of the super continent Rodinia in the Neoproterozoic Era (about 750 million years ago) (Van Schmus et al., 1996) and later failed and remained as an aulacogen. The area was then flooded by an ancient ocean, depositing layers of sediment on the rift. During the Mesozoic Era (about 200 million years ago), as the Atlantic Ocean was opening in the east, rifting was once again re-activated and intrusive igneous rocks were emplaced. But again the rifting failed and the continent remained intact, although with a significant zone of weakness (Keller et al., 1983).

The Mississippi embayment is a southwest-trending aulocogen of late Precambrian-early Paleozoic origin (Braile et al., 1982). Reelfoot rift was reactivated in the Mesozoic to form the Mississippi embayment and is the site of modern seismicity which suggests reactivation in a contemporary stress field of ENE compression. Even though the importance of rifting can be established, recognition of rifts and delineation of their complexities remain a major problem which requires more study (Keller et al., 1983). Geodynamic processes within the rift have had a major influence on basin geometry and subsidence (Kolata and Nelson, 1997). Two distinct regions of deformation are known to overlap, trending from southwest to northeast (Bexfield et al., 2006; Woolery et al., 2003) in the NMSZ (Figure 2.1). Deep seated Paleozoic normal faults (Kolata and Nelson, 1991) propagating from the northeast were initiated during the Cambrian with the formation of the Reelfoot rift and have been mapped extensively where exposed in southeastern Illinois. The faults were contractionally reactivated during the late Paleozoic and were again reactivated as normal faults in Mesozoic

time (Kolata and Nelson, 1991). The second trend of deformation propagates from the southwest and is associated with contemporary seismicity in the northeast-striking NMSZ (Chiu et al., 1992).

The major terrains (Figure 2.1) in the NMSZ include the extensive Northern Rhyolite terrain (1.69–1.78 Ga), the Mazatzal belt (1.61-1.68 Ga), and the Granite–Rhyolite terrane (1.48–1.45 Ga). The tectonic blocks are interpreted to have been assembled during two main periods of convergent tectonism: 1.74 to 1.70 Ga (Yavapai orogeny) and 1.65 to 1.63 Ga (Mazatzal orogeny, Holm et al., 2007). The Yavapai-Mazatzal province is made up of supracrustal rocks of the 1.79 to 1.70 Ga Yavapai Supergroup containing mafic to intermediate volcanic rocks, volcaniclastic, and sedimentary rocks (Eisele and Isachsen, 2001). These are intruded by calc-alkaline batholiths of 1.75 to 1.69 Ga age. The Mazatzal province comprises several blocks with varying ages (Holm et al., 2007). Ages in the Mazatzal block range from 1.74 Ga for a gabbro and 1.70 to 1.69 Ga for a suite of volcanic rocks to a 1.65 Ga age for post-tectonic granite (Karlstrom and Bowring, 1988).

## 2.4. DATA

This study uses PKS, SKKS and SKS waveforms recorded by 25 stations, among which 17 are permanent and 8 are portable stations. The epicentral distances are $85^{o}$ to $140^{o}$ for SKS, $120^{o}$ to $180^{o}$ for PKS and $85^{o}$ to $140^{o}$ for SKKS. The data used in this study were recorded from 1980 to 2008 by broadband permanent and temporary stations.

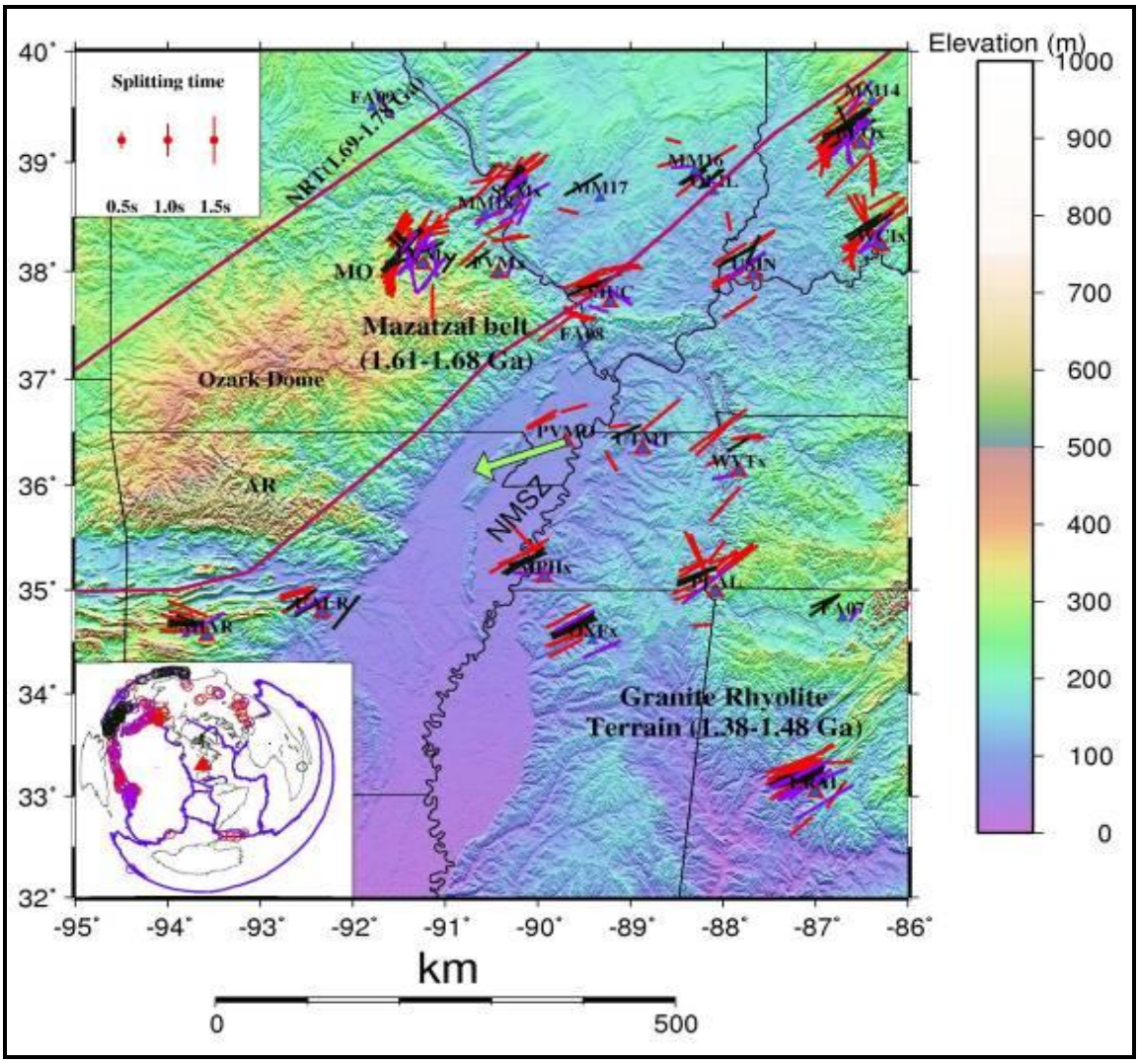


**Figure 2.1:** A Mercator projection map showing the seismic station locations, major terrains and shear wave splitting results of the NMSZ. Red, black and purple represent splitting parameters determined from SKS, PKS and SKKS respectively. Event locations are also shown in the Figure above. Azimuthal distribution at stations CCM, BLO, PLAL SIUC, WCI is complex and hence cannot be explained by single layer model. Station MPH UTMT and PVMO within the Mississippi embayment show some degree of alignment with the absolute plate motion (APM). The green arrow at station PVMO represents the direction of plate motion. NRT: Northern Rhyolite Terraine.

Five of the temporary network stations (MM14-MM18) (Figure 2.1) are part of the Missouri to Massachusetts (MOMA) array, deployed from January 1995 to April 1996 with a station spacing of approximately 90 km (Fouch et al., 2000). Mean splitting parameters were presented at the five stations (Fouch et

al., 2000). Three of the stations (FA07-FA09) are from the Florida to Edmonton (FLED) array. Seismometers of the FLED array were deployed in May 2001 and data collection continued through October 2002 (Fischer et al., 2006). All analyzed phases have steeply dipping incidence angles and sample the upper mantle almost directly beneath the station, providing very good lateral resolution but poor vertical resolution. As demonstrated below, in spite of limited azimuthal coverage, the combined shear wave splitting results from the PKS, SKKS, and SKS phases are sufficient at most stations to discriminate between splitting from a single-layer model with double layer model.

## 2.5. METHODS

The seismograms were band-pass filtered between 0.04 and 0.5 Hz in order to reduce non-XKS arrivals that would impede the splitting measurement. The XKS time window used to compute the splitting parameters is initially set as 'a' = 15 s before and 'f' = 35 s after the predicted phase arrival times based on the IASP91 earth model. About 1127 seismograms were visually checked (328 for PKS, 278 for SKKS and 521 for SKS) to adjust the 'a' and 'f' values, and to reject the ones with strong non-XKS arrivals in the XKS window.

The polarization angle $\Phi$ and the splitting time $\delta t$ are determined by grid search over the possible splitting parameters to reverse the process of generating the split shear waves. This is achieved by minimizing the component that is perpendicular to the incoming polarization angle of the shear wave before entering the anisotropic medium (Silver and Chan, 1991). The method of Silver and Chan (1991) was used to determine the splitting parameters $\Phi$ and $\delta t$ that

best remove energy on the transverse component. Examples of splitting measurements are shown in Figure 2.2.

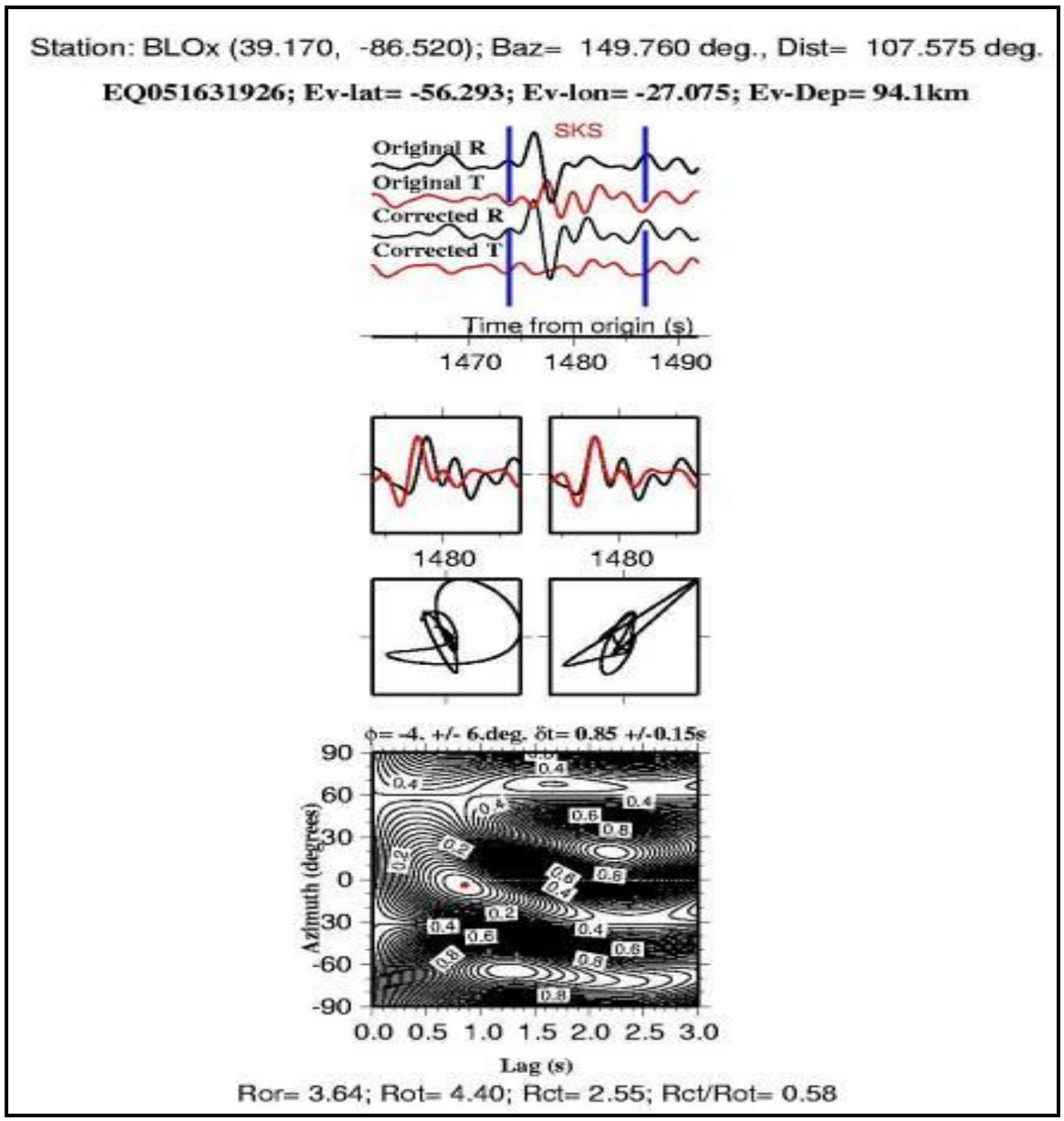


Figure 2.2a: Example of shear wave splitting plots for station BLO. Station: BLOx (39.170, -86.520). The vertical thick blue lines give the time window on which the splitting measurement is made. The four diagrams in the middle represent uncorrected and corrected fast and slow components of the split shear waves.

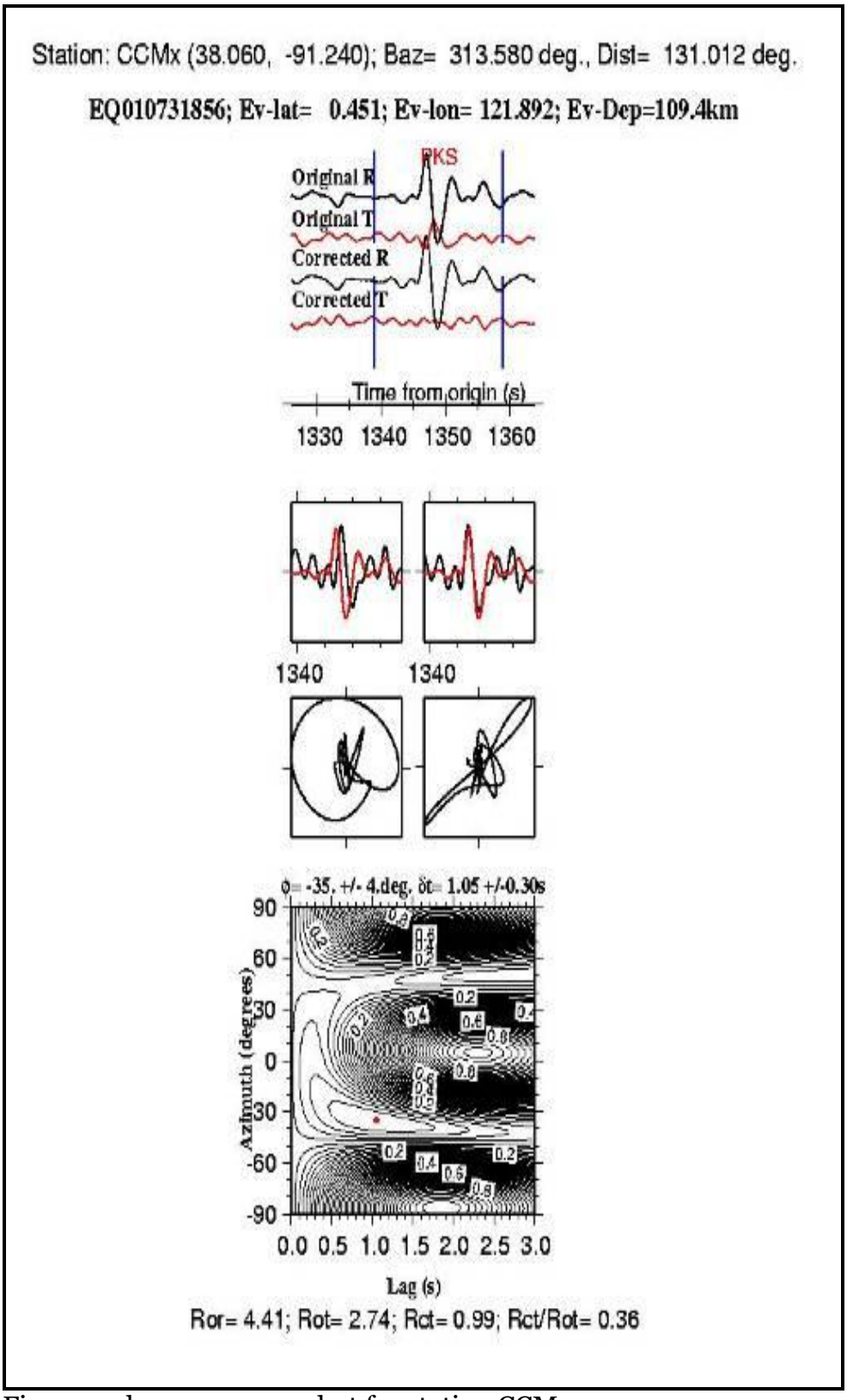


Figure 2.2b: same as 2.2a but for station CCM.

Silver and Savage (1994) have shown that for two anisotropic layers, the splitting parameters measured under the assumption of single anisotropic will be apparent parameters (Φa, δta) and will display azimuthal variations. The basis for this double layer is the fact that an incoming near vertical incident phase passes though two homogeneous anisotropic layers split twice. Splitting parameters for a double layer model are found by calculating the misfit to the apparent parameters by finding the pairs (Φ1, δt1) for the lower layer and (Φ2, δt2) for the upper layer that minimizes the misfit. This procedure for calculating the parameters for double layer model generates many possible solutions that fall within the set misfit. The bottom layer was fixed at $\Phi 1=70^{o}$ and δt1=0.5 s to minimize the ambiguity. The direction used for the bottom layer corresponds to the direction of the APM in the study area. Parameters for the upper layer are those providing the smallest misfit. The double layer anisotropy parameters are then checked for consistency by comparing the two layer curve with variation of Φ against BAZ Modulo ($90^{o}$). Double layer anisotropy causes the estimated splitting parameter to have a periodicity of π/2 as function of back azimuth (Silver and Savage, 1994). The method of Silver and Savage (1994) was used to perform grid search over the four trial parameters (Φ and δt for both upper and lower layers) to determine the optimum two-layer anisotropy model.

## 2.6 RANKING of RESULTING SPLITTING PARAMETERS

The results were objectively ranked as quality A (outstanding), B (fair), C (usable), N (null), or S (special) by using the method of Liu et al. (2008) which involves a combinations of the following three parameters: (1) $R_{or}$, the signal-to-

noise ratio on the original radial component that determines the strength of the XKS signal; (2) $R_{ot}$, the signal- to-noise ratio on the original transverse component and is related to the signal strength, magnitude of anisotropy, thickness of the anisotropic layer, and the angle between the fast direction and the arriving azimuth of the SKS ray-path; and (3) $R_{ct}$, the signal-to-noise ratio on the corrected transverse component. Its ratio with Rot is a measure of the significance of reduction of the energy on the corrected transverse component. In this study, quality A and B results which require Ror ≥10.0, Rot≥2.0, and Rct/Rot ≤0.7) are considered as "well-defined" measurements and are used in the discussion.

## 2.7. RESULTS AND DISCUSSION

Shear-wave splitting parameters have been measured at some of the stations in the study area. Stations CCM, MM14, MM15, MM16, MM17 and MM18 were measured by Fouch et al. (2000) using data from the Missouri to Massachusetts array (MOMA). They have found spatially uniform mean shear-wave splitting parameters at the stations, with a fast direction that is parallel to the absolute plate motion (APM) direction. Rowland et al. (1993) measured upper crustal anisotropy using short-period data from local earthquakes in the NMSZ, recorded by a PANDA (Portable Array for Numerical Data Acquisition) array, and found that the fast polarization directions at most stations are in ENE, which is consistent with the regional maximum compressional stress direction. Such a relationship is attributed to the presence of vertical stress aligned cracks, which are considered as the major cause of shear-wave splitting in the Earth's crust

(Crampin 1994). Crustal anisotropy related to upper crustal fracturing or to lower crustal pervasive fabric may contribute a small amount in splitting times (e.g. Barruol and Mainprice, 1993) in the splitting of SKS waves, which is 1 s on average (Silver, 1996). Recent shear wave splitting measurements by Gao et al. (2008) at Arkansas (station MIAR) has shown fast axis directions parallel to the trend of the Ouachita orogeny. MIAR, OXF and FVM were also studied by Barruol et al. (1997) who found $\Phi=89^{o}$ and $\delta t = 1.15$ s for MIAR, $\Phi=61^{o}$ and $\delta t = 1.55$ s for OXF and $\Phi=42^{o}$ and $\delta t = 0.83$ s for FVM. Figure 2.3 shows the mean splitting parameters from this study.

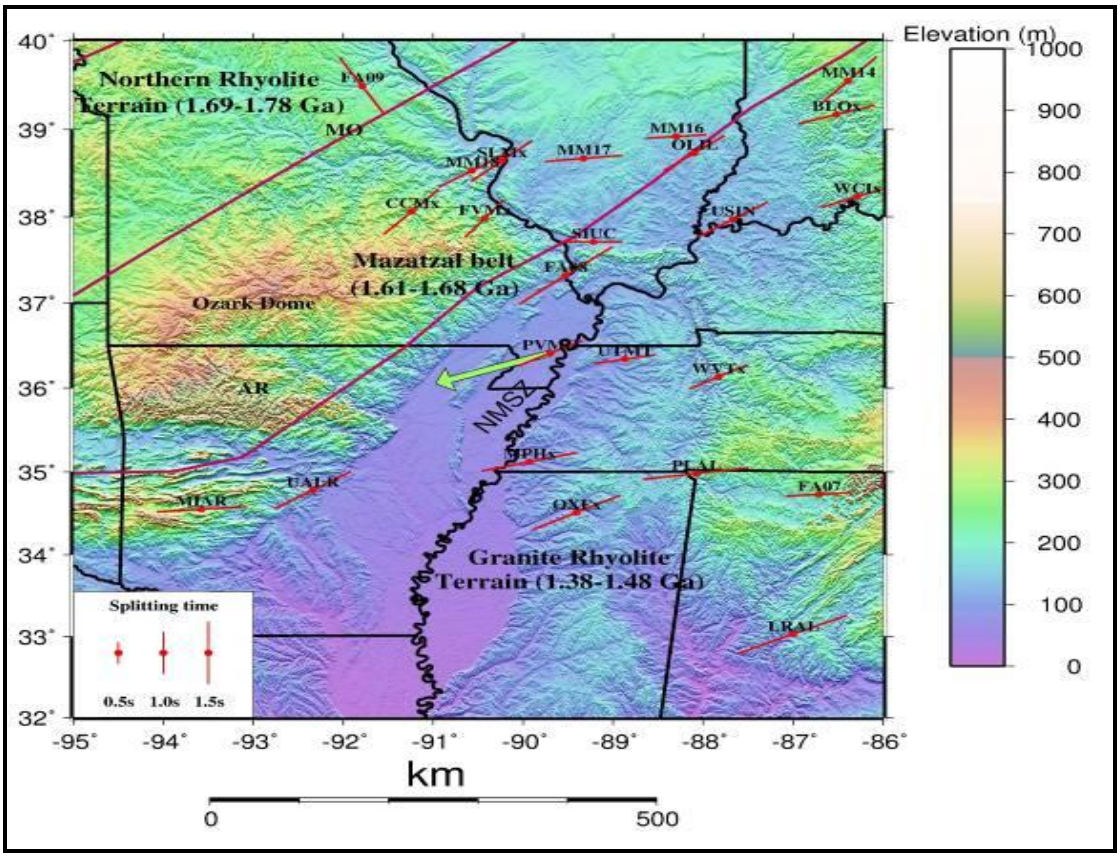


Figure 2.3: Mercator projection map of mean values of all phases per station. Large mean delay times are observed at LRAL and small mean delay times are found at stations FVM, UTMT, SIUC and PVMO.

Studies by Marone and Romanowicz (2007) present evidence for the presence of two layers of anisotropy with different fast-axis orientations in the cratonic part of the North American upper mantle. Their study revealed that beneath the stable interior of North America, at the asthenospheric depths of 200–400 km the fast axis is sub-parallel to the absolute plate motion, whereas in the lithosphere, the orientation is significantly more northerly, and is most likely caused by past orogenic events.

**2.7.1 Azimuthal Variation of Splitting Parameters and the Existence of Two-Layer Anisotropy.** To show azimuthal dependence in splitting, plots of Φ and δt against BAZ (modulo $90^{o}$) (Figures 2.4 and 2.5) are shown. The variation in the plots (Figures 2.4 and 2.5) could result from a single layer of anisotropy, spatially variable anisotropy within the station Fresnel zone, or more complicated anisotropy. The plot of Φ and δt as function of BAZ Modulo $90^{o}$ for most stations show a variable or complex distribution of events and polarization direction. The strongest azimuthal dependence is shown by CCM, BLO, SIUC, FVM, PLAL, MPH, OLIL, WCI, USIN, FVM, SLM, MIAR, LRAL, UTMT, WVT, OXF and MPH.

To investigate the existence of a two layer model, the grid search method (Silver and savage 1994) was employed to find the four parameters (Φ1, δt1 and Φ2, δt2) for all the stations. From the calculated four parameters for each station, it was very clear that the bottom layer has trending direction close to the APM direction except for MIAR. From this observation the bottom layer was fixed at $\Phi 1 = 70^{o}$ and δt1=0.5 s to obtain splitting parameters of the top layer for each

station group. The theoretical two-layer curves with parameters in Table 3.2 are plotted in Figure 2.4 and Figure 2.5. These curves fit fairly well to the variation of Φ and δt as a function of BAZ Modulo 90$^{o}$ for most stations.

**Table 2.1: Average SKS, PKS, and SKKS splitting results for the NMSZ. Stations with '*' have not been analyzed for shear wave splitting before.**

| Station name | Coordinates Latitude (Deg.) | Longitude (Deg.) | Fast Direction (Deg.) | Fast, Direction Δ° | Splitting time s | Splitting time Δs | Number of events | Weighted mean ΔΦ | Δs | Phase |
|---|---|---|---|---|---|---|---|---|---|---|
| BLO* | 39.17 | -86.52 | 63.53 | 26.13 | 1.04 | 0.26 | 12 | 0.48 | 0.02 | PKS |
| BLO* | 39.17 | -86.52 | 102.51 | 72.38 | 0.88 | 0.24 | 9 | 0.91 | 0.04 | SKKS |
| BLO* | 39.17 | -86.52 | 50.51 | 23.35 | 0.96 | 0.32 | 25 | 0.34 | 0.01 | SKS |
| CCM | 38.06 | -91.24 | 52.86 | 32.62 | 1.14 | 0.49 | 14 | 0.28 | 0.02 | PKS |
| CCM | 38.06 | -91.24 | 38.57 | 28.3 | 0.92 | 0.23 | 18 | 0.38 | 0.02 | SKKS |
| CCM | 38.06 | -91.24 | 37.46 | 29.85 | 0.82 | 0.38 | 53 | 0.28 | 0.01 | SKS |
| FA07* | 34.73 | -86.71 | 54.1 | 7.78 | 0.94 | 0.04 | 2 | 1.9 | 0.06 | PKS |
| FA07* | 34.73 | -86.71 | 29 | 4 | 0.45 | 0.6 | 1 | 10 | 0.22 | SKKS |
| FA07* | 34.73 | -86.71 | 175 | 12 | 0.95 | 0.4 | 1 | 6 | 0.2 | SKS |
| FA08* | 37.32 | -89.53 | 51 | 14 | 1.45 | 0.25 | 1 | 3.5 | 0.24 | SKS |
| FA09* | 39.49 | -91.79 | 149 | 6 | 1.05 | 0.3 | 1 | 3 | 0.15 | SKKS |
| FVM | 37.98 | -90.43 | 53 | 7 | 0.8 | 0.2 | 1 | 7.5 | 0.15 | PKS |
| FVM | 37.98 | -90.43 | 13 | 7 | 0.55 | 0.12 | 1 | 3.5 | 0.06 | SKKS |
| FVM | 37.98 | -90.43 | 49.28 | 16.96 | 0.88 | 0.09 | 4 | 0.9 | 0.04 | SKS |
| LRAL* | 33.03 | -87 | 70.52 | 2.05 | 1.31 | 0.15 | 13 | 0.48 | 0.02 | PKS |
| LRAL* | 33.03 | -87 | 61.77 | 3.8 | 1.74 | 0.32 | 8 | 0.78 | 0.05 | SKKS |

**Table 2.1: Average SKS, PKS, and SKKS splitting results for the NMSZ. Stations with '*' have not been analyzed for shear wave splitting before (cont.).**

| Station name | Coordinates Latitude (Deg.) | Longitude (Deg.) | Fast Direction (Deg.) | Fast, Direction Δ° | Splitting time s | Splitting time Δs | Number of events | Weighted mean ΔΦ | Δs | Phase |
|---|---|---|---|---|---|---|---|---|---|---|
| LRAL* | 33.03 | -87 | 63.22 | 7.16 | 1.25 | 0.31 | 14 | 0.91 | 0.04 | SKS |
| MM18 | 38.53 | -90.57 | 57 | 22 | 0.95 | 2.62 | 1 | 2.5 | 0.05 | SKS |
| MIAR | 34.55 | -93.58 | 95.43 | 8.36 | 0.83 | 0.14 | 6 | 1.15 | 0.03 | PKS |
| MIAR | 34.55 | -93.58 | 59 | 22 | 1.4 | 0.5 | 1 | 3.5 | 0.24 | SKKS |
| MIAR | 34.55 | -93.58 | 101.72 | 8.58 | 1 | 0.27 | 7 | 0.81 | 0.04 | SKS |
| MM14 | 39.55 | -86.39 | 35 | 8 | 1.2 | 0.4 | 1 | 4 | 0.2 | SKKS |
| MM14 | 39.55 | -86.39 | 48.56 | 2.83 | 0.86 | 0.18 | 2 | 1.56 | 0.03 | SKS |
| MM16 | 38.92 | -88.3 | 99.36 | 18.38 | 0.63 | 0.04 | 2 | 3.34 | 0.08 | SKKS |
| MM16 | 38.92 | -88.3 | 72 | 8 | 0.8 | 0.1 | 1 | 3 | 0.05 | SKS |
| MM17 | 38.67 | -89.33 | 58 | 16 | 1.25 | 0.43 | 1 | 8 | 0.22 | PKS |
| **MM17** | 38.67 | -89.33 | 110 | 20 | 0.6 | 0.48 | 1 | 9 | 0.16 | SKS |
| MPH* | 35.12 | -89.93 | 57.1 | 7.21 | 1.2 | 0.19 | 4 | 0.78 | 0.03 | PKS |
| MPH* | 35.12 | -89.93 | 91 | 22 | 1.05 | 2.6 | 1 | 4 | 0.14 | SKKS |
| MPH* | 35.12 | -89.93 | 79.05 | 39.39 | 1.33 | 0.42 | 5 | 0.5 | 0.04 | SKS |
| OLIL* | 38.73 | -88.1 | 53.83 | 3.07 | 0.87 | 0.13 | 5 | 1.12 | 0.05 | PKS |
| OLIL* | 38.73 | -88.1 | 51.88 | 5.66 | 0.94 | 0.04 | 2 | 2.4 | 0.04 | SKS |
| OXF | 34.51 | -89.41 | 64.48 | 1.8 | 1.27 | 0.11 | 4 | 0.54 | 0.02 | PKS |
| OXF | 34.51 | -89.41 | 61.78 | 3.43 | 1.1 | 0.16 | 3 | 1.95 | 0.08 | SKKS |
| OXF | 34.51 | -89.41 | 61.83 | 4.64 | 1.19 | 0.14 | 4 | 0.63 | 0.03 | SKS |
| PLAL | 34.98 | -88.08 | 62.41 | 2.11 | 1.21 | 0.11 | 3 | 0.86 | 0.04 | PKS |
| PLAL | 34.98 | -88.08 | 50 | 2 | 1.8 | 0.32 | 1 | 1.5 | 0.17 | SKKS |
| PLAL | 34.98 | -88.08 | 132.6 | 55.86 | 0.89 | 0.29 | 13 | 0.38 | 0.02 | SKS |
| PVMO* | 36.41 | -89.7 | 62.61 | 5.65 | 0.87 | 0.1 | 3 | 1.58 | 0.05 | SKS |
| SIUC* | 37.71 | -89.22 | 72.99 | 13.72 | 0.81 | 0.43 | 3 | 1.61 | 0.04 | PKS |
| SIUC* | 37.71 | -89.22 | 110 | 18.1 | 0.55 | 0.09 | 5 | 2.24 | 0.02 | SKKS |
| SIUC* | 37.71 | -89.22 | 88.62 | 16.77 | 0.7 | 0.13 | 21 | 0.81 | 0.01 | SKS |
| SLM* | 38.64 | -90.24 | 49.25 | 14.73 | 0.84 | 0.11 | 6 | 0.82 | 0.03 | PKS |
| SLM* | 38.64 | -90.24 | 56.45 | 7 | 1.19 | 0.42 | 9 | 0.37 | 0.04 | SKKS |
| SLM* | 38.64 | -90.24 | 40.59 | 9.67 | 0.91 | 0.16 | 11 | 0.66 | 0.03 | SKS |
| UALR* | 34.78 | -92.34 | 42.38 | 12.97 | 1.18 | 0.12 | 3 | 2.45 | 0.08 | PKS |
| UALR* | 34.78 | -92.34 | 60 | 6 | 1.15 | 0.25 | 1 | 3 | 0.12 | SKKS |

**Table 2.1: Average SKS, PKS, and SKKS splitting results for the NMSZ. Stations with '*' have not been analyzed for shear wave splitting before (cont).**

| Station name | Coordinates Latitude (Deg.) | Longitude (Deg.) | Fast Direction (Deg.) | Fast, Direction Δ° | Splitting time s | Splitting time Δs | Number of events | Weighted mean ΔΦ | Δs | Phase |
|---|---|---|---|---|---|---|---|---|---|---|
| UALR* | 34.78 | -92.34 | 68.92 | 7.72 | 0.9 | 0.03 | 3 | 2.05 | 0.05 | SKS |
| USIN* | 37.97 | -87.67 | 58.49 | 2.12 | 0.99 | 0.17 | 4 | 1.48 | 0.06 | PKS |
| USIN* | 37.97 | -87.67 | 53.55 | 2.83 | 1.05 | 0.07 | 2 | 1.86 | 0.07 | SKKS |
| USIN* | 37.97 | -87.67 | 57.68 | 5.35 | 0.95 | 0.2 | 6 | 0.78 | 0.03 | SKS |
| UTMT* | 36.34 | -88.87 | 64 | 8 | 0.9 | 0.23 | 1 | 4 | 0.12 | PKS |
| UTMT* | 36.34 | -88.87 | 120 | 7 | 0.35 | 0.2 | 1 | 11 | 0.31 | SKKS |
| UTMT* | 36.34 | -88.87 | 54.6 | 66.19 | 0.95 | 0.5 | 3 | 0.96 | 0.06 | SKS |
| WCI* | 38.23 | -86.29 | 53.62 | 1.64 | 0.92 | 0.19 | 3 | 1.23 | 0.04 | PKS |
| WCI* | 38.23 | -86.29 | 32.38 | 7.78 | 1 | 0 | 2 | 3.33 | 0.08 | SKKS |
| WCI* | 38.23 | -86.29 | 119.21 | 61.11 | 0.82 | 0.25 | 14 | 0.67 | 0.02 | SKS |
| WVT* | 36.13 | -87.83 | 56 | 6 | 0.65 | 0.12 | 1 | 3 | 0.06 | PKS |
| WVT* | 36.13 | -87.83 | 79 | 1 | 0.8 | 0.2 | 1 | 3.5 | 0.15 | SKKS |
| WVT* | 36.13 | -87.83 | 49.71 | 10.14 | 0.95 | 0.55 | 6 | 0.8 | 0.07 | SKS |

**Table 2.2: Station groups and upper layer parameters.**

| Groups | Station names | Φ1(deg.) | δt1(s) | Φ2 (deg.) | δt1(s) |
|---|---|---|---|---|---|
| A | CCM, FA09 | 70 | 0.5 | 28 | 1.05 |
| B | FVM, SLM, MM16, MM17, MM18, OLIL, USIN | 70 | 0.5 | 66 | 0.35 |
| C | SIUC, FA08 | 70 | 0.5 | -83 | 0.3 |
| D | BLO, WCI, MM14 | 70 | 0.5 | 26 | 0.45 |
| E | LRAL, FA07 | 70 | 0.5 | 61 | 0.8 |
| F | UALR | 70 | 0.5 | 55 | 0.5 |
| G | MIAR | | | | |
| H | PVMO, UTMT, WVT, MPH, OXF, PLAL | 70 | 0.5 | 46 | 0.35 |

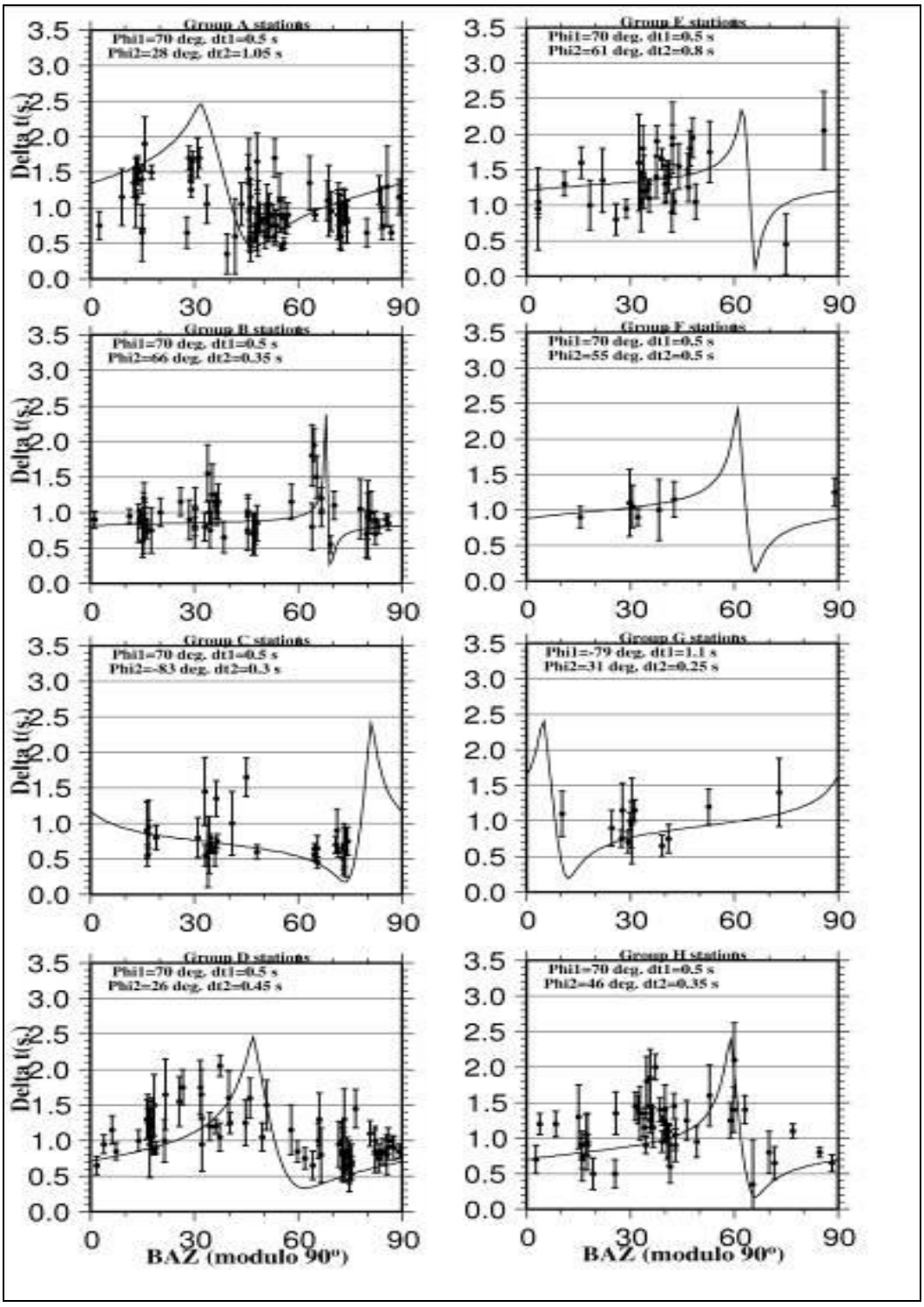


Figure 2.4: High quality measurements of δt vs. BAZ (modulo 90°) for the stations in the NMSZ and nearby stations. The double anisotropic was estimated with a theoretical two-layer model calculated with bottom layer fixed at Phi= 70 deg. and Dt at 0.5 s.

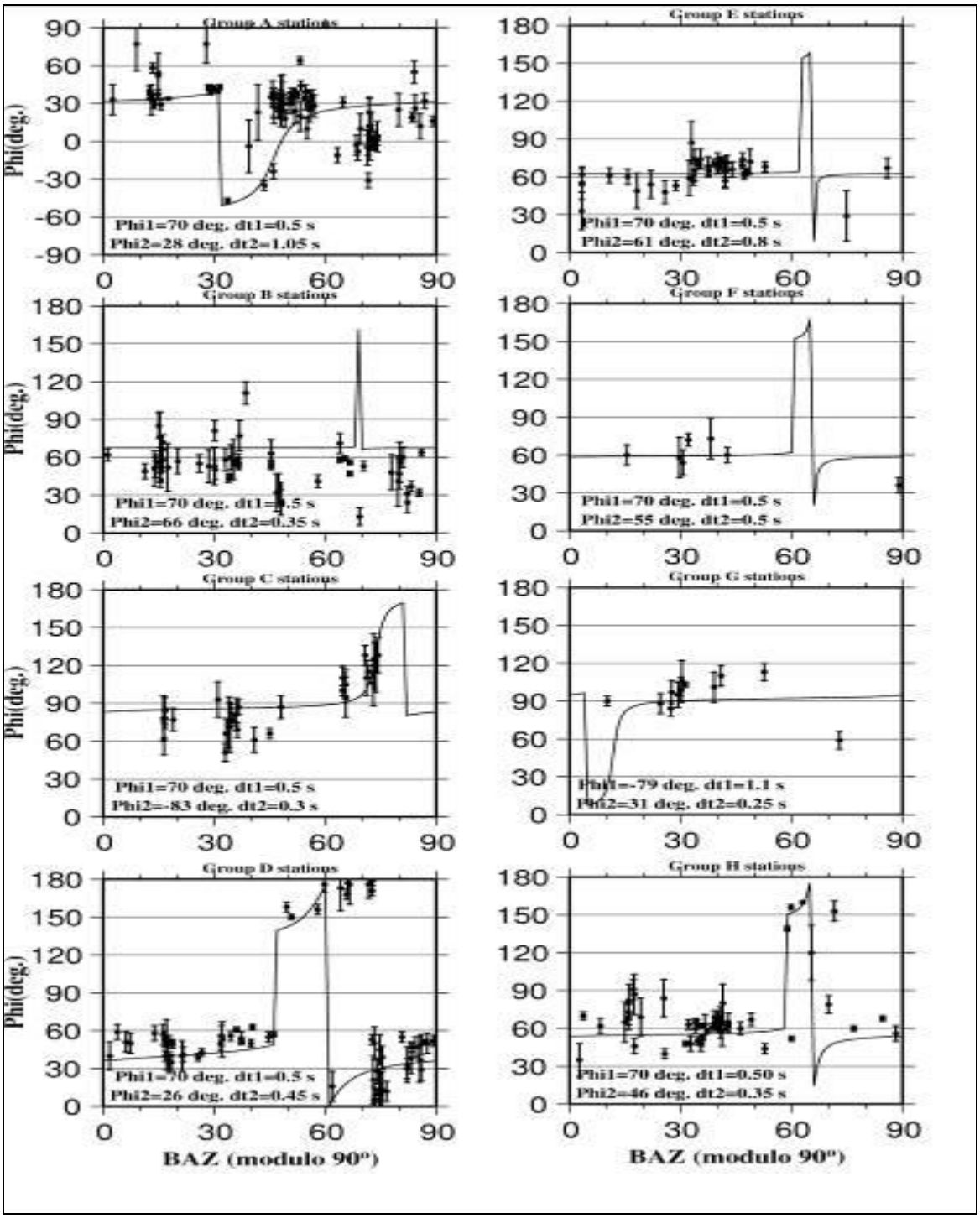


Figure 2.5: High quality measurements of Φ vs. BAZ (modulo 90°) for the stations in the NMSZ and nearby stations. The stations have been modeled by double anisotropic layers with theoretical two-layer curves plotted. The bottom layer was fixed at 70 deg. and Dt= 0.5 s.

**2.7.2 Spatial Grouping of the Stations.** The data from this study is divided in to eight groups based on the location of each station with respect to nearby stations and azimuthal coverage of events. The parameters for the upper layer in a double-layer anisotropy were then calculated for each group using the method of Silver and Savage (1994) with the bottom layer fixed at $\Phi 1=70^{o}$ and $\delta t1$ at 0.5 s (Table 2.2 and Figure 2.6).

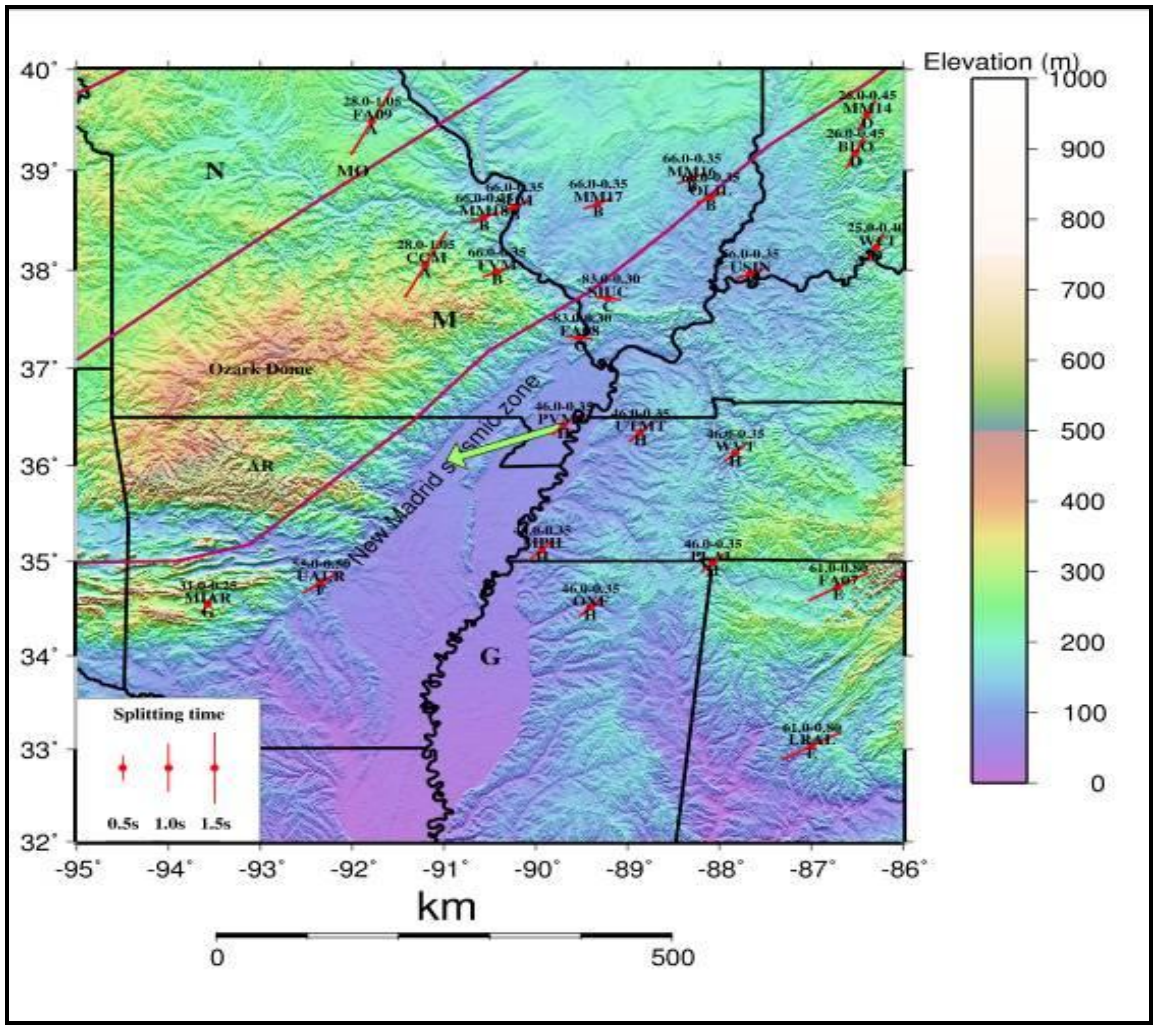


Figure 2.6: Distribution of fast directions for the upper layer with lower layer fixed at Phi1=70 deg. and Dt1=0.5 s. The letters below the station names are station groups.

**Group A** stations include CCM and FA09 even though FA09 has fast axis trending in the NW direction. These stations are on the Mazatzal Belt (1.61-1.68 Ga), a NE trending Precambrian belt. Stations within this group show well defined splitting parameters on XKS phases. These stations are grouped together because BAZ from FA09 falls within the azimuthal distribution of events in CCM. **Group B** has the following stations: FVM, SLM, MM16, MM17, MM18, OLIL and USIN. These stations are within the Illinois Basin which is underlain by Precambrian basement. The stations are grouped together because the fast axis direction from plot of individual splitting parameters show a NE direction with events having limited BAZ. Station FVM seems to be at the boundary between CCM and MM18. **Group C** stations include SIUC and FA08. SIUC show a complex splitting pattern which is different from the surrounding stations. **Group D** stations: BLO, WCI and MM14. These stations show complex splitting patterns and the events have similar azimuthal distribution except MM14 which has a narrow azimuthal window of the events. **Group E** stations: LRAL and FA07. The stations are on the Appalachian Orogeny and have consistent splitting pairs trending in the NE direction. **Group G**: MIAR. This station is situated on the Ouachita Orogeny and has fast axis direction in EW direction. **Group H**: PVMO, UTMT, WVT, MPH, OXF, and PLAL stations inside or in the immediate vicinity of the NMSZ belong to this group. The station names referred above are as shown in Figure 2.1.

**2.7.3. Group A Stations**: Station CCM was previously studied by Fouch et al. (2000) who observed a mean $\Phi = 30°$ and mean $\delta t = 0.9$ s with 3 splitting measurements. Using data that spans nearly two decades, the anisotropy

measurements at CCM from 53 SKS, 14 PKS, and 18 SKKS show a complex pattern of splitting with fast axis directions showing a counterclockwise rotation of Φ ranging from 1±7° to 179±14° with a mean value of 50°±7.8° and δt ranging from 0.35 s to 1.9 s with mean splitting time of 1.0±0.2 s. CCM located on the Mazatzal belt (1.61-1.68 Ga) and shows complex splitting parameters (Figures 2.4 and 2.5) of Φ and δt as a function of BAZ (modulo 90°). The observed splitting pattern for this station is a strong indication that anisotropy cannot be estimated by assuming single layer anisotropy. The direction of the APM at the NMSZ is N250.9°E (Gripp and Gordon, 2002) on a hotspot reference frame.

FA09 is situated north-west of the Mazatzal belt in the Northern Rhyolite terrain. XKS splitting measurements for this station resulted in one SKKS splitting with Φ1=149±6° and δt1=1.05 ±0.3 s. The theoretical two layer curve for this group are plotted in Figure 2.4 and Figure 2.5 with Φ2=28°, and δt2=1.05 s for the top layer and the bottom layer fixed at Φ1=70°, and δt1=0.5 s. Thelayer thickness of the upper layer is about 117 km for 4% anisotropy. These curves fit fairly well to the azimuthal variations of Φ, and δt.

**2.7.4 Group B Stations.** Station FVM was previously studied by Barruol et al. (1997) who obtained a Φ of 42° and a δt of 0.83 s. In this study, 1 PKS, 1 SKKS and 4 SKS measurements were obtained with Φ ranging from 13±7° to 81±8° with a mean Φ of 55 ± 9.5° and δt ranging from 0.55±0.12 s to 1.0±0.17 s with a mean of 0.8±0.2 s.

Station SLM is between MM18 and MM17 and has 6 PKS, 9 SKKS and 11 SKS measurements with Φ values ranging from 24±8° to 77± 12° with a mean of

46.5±7.4° and δt ranging from 0.7±0.1 s to 1.95±0.43 s with a mean of 1.04±0.2 s. This station show complex splitting behavior which is not revealed by MM18 and MM17 probably because the short duration in which the data was acquired for the MOMA array.

MM16 has 4 SKS measurements with Φ values ranging from 72° ±6 to 111° ± 9 with a mean of 93.5±8.3, and δt values ranging from 0.4±0.1 s to 0.8±0.1 s with a mean of 0.6±0.12 s. Fouch et al. (2000) obtained a mean Φ of 61° and a mean δt of 0.8 s for SKS phase. This station has a poor azimuthal coverage with events having back azimuth of 285° to 319°.

One SKS event from MM17 yielded good splitting pairs with Φ of 58±16° and δt 1.25±0.4 s. For this station, Fouch et al. (2000) obtained a mean Φ of 60° and a mean δt of 0.9 s using the SKS phase.). Determination of double layer parameters was not performed because of insufficient data.

The SKS splitting determined by Fouch et al. (2000) shows that the mean Φ is about 57° with a mean δt of 1.05 s using the SKS phase. This study has obtained one SKS event with Φ=57±5° and δt=0.95±0.1 s. There is very little variation in the splitting parameters from this study with previous measurements. Double layer anisotropy cannot be estimated for this station based on one measurement and hence the existence of two layer anisotropy cannot be ruled out.

OLIL station is situated within the Mazatzal belt and is close to MM16. No previous measurements exist from this station but splitting parameters at MM16 show fast directions align with the APM (Fouch et al., 2000). 5 PKS events and 3 SKS events yielded good splitting parameters with Φ ranging from 41± 20°to

170±12° with a mean of 67.8±9° and δt ranging from 0.55±0.18 s to 1.0±0.18 s with a mean of 0.8±0.2 s.

The earthquakes from this station yielded 3 PKS, 3 SKKS and 6 SKS phases with Φ ranging from 52±19° to 64±3° with a mean of 57±8.1° and δt ranging from 0.75 ±0.28 s to 1.2±0.2 s with a mean of 0.95±0.23 s. The fast axis direction coincides with the APM direction. Double layer inversion for this group has Φ2=66°, δt2=0.35 s for the top layer with the bottom layer fixed at Φ1=70°, δt1=0.5 s. The layer thickness of the upper layer is about 39 km for 4% anisotropy.

**2.7.5 Group C Stations.** Station SIUC is located south of MM17 and shows complex splitting as observed in other stations like BLO and CCM. 29 earthquakes from this station result in 3 PKS, 5 SKKS and 21 SKS phases with Φ ranging from 61±10° to 129±14° with a mean of 91.7±11.7°, and δt ranging from 0.45±0.08 s to 1.65±0.27 s with a mean of 0.75±0.22 s.

FA08 is at the tip of the Mississippi embayment/Reelfoot escarpment and has one SKS measurement with Φ = 51±7° and δt=1.45±0.48 s. The four parameters for double layer anisotropy could not be determined because of the limited number of events. Because of the close proximity of FA08 to SIUC, the theoretical curve shown in Figure 2.4 and Figure 2.5 were calculated using the combined splitting parameters from these two stations. This group has Φ2=-83°, δt2=0.3 s for the top layer with the bottom layer fixed at Φ1=70°, δt1=0.5 s. The anisotropic layer thickness of the upper layer is about 33 km for 4% anisotropy

**2.7.6 Group D Stations.** Station BLO is in the northern most of the study area on the Mazatzal Belt and no previous splitting parameters were determined for this station. The splitting parameters from 12 PKS, 9 SKKS, and 24 SKS phases ranges from $\Phi$=5 ±11$^{o}$ to 179±4$^{o}$ with a mean of 60.6±7.7$^{o}$ and $\delta$t from 0.6±0.2s to 2.05±0.25 s with a mean of 1.06±0.24 s. The direction of the fast axis show a counter clockwise rotation pattern (Figure 2.1). This rotation pattern is an indication that the anisotropy beneath BLO is complex and cannot be explained by single layer model or simple asthenospheric flow.

Station WCI has shown a complex pattern of fast axis direction. The $\Phi$ for this station ranges from 4±10$^{o}$ to 173±18$^{o}$ with a mean of 67.5±8.8o and $\delta$t values ranging from 0.45±0.17 s to 1.75±0.38 s from 3 PKS, 3 SKKS and 14 SKS phases. The mean fast axis in this area has been found to align with the APM (Fouch et al., 2000), but plotting the individual splitting measurements reveal a much more complicated pattern of splitting. Interpretation of splitting parameters from MOMA array suggests single layer anisotropy in this area (Fouch et al., 2000).

Three SKS measurements from MM14 (mean $\Phi$ =53$^{o}$ and mean $\delta$t= 0.95 s for SKS phase; Fouch et al., 2000) show $\Phi$ values ranging from 35±8$^{o}$ to 51±5$^{o}$ with a mean of 44.3±5.7 and $\delta$t values ranging from 0.8±0.07 s to 1.2±0.4 s with a mean of 1.01±1.2 s.

MM15 did not yield good splitting parameters because of low signal to noise ration within the expected shear wave splitting window, but Fouch et al. (2000) found mean $\Phi$ of 60$^{o}$ and mean $\delta$t= 0.9 s for SKS phase.

**2.7.7 Group E Stations.** LRAL has the largest delay times (Table 2.1) and the splitting pattern is consistent for all the phases. Individual splitting measurements for this station are shown in Figure 2.1. Φ measurement from 13 PKS, 7 SKKS and 14 SKS phases ranges from 33±15° to 87±17° with a mean of 64.6±6.9° and δt ranges from 0.8±0.22s to 1.95±0.28 s with a mean of 1.38±0.28.

This station is situated on the 1.38 to 148 Ga Granite Rhyolite Terrains. Three measurements (2 PKS and 1 SKKS) from this station revealed Φ in the range of 29±20° to 64±12° with a mean of 48.6±12° and δt in the range of 0.45±0.43 s to 0.95±0.13 s with a mean of 0.76±0.28 s. The grid search method for this group resulted to Φ2=61°, δt2=0.8 s for the top layer with the bottom layer fixed at Φ1=70°, δt1=0.5 s. The layer thickness of the upper layer is about 89 km for 4% anisotropy.

**2.7.8 Group F Stations.** UALR is approximately 130 km from MIAR, but the average splitting parameters are different from MIAR. The Φ from 3 PKS, 1 SKKS, and 3 SKS phases range from 36±6° to 73±16° with a mean of 46.5±7.4° and δt ranging from 0.9 ±0.15 s to 1.25±0.2 s with a mean of 1.05±0.27 s. With the bottom layer fixed at Φ1=70°, δt1=0.5 s, the top anisotropic layer has Φ2=55°, δt2=0.5 s with a thickness of about 55 km calculated for 4% anisotropy.

**2.7.9 Group G Stations.** MIAR was previously studied by Gao et al. (2008) and showed a mean Φ of 112±8° and splitting time of 0.7±0.2 s using the SKS phase. The same station was studied by Barruol et al. (1997) who obtained a mean Φ of 89° and δt of 1.15 s. In this study, the anisotropy

beneath MIAR was studied using the XKS phases and the measurements are shown in Figure 2.1. The observed Φ values from 6 PKS, 1 SKKS and 7 SKS phases vary from 59±7° to 113±7° with a mean of 96.8±7.8° and δt ranges from 0.65±0.15 s to 1.2±0.25 s with a mean of 0.99±0.27 s. The fast axis direction coincides with strike of the Ouachita orogeny. With bottom layer fixed at Φ1=70° and δt1 at 0.5 s, the grid search method did not yield a good fit for this station. The grid search method of Savage and Silver (1994) without fixing the bottom layer resulted in the following parameters for the double layer model: Φ1=-79°, δt1=1.1 s for the lower layer and Φ2=31°, δt2=0.25 s for the upper layer. The lower layer coincides with the trend of the Ouachita orogenic belt. Previous studies for this station have indicated that upper mantle anisotropy beneath MIAR could be represented by a single layer model (Gao et al., 2008).

**2.7.10 Group H Stations.** Station PVMO shows three well constrained SKS splitting parameters with Φ ranging from 58±6° to 73±4° with a mean of 64.6±6.6°, and δt ranging from 0.75±0.18 s to 0.95±0.22 s. PVMO is located within the Mississippi embayment and the general sense of direction for the fast axis of polarization is NE similar to the direction of APM. The splitting times are much greater than expected for crustal anisotropy. The deviations of the apparent splitting parameters from the theoretical curves are likely to be caused by scattering effects in the data and due to using only a single frequency (0.15 Hz) in calculating the curves.

Station UTMT is situated east of PVMO within the Mississippi embayment, a southwest-trending aulocogen of late Precambrian-early Paleozoic origin (Braile et al., 1982). Well defined splitting parameters from all the phases are observed for this station. The polarization angle (Φ) from 1 PKS and 3 SKS phases ranges from 48±2 to 153±8° with a mean of 85±8.25 and the delay times δt range from 0.6 ±0.23 s to 1.45±0.2 s with a mean of 0.9±0.22 s. The average splitting parameters for UTMT are shown in Table 2.1.

WVT is on the eastern side of the Mississippi bluff. 1PKS, 1 SKKS and 5 SKS phases have Φ ranging from 40±4° to 87±16° with a mean of 65.1±9.4° and the delay times δt range from 0.5±0.22 s to 1.6±0.43 s with a mean of 0.93±0.29 s. The fast axis directions show an NE trending direction which is similar to the APM direction.

Splitting parameters from 4 PKS, 1 SKKS and 5 SKS phases for MPH show Φ ranging from 53±2° to 139±2° with a mean of 71.9±3.9 ° and δt values ranging from 0.95±0.15 s to 2±0.18 s with a mean of 1.2±0.2 s. Even though this station is south east of the Reelfoot faults, the fast axis direction for this station aligns with the APM. This is an indication that crustal contribution to the observed splitting parameters does not play a significant role.

OXF is located south of MPH and has Φ values (from 4 PKS, 3 SKKS and 4 SKS phases) in the range of 60±2° to 70±3° with a mean of 63.4±4.1° and the delay times δt in the range of 0.95±0.25 s to 1.45±0.18 s with a mean of 1.21±0.16 s.

PLAL shows a complex splitting pattern from 3 PKS, 1 SKKS and 13 SKS phases with polarization angle ranging from 35±13° to 160±1° with a mean of

70.3±6.6° and the delay times δt ranging from 0.5±0.2 s to 1.8±0.4 s with a mean of 1.15±0.26 s. Previous mean measurements using the SKS phase alone for this station by Fouch et al. (2000) revealed a Φ of 170° and a δt of 1.35 s. Their mean Φ is different from the mean from this study which (from 17 events) is 70.3±6.6° and δt =1.15±0.26 s. The fast axis direction from this study has a similar trend as APM. The grid search method resulted in Φ2=46°, and δt2=0.35 s for the top layer with the bottom layer fixed at Φ1=70°, δt1=0.5 s. The layer thickness of the upper layer is about 39 km for 4% anisotropy

## 2.8. DISCUSSION

**2.8.1 Source of Anisotropy.** The hypotheses to explain the observed anisotropy beneath the NMSZ include: (1) mantle anisotropy induced by extension due to LPO of olivine, (2) anisotropy due to an alignment of parallel dikes or melt-filled lenses along the strike of the rift, (3) fossilized anisotropy in the lithospheric mantle from previous orogenic events, and (4) mantle anisotropy due to shear related flow at the base of the lithosphere or cratonic keel, (5) asthenospheric flow in the direction of absolute plate motion .

**2.8.2 Anisotropy Due to Extension/Compression.** Continental regions have been shown to exhibit splitting patterns that are closely related to surficial geologic features, suggesting a lithospheric origin related to the fabric that was generated by the most recent significant tectonic event (e.g., Silver, 1996; Barruol et al., 1997) or that lithospheric and sublithospheric deformation is coherent. Splitting measurements in the NMSZ are not pervasively consistent with surface geologic features (Figure 2.1) and hence lithospheric anisotropy

cannot be invoked as the only cause of the observed anisotropy. Shear wave splitting on ocean ridges (e.g., the Red Sea; Vinnik et al., 1989) and on continental rifts (e.g., Baikal rift; Gao et al., 1997) show fast splitting directions parallel to the extension direction. In extensional regimes, ductile stretching of the mantle lithosphere should produce a lattice preferred orientation of olivine fast axes in the direction of extension if strain is controlled by dislocation creep (Christensen, 1984; Nicolas and Christensen, 1987; Mainprice and Silver, 1993). Lattice preferred orientation (LPO) of olivine aligns the a-axes with the direction of extension, whereas in compressive regimes the fast axis is aligned perpendicular to the direction of compressive forces (Zhang and Karato, 1995). Our results are subparallel to the extension direction, and so extension-driven rift-perpendicular material flow is also likely to be a possible cause of the observed anisotropy.

The splitting measurements on the NMSZ and the surrounding area presented in Figure 2.1 show sub-parallelism of fast axis of polarization with the local structural trend. This suggest that the old lithospheric structures control the observed splitting parameters to some degree but the splitting time is more than expected for crustal anisotropy (Savage, 1999). Parallelism of the fast axis direction and the strike of geological features are observed at most stations in Figure 2.1 even though CCM, BLO, MIAR, WCI show complex splitting patterns. This type of alignment has been observed in areas of active transpression (Savage, 1999; Fouch et al., 2000). The average fast directions of the stations within the rift are approximately subparallel to trend of the rift. Such parallelism suggests that anisotropy could be related to deep seated rift structures and rift

processes. Fast directions along the trend of the rift could be related to the preferred alignment of magma filled pockets/dikes with a long axis parallel to the maximum compressive direction and a short axis parallel to the minimum compressive (extension) direction (Gao et al., 1997). Rift parallel dikes may form a transverse anisotropy with a rift orthogonal axis of symmetry. The fast direction of the anisotropy would be parallel to the strike of the dikes/rift axis. The crustal contribution is not likely to be significant and typically amounts to 0.04-0.2 s of splitting (Gledhill and Stuart, 1996; Savage, 1999) indicating that the majority of XKS shear wave splitting occurs in the mantle. The effect of crustal anisotropy is thus not apparent and, the upper mantle is considered the most likely source of the observed anisotropy in NMSZ.

Significant anisotropy may also be induced by flow of asthenospheric material between steeply dipping rift border faults (Barruol and Ben-Ismail, 2001). It is widely observed that the fast direction of crustal shear waves is parallel to the local strike of cracks or direction of the maximum horizontal compressive stress (Crampin and Peacoch, 2005). However in the NMSZ, subtle correlation between splitting parameters and the trend of the Reelfoot faults were observed. The observed splitting parameters could be olivine LPO anisotropy due to ductile lithospheric compression associated with NE/SW compressive forces at the NMSZ. Zoback and Zoback (1980) indicated that the direction of maximum stress in the central United States is approximately east-west compressive, but in the central part of the NMSZ (the area surrounding Kentucky Bend), the stress-direction data indicate a rotation to northeast-southwest compression.

**2.8.3 Anisotropy Due to APM.** Some of the stations in the NMSZ and elsewhere exhibit patterns of seismic anisotropy more closely related to the local direction of absolute plate motion (APM) in the hotspot reference frame (e.g., Nicolas and Christensen, 1987; Vinnik et al., 1992), suggesting that seismic anisotropy exists primarily in the sublithospheric mantle and is generated by fabric resulting from mantle flow. The current APM direction of NMSZ is 250° (Gripp and Gordon, 2002). Our observed fast azimuths show a strong correlation with this N250°E APM direction in the vicinity of the NMSZ. Observed anisotropy results in NMSZ are therefore partly explained by the simple asthenospheric flow hypothesis. Mantle material may flow beneath and around continental keels with complex morphologies, generating a fabric that mimics the keel shape (Fouch et al., 2000). Observations of seismic anisotropy have led to the conclusion that the observed anisotropy on continental settings is a combination of both lithospheric and sublithospheric fabric (Savage and Silver, 1993; Fouch et al., 2000).

The observed fast direction at MAIR shows large deviation between the fast direction from the lower layer and APM direction with the upper layer at N31°E. The large deviation between the lower layer and APM direction could be caused by asthenospheric flow around the continental root. The most intriguing observation for this station is the parallelism of the trend of surface expressions of Ouachita orogeny with fast axis of the lower later. This suggests that the observed anisotropy has contributions from both the lithosphere and asthenosphere. A geophysical model by Mickus and Keller (1986) suggests that the strike of orogeny observed on the surface does not necessarily represent

regional trend of the orogeny or lithospheric deformation at depth. Studies by Fouch et al. (2000) show NE-SW fast directions on the North American craton that are parallel the APM and are different from the fast directions at MIAR. Station UALR is close to MIAR (Figure 2.1) but the direction of the fast direction is consistent with the North American APM. There is a significant change in the fast directions between the two stations suggesting that UALR is situated on the edge of the craton and hence the splitting pattern at these stations resembles that of cratonic stations.

Station CCM, FVM, SLM, MM18, MM17, MM16, SIUC and OLIL are located on Mazatzal belt (1.61-1.68Ga) which is made up of several blocks with varying ages (Holm et al., 2007). The age differences of the Mazatzal belt are likely to cause spatial variations of the splitting parameters as shown in Table 2.2. Station MM14, BLO, WCI, FA08 and USIN are on the granite rhyolite terrain (1.38-1.48 Ga). These terrains belongs the North American craton. Splitting patterns from these stations are complex and cannot be explained by simple asthenospheric flow alone. Our splitting measurements for cratonic stations are explained well by the double layer parameters shown in Table 2.2. The lower layer has fast directions of approximately N70$^{o}$E while the top layer is approximately N22$^{o}$E. The lower layer is consistent with the direction of the APM while anisotropy on the upper layer is most likely due to lithospheric contribution. This double layer anisotropy is consistent with the result of a recent joint inversion of surface waveforms and shear wave splitting measurements which revealed a two-layer anisotropy model (Marone and Romanowicz, 2007)

for stable North America. Stations within the New Madrid seismic zone show double anisotropy model with the parameters shown in Table 2.2.

**2.8.4 Anisotropy due to Proximity to the Bermuda Hotspot.** The mantle plume hypothesis predicts that ascending plume material is deflected by the lithosphere, which could lead to the development of olivine LPO and bulk anisotropy. The deflection of plume material can be tested by measurements of mantle anisotropy (Savage and Sheehan, 2000). Cox and Van Arsdale (1997) related the formation of the NMSZ to the Bermuda hotspot. Theoretical models predict that the polarization angle of the fast axis would approximately align with radial asthenospheric flow outwards from the plume head sheared in the direction of plate motion at significant distances from the conduit (Kaminski and Ribe, 2002). Splitting measurements observed around Hawaii (Walker et al., 2001) and in the Great Basin (Walker et al., 2004) fit such a parabolic flow pattern. Splitting measurements from the NMSZ does not show evidence of the splitting pattern expected from plume upwelling beneath Reelfoot rift.

**2.8.5 Depth Extent of Faults.** Seismic studies by Van Arsdale et al. (1998) at Reelfoot rift revealed a westerly dipping reverse fault zone, with the Ridgely right-lateral transpressive fault zone on the east, and the Cottonwood Grove right-lateral strike-slip fault in the middle of the basin. The depth extent of these major faults system in the NMSZ is unknown. High resolution seismic reflection surveys (McBride and Stephenson, 2003; Bexfield et al., 2006) have been used to study subsurface faulting. The results revealed that the faults systems are confined in the upper crust. The Ridgely fault zone consists of two

northeast-striking faults within the Mississippi embayment and has 15 m of post-Eocene, up-to-the-east displacement and appears to locally control the eastern limit of Mississippi River migration (Bexfield et al., 2006). Our observed splitting parameters have a nearly parallel trend with this fault system. The Cottonwood Grove fault zone passes through the center of the NMSZ close to station MPH and PVMO and has approximately 5 m of up-to-the-east displacement. Work by Chiu et al. (1992) suggests that a 31° to 48°, southwest-dipping reverse fault lies beneath the Lake County uplift at hypocentral depths of 4 to 13 km.

A preferred orientation of cracks, faults, fractures, and availability of intrusion bodies make a homogeneous medium anisotropic for wavelengths much larger than the spacing of the parallel structures (Crampin, 2003). When these structures are vertical, the fast direction is parallel to the strike of the structures, and δt is proportional to the volume fraction of and velocity contrast across the structures. Cracks, faults, and fractures are confined to the brittle upper crust (0–15 km), and thus the δt associated with such aligned structures are probably within the noise of teleseismic shear wave splitting. This is consistent with the typically observed crustal δt of 0.1–0.3 s (Crampin, 1994; McNamara et al., 1994). However, partially molten tabular intrusions (dikes) are a possible cause of teleseismic splitting because the velocity contrast between magma and the surrounding rock is large, and parallel dikes could penetrate through the entire lithosphere, leading to considerable δt. Magma-filled (Kendall, 1994) lenses can also lead to effective anisotropy and splitting where Φ is parallel to the strike of the lenses. Because parallel dikes or magma-filled lenses would be a result of partial melt collecting along planes that are perpendicular to the least

principal stress direction, this hypothesis predicts that the fast directions would be parallel to the current maximum horizontal compressive stress if there was a steady state active source of partial melt in the asthenospheric mantle and the region of partial melt was currently in a normal faulting stress state. Predicted δt would be the highest in the center of the rift and would decrease away from the rift because of cooling of the dikes/magma lenses over time. The data set allows a more spatially comprehensive study of splitting in NMSZ, and there is some evidence for splitting parallel to maximum compressive stress in stations that are far from the rift but not enough to conclude that either parallel dikes or magma-filled lenses are the dominant causative mechanism of anisotropy.

**2.8.6 Simple Asthenospheric Flow.** Lattice preferred orientations of the fast olivine axis develop in the asthenosphere because of dislocation-creep deformation associated with simple shear at the base of the plate (e.g., Nicolas, 1989; Zhang and Karato, 1995). These orientations are roughly horizontal and in the direction of shear. Simple asthenospheric flow due to the passive shearing of the asthenosphere by the moving plate has been invoked to interpret splitting fast directions parallel to absolute plate motion (APM) (Vinnik et al., 1992). Our fast directions show spatial and azimuthal variation throughout the study area (Figure 2.1) and are therefore not explained by the simple asthenospheric flow hypothesis. The polarization for cratonic stations are consistent with the asthenospheric flow hypothesis if the plate is moving with respect to the underlying mantle, creating simple shear at the base of the craton. If there is relative motion between the lithosphere and the underlying mantle, the

asthenosphere must flow around and/or beneath craton keels. Fouch et al. (2000) interpreted splitting parameters in North America as due to asthenospheric flow associated with basal lithospheric topography. In most regions of gentle topographical gradients, the fast axis is parallel to APM (Gripp and Gordon, 2002). In regions where the topographic gradients are large, the fast direction tends to be parallel to the topographic contours of the keel topography. Stations CCM and stations from the MOMA array were previously studied by Fouch et al. (2000) who suggest that the fast directions are approximately parallel to the craton edge and can be explained by edge flow around the keel. Their calculations predict that splitting beneath flat lithospheric keel would have Φ parallel to APM, whereas splitting elsewhere would have Φ parallel to the depth contours at the base of the lithosphere because the rigid lithosphere is moving through the asthenosphere.

**2.8.7 Vertical Asthenospheric Flow.** A recent study by Forte et al. (2007) based on tabular slab geometry descending into the mantle below the Central Mississippi River Valley demonstrated dramatic changes in mantle flow direction associated with the subducting Farallon slab. For vertical asthenospheric flow, the expected splitting times would be small or close to zero. However, the observed splitting times in the vicinity of the NMSZ are greater than the global average, and hence cannot be explained by vertical asthenospheric flow.

**2.8.8 Fossilized Anisotropy in the Lithosphere.** The North American plate has been modified by multiple orogenic events, and therefore

vertically incoherent anisotropy and inconsistent splitting are expected. The fast directions within the NMSZ are subparallel to the geologic structural trends exposed at the surface. Correlation of increasing δt with increasing lithospheric thickness for the North American craton observed previously were explained by fossilized lithospheric anisotropy (Silver and Chan, 1988, 1991). The double layer model with the bottom layer fixed at $\Phi = 70^{o}$ and $\delta t = 0.5$ s reveal the presence of fossilized anisotropy (Figure 2.6) with the upper layer with splitting times ranging from 0.3 s to 1.05 s. Splitting observed on the Kaapvaal craton (Silver et al., 2001; Fouch et al., 2004) has also been interpreted to represent the effects of fossilized anisotropy. The Australian (Clitheroe and van der Hilst, 1998) and east European (Wylegalla et al., 1999) cratons and parts of the Siberian (Gao et al., 1997) craton demonstrate small, inconsistent, or no splitting.

**2.8.9 Pervasive two Layer Anisotropy.** The shear waves splitting for the PKS, SKS, and SKKS were combined for each station to search for two layer anisotropy. Strong double layer anisotropy is revealed by most stations shown in Figures 2.4, 2.5, 3.1. The two layer system consists of a lower and upper layer with splitting parameters shown in Table 2.2. The curve fit fairly well to the variation of apparent splitting angle and apparent splitting time. Fouch et al. (2000) analyzed data from CCM using three events which were not sufficient to show any complexity in shear wave splitting. The double layer inversion at CCM shows a lower layer with $\Phi 1 = 49^{o}$, $\delta t1 = 0.8$ s and upper layer with $\Phi = 21^{o}$, $\delta t = 0.55$ s and BLO has lower layer with $\Phi 1 = 74^{o}$, $\delta t1 = 1.05$ s and upper layer with $\Phi = 22^{o}$, $\delta t = 0.65$ s. Individual splitting measurements at these stations show a counter

clockwise splitting pattern. The fast directions of the lower layers of the two stations are not consistent which could result from complex asthenospheric flow beneath the stations.

## 2.9. CONCLUSION

XKS splitting observations in the NMSZ and the surrounding areas suggest a complex pattern of anisotropy across the region. A single layer of anisotropy is inferred beneath some of the stations while other stations show evidence of the asthenosphere as the source of the anisotropy. Since the observed fast directions are sub-parallel to the Reelfoot fault system, it is likely that asthenospheric flow is responsible for the observed anisotropy. Plate-mantle interaction is dominated beneath the Eastern North America due to the higher level of shear stress and the larger spatial extent. Thus the mantle under NMSZ may move in a different direction without affecting the motion of North America. On the other hand, the motion of deep lithospheric roots is probably to some degree correlated with the motion of the mantle below. Our shear wave splitting measurements suggest that the anisotropy observed at the NMSZ is complex and hence a combination from different sources and that the depth extent of Reelfoot fault system is confined to the upper part of the brittle-ductile transition. The two layer model proves to be the ideal model to explain the measured splitting parameters beneath the New Madrid Seismic Zone.

# 3. EVIDENCE OF RIFT-PARALLEL FAST POLARIZATION DIRECTIONS BENEATH THE MIDCONTINENT RIFT REVEALED FROM SHEAR-WAVE SPLITTING ANALYSIS

## 3.1 ABSTRACT

Upper mantle anisotropy beneath the Mesoproterozoic Midcontinent Rift (MCR) and adjacent areas is investigated using splitting of P-to-S converted phases (SKS, SKKS and PKS) at the core-mantle boundary. Available data from all the portable or permanent broadband seismic stations in the area of 38-46$^{o}$N and 92-102$^{o}$W are used in the study. Well-defined measurements were obtained at about 21 stations, with a mean splitting time of about 1 s which corresponds to a layer of anisotropy of about 110 km thick (4% anisotropy). The most interesting feature in the spatial distribution of the splitting parameters (fast polarization direction $\Phi$ and splitting time t) is that beyond the 1.1 Ga MCR, the $\Phi$ observations are mostly parallel to the absolute plate motion (APM) direction, while in the vicinity of the rift, the majority of the $\Phi$ values are consistent with the strike of the rift. The APM direction in the study area is about 250$^{o}$ clockwise from the north, while the strike of the MCR is 215$^{o}$-220$^{o}$. The most likely cause for the intriguing observation is azimuthal anisotropy related to sub-vertical magmatic dykes along the strike of the rift. Although the dykes have long become inactive, the slight difference in seismic velocity between the dykes and the surrounding lithospheric rocks can lead to the observed anisotropy. This interpretation is consistent with the notion that igneous activities were pervasive while the rift was active, leading to a layer of basaltic rocks of up to 20 km thick in the rift.

## 3.2. INTRODUCTION

Polarization anisotropy on the Mid-continent Rift (MCR) is determined by splitting of P-to-S converted phases at the core-mantle boundary in order to study the deformation in the upper mantle (Silver, 1996; Savage, 1999). The MCR provides an excellent place to study upper mantle deformation beneath an inactive rift (Figure 3.1).

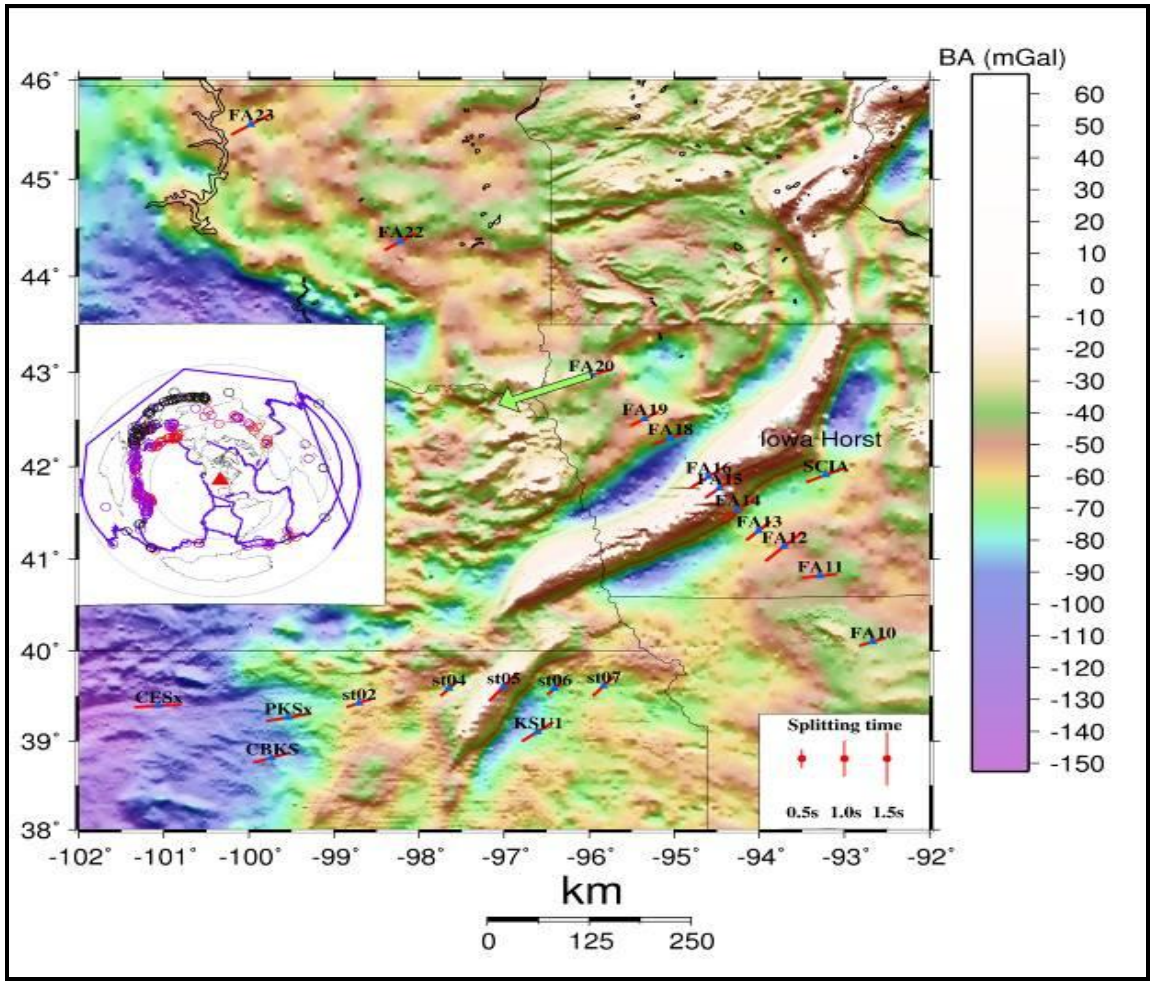


Figure 3.1: Mean shear wave splitting measurements and Bouguer anomaly of the MCR showing two profiles used for shear wave analysis. Orientation, length of bars give fast polarization directions, splitting delay time at stations shown in the figure. The blue triangles represent the location of temporary broadband stations. Gravity data was obtained from PACES: Pan-American Center for Earth and Environmental Studies.

In this paper, the results from teleseismic shear wave splitting parameters from XKS (SKS, PKS and SKKS) are used to (1) constrain the spatial variation of anisotropy, (2) quantify the orientation and strength of mantle fabrics beneath the MCR in North America, (3) explore the existence of fossil fabrics related to Archean rifting, and (4) provide insights on the "healing process" of continents.

## 3.3 GEOLOGIC SETTING

The MCR delineated by high gravity anomaly (Van Schmus and Hinze, 1985) cuts across several Precambrian basement terranes of different age, structure, and composition in the craton that existed prior to 1.2 Gyr ago. The northern portion of the MCR is situated in the Lake Superior basin and occurs in the Archean Superior Province of the Canadian Shield. South of the Lake Superior basin, the southeastern and southwestern segments occur for the most part in early Proterozoic crust, although the northern part of the MCR segment occurs in the Archean terrane. Archean crust is not found south of central Wisconsin and southern Minnesota (Van Schmus and Bickford 1981; Nelson and DePaolo, 1985). The Proterozoic crustal basement rocks in the Midcontinent region were formed 1300-1900 Myr ago and consist of 1600-1900-Myr old crust probably formed as orogenic continental margin assemblages (Van Schmus and Bickford, 1981) and 1300-1500-Myr-old anorogenic plutonic and volcanic rocks that formed by re-melting of the older Proterozoic crust (Thomas et al., 1984; Nelson and DePaolo, 1985; Anderson, 1983).

## 3.4. DATA ACQUISITION

XKS data from broadband seismic stations were used for this study. Data came from 14 temporary stations from the Florida to Edmonton (FLED) array, 8 temporary stations from a Kansas array, and 4 permanent broadband stations. XKS phases from earthquakes with magnitude >5.5 that occurred at distances between 85$^{o}$ and 180$^{o}$ for SKKS and SKS phases and between 120$^{o}$ and 180$^{o}$ for the PKS phases are used. Seismometers of the FLED array were deployed in May 2001 and data collection continued through October 2002 (Fischer et al., 2006). A total of 232 phases were chosen from 35 earthquakes where XKS phase energy was above the noise level. Seismograms were band-pass filtered with corner frequencies 0.04 and 0.15 Hz. Band-pass filtering is required to remove the high levels of micro-seismic and cultural noise in the data. In cases of excellent signal-to-noise earthquakes, this approach gives robust measurements on individual seismograms. However, most of the data from the MCR is noisy and resulted in splitting parameters with large errors (>=0.5 s in $\delta t$, >=22$^{o}$ in $\Phi$) for individual earthquakes.

The data was obtained from IRIS data management center. Events used in this study are shown in Figure 3.1. The events recorded at most of stations have limited distribution of back azimuths (BAZ). All analyzed phases have steeply dipping incidence angles and sample the upper mantle almost directly beneath the station, providing very good lateral resolution.

## 3.5. METHOD

The polarization angle Φ and the splitting time δt are determined based on a grid search over the possible splitting parameters to reverse the process of generating the split shear waves (Silver and Chan 1991). This is achieved by minimizing the component that perpendicular to the incoming polarization angle of the shear wave before entering the anisotropic medium (Ozalaybye and Savage, 1992). A visual inspection for all events allowed us to keep about 93 events for which XKS phases were clearly identified. The method of Silver and Chan (1991) determines the anisotropy parameters Φ and δt that best remove energy on the transverse component of the seismogram for a selected time window. Several events show null measurements which are characterized by the absence of signal on the transverse component. They indicate either the absence of anisotropy beneath the station or that the initial polarization direction of the SKS wave is parallel to the fast or slow direction in the anisotropic layer. An example of splitting measurements is shown in Figure 3.2.

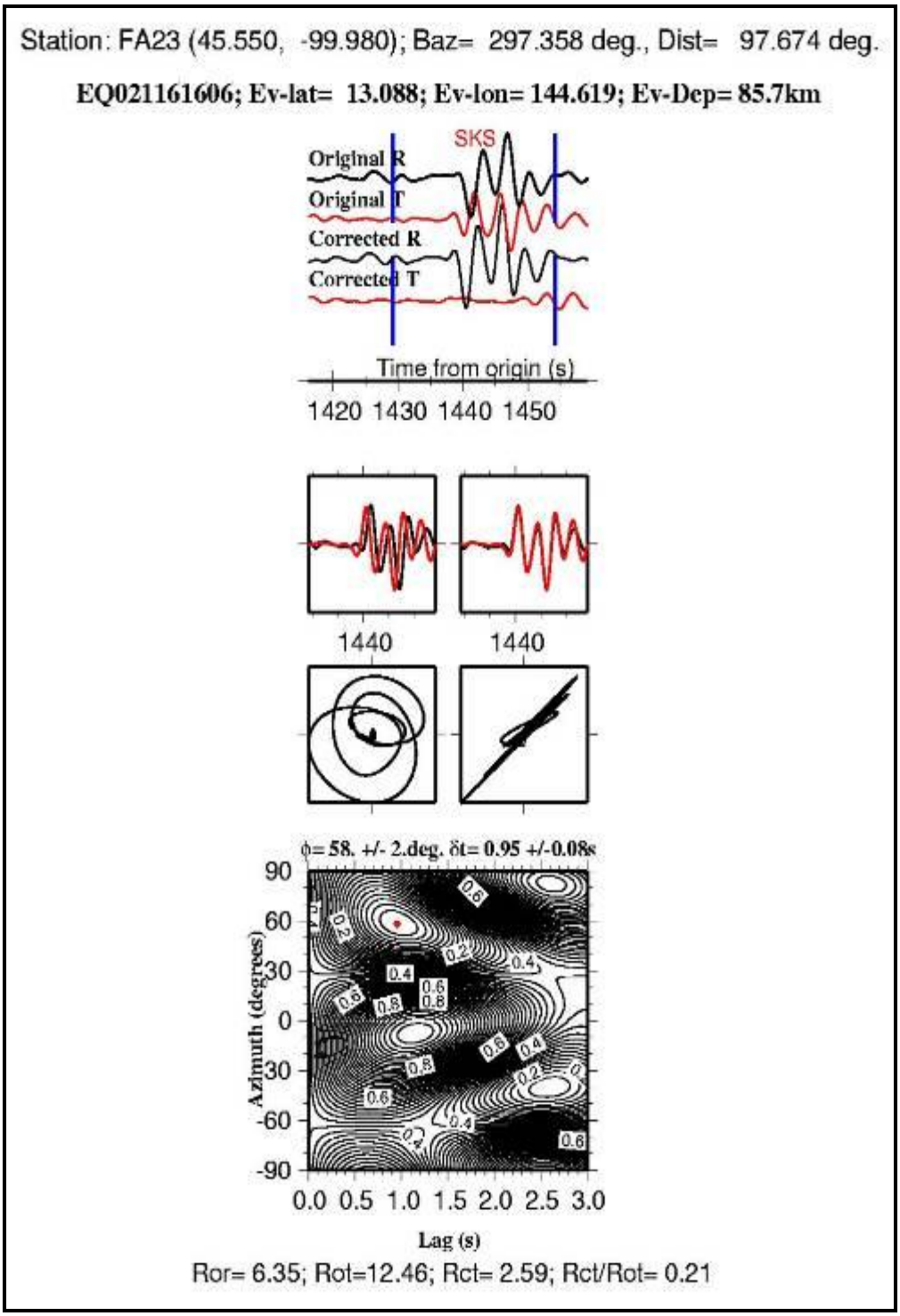


Figure 3.2a: Example of shear wave splitting plots for station FA23; this station is situated off the rift on the NW side of the MCR.

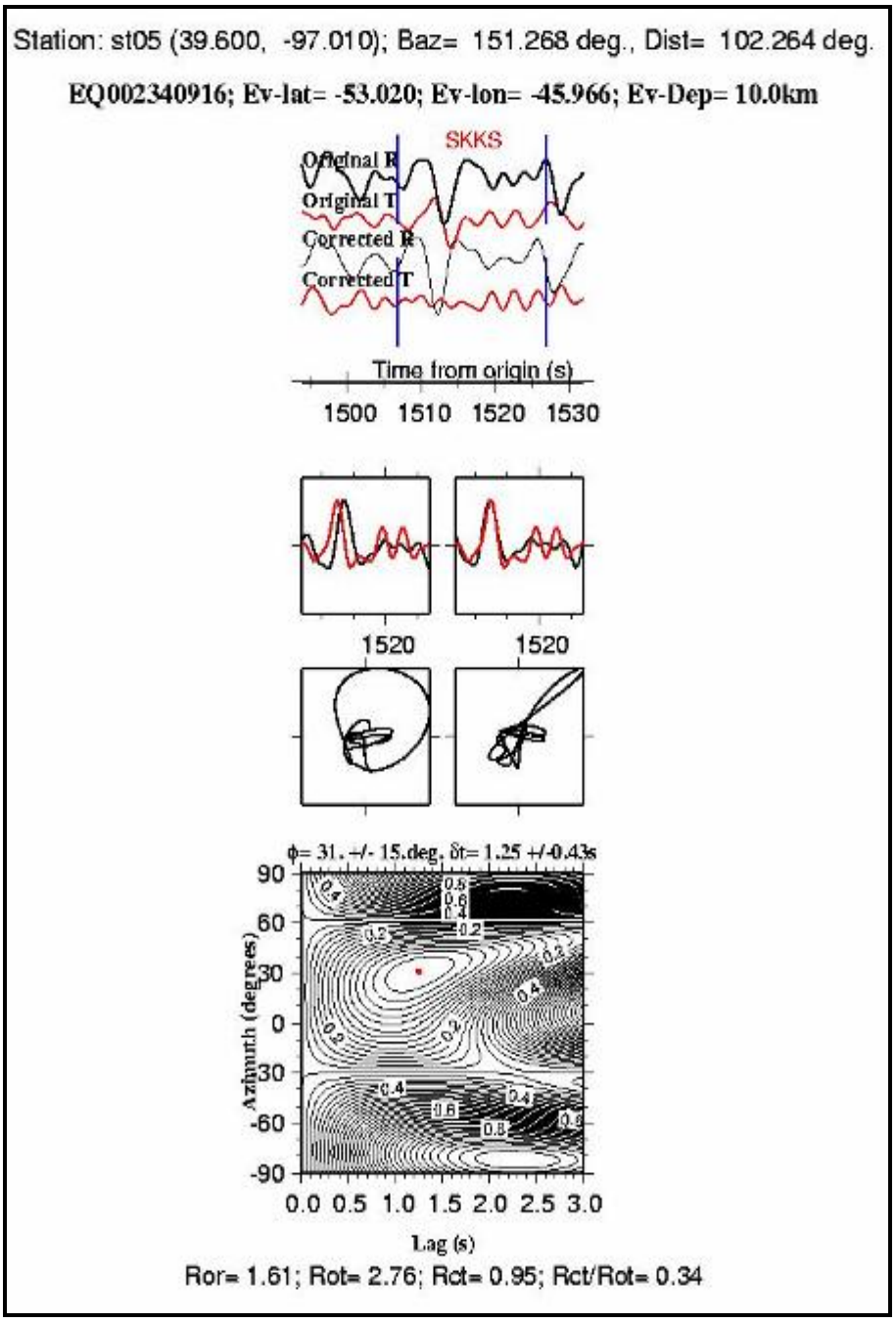


Figure 3.2b: Example of shear wave splitting plots for station st05 situated on the Kansas Horst.

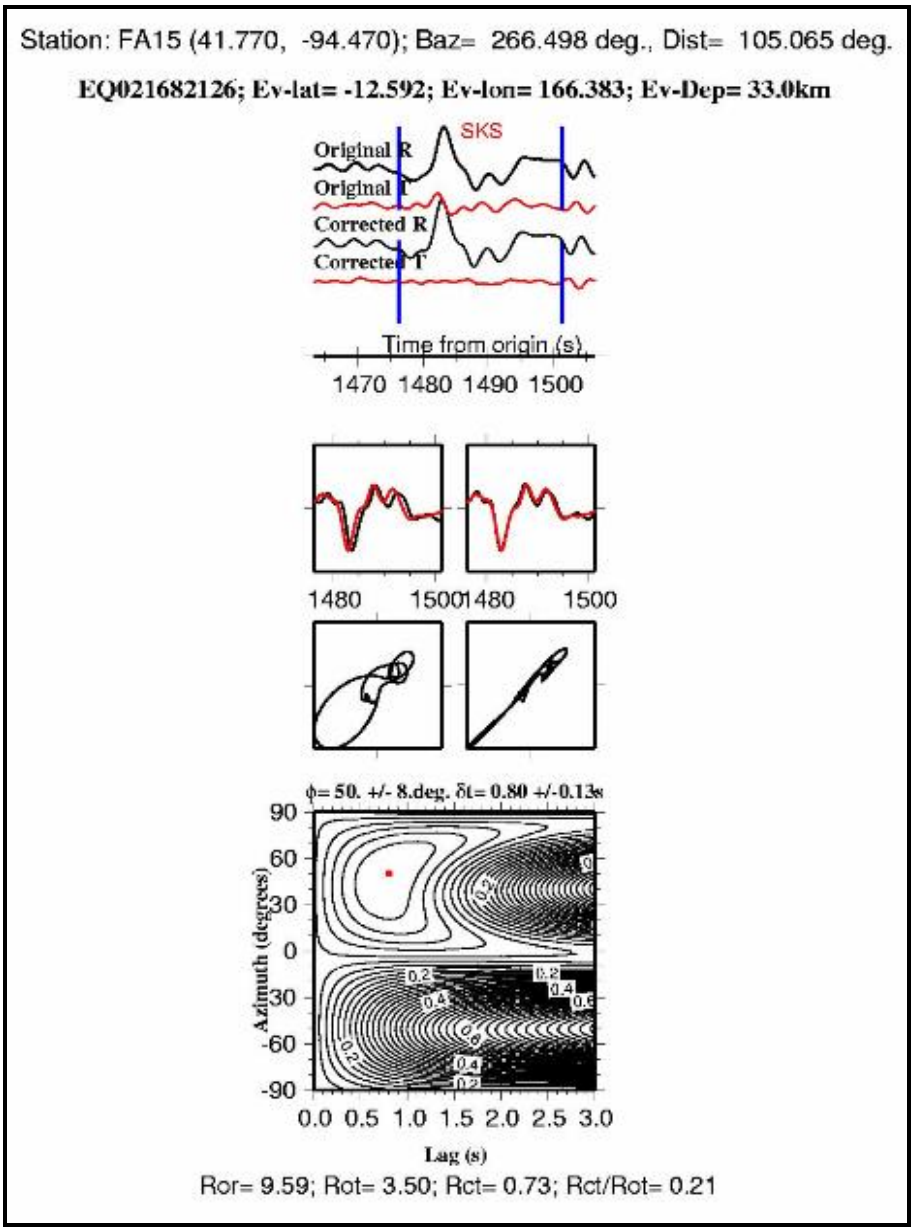


Figure 3.2c: Example of shear wave splitting plots for station FA15 situated on the Iowa Horst.

## 3.6 RANKING OF RESULTING SPLITTING PARAMETERS

The reduction of the energy on the XKS phase of the corrected transverse component, small errors in Φ and δt and the clear arrival of the XKS phases on the original radial and transverse components are the basic requirements for a

well defined splitting parameter. The procedure used by Liu et al. (2008) was adopted for ranking the splitting parameters in this study. This procedure requires that the following conditions be met to obtain a well-defined splitting measurement: (1) high S/N for pre-splitting SKS arrivals; (2) a large (>22$^{o}$) difference between the back azimuth (BAZ) and the fast direction; and (3) strong azimuthal anisotropy with a horizontal axis of symmetry. Deviations from these conditions lead to poorly determined splitting results. Events were objectively ranked as quality A, B, C, N, or S by using the method of Liu et al (2008) which involves a combinations of the following three parameters: (1) Ror, the signal-to-noise ratio on the original radial component that determines the strength of the SKS signal; (2) Rot, the signal- to-noise ratio on the original transverse component. Rot is related to the signal strength, magnitude of anisotropy, thickness of the anisotropic layer, and the angle between the fast direction and the arriving azimuth of the SKS ray-path; and (3) Rct, the signal-to-noise ratio on the corrected transverse component. Its ratio with Rot is a measure of the significance of reduction of the energy on the corrected transverse component. Events ranked A or B with $\delta t$ <2 s are used in obtaining station averages.

## 3.7. RESULTS

Most of the events analyzed did not yield good splitting parameters because of the following reasons: (1) The Earth beneath the station could be weakly anisotropic to steeply incident shear phases; (2) simple anisotropy exists, and the initial polarization angle is parallel or perpendicular to the fast axis; (3) complex anisotropy exists, and interference between multiply split phases creates

a complicated waveform that is not explained well by the optimum apparent splitting parameters, (4) the signal does not contain an adequate frequency bandwidth to calculate the error bars, perhaps because of large earthquake source dimensions, attenuation along the ray path, and/or intra-crustal scattering/reverberation; or (5) the SNR is too low. Examples of good splitting measurements are shown in Figures 3.1, and 3.2., and Table 3.1 shows mean splitting results.

The minimum and maximum splitting times for the FLED array are 0.4±0.1 to 1.35±0.3 s respectively with an average of 0.9±0.25 s and the polarization angle ranges from 36±4$^{o}$ to 146±6$^{o}$ with an average of 63.2±9.9$^{o}$. Stations in the Kansas array show splitting times in the range of 0.45±0.62 s to 1.8±0.35 s with an average of 0.87±032 s, and Φ values in the range of15±16$^{o}$ to 176±8$^{o}$ with an average of 60.7±11$^{o}$. Permanent stations considered in this study are CES, SCIA, PKS and ECSD. Stations SCIA is situated NE of FA14 and has an average splitting time of 0.94±0.3 s and average Φ of 65.6±9.8$^{o}$. The trend of the MCR in the vicinity of SCIA is about N45$^{o}$E. NW of the Iowa Horst (FA17 to FA23) Φ is consistently oriented NE-SW, approximately coincident with the APM direction and the orientation of the Great Lakes Transfer Zone and Spirit lake Trend. The splitting time (δt) for this stations ranges from range 0.75–1 s. Stations FA14 to FA16 are within the Keweenawan rift and have δt and Φ values ranging from 0.5 s to 1.6 s and Φ values from 45$^{o}$ to 78$^{o}$, which are approximately coincident with the strike of the surface expression of the fault. On the Southern side of the Iowa Horst (FA10 to FA14), Φ ranges from 45$^{o}$ to 68$^{o}$, and δt increases to 1 s. Splitting measurements from the permanent stations show a NE trend of

fast directions, similar to both FLED and Kansas array. Splitting parameters for CBKS were previously determined by Barruol et al. (1997) ($\Phi$=42$^o$, $\delta$t=0.61 s and $\Phi$=58$^o$, $\delta$t=0.95 s) and Fouch et al. (2000) ($\Phi$=46$^o$, $\delta$t=0.45 s). Average measurements of splitting parameters from this study show $\Phi$=62.5$^o$, $\delta$t=0.7 s for SKS and $\Phi$=54$^o$, $\delta$t=0.9 s for PKS phases. FLED stations on the Iowa horst are FA15, FA16 and FA17 and have the following splitting parameters: $\Phi$=42$^o$, $\delta$t=0.61 s and $\Phi$=58$^o$, $\delta$t=0.95 s. The polarization angle for these stations shows a deviation of about 25$^o$ from the APM direction. Plotting of the gravity profiles with splitting parameters from both Kansas and FLED array shows that the high Bouguer gravity anomaly within the rift axes coincides with the more northerly polarization angles observed for stations within the rift (Figure 3.3).

**Table 3.1: Mean splitting results for stations used in the study area.**

| Station | St-lat. | St-lon. | Phi | STD of Phi | DT | STD of DT |
|---|---|---|---|---|---|---|
| FA23 | 45.55 | -99.98 | 57.5 | 3.25 | 1.02 | 0.1425 |
| FA22 | 44.36 | -98.22 | 56.5 | 9.5 | 0.82 | 0.19 |
| FA20 | 42.97 | -95.98 | 71 | 13 | 0.91 | 0.31 |
| FA19 | 42.51 | -95.35 | 58 | 18 | 0.70 | 0.25 |
| FA18 | 42.3 | -95.05 | 66.6 | 11.8 | 0.81 | 0.28 |
| FA16 | 41.89 | -94.60 | 52.5 | 5.5 | 0.95 | 0.23 |
| FA15 | 41.77 | -94.47 | 50.00 | 8.0 | 0.80 | 0.13 |
| FA14 | 41.54 | -94.26 | 52.00 | 7.5 | 1.00 | 0.25 |
| FA13 | 41.31 | -94.01 | 46.50 | 13.0 | 0.725 | 0.43 |
| FA12 | 41.14 | -93.71 | 46.00 | 4.0 | 1.15 | 0.2 |
| FA11 | 40.82 | -93.29 | 82.50 | 11.5 | 0.74 | 0.24 |
| SCIA | 41.91 | -93.22 | 65.60 | 9.8 | 0.94 | 0.30 |
| FA10 | 40.1 | -92.67 | 69.00 | 14.0 | 0.6 | 0.13 |
| CESx | 39.39 | -101.07 | 86.00 | 2.0 | 1.05 | 0.27 |
| CBKS | 38.81 | -99.74 | 71.00 | 8.75 | 0.81 | 0.23 |
| PKSx | 39.26 | -99.54 | 78.20 | 9.6 | 0.98 | 0.35 |
| st05 | 39.6 | -97.01 | 39.25 | 15.5 | 0.96 | 0.49 |
| st04 | 39.58 | -97.65 | 42.00 | 6.0 | 0.50 | 0.10 |
| st06 | 39.58 | -96.41 | 44.00 | 10.0 | 0.40 | 0.08 |
| St07 | 39.61 | -95.83 | 41.00 | 5.0 | 0.70 | 0.12 |
| KSU1 | 39.1 | -96.61 | 53.00 | 11.85 | 0.84 | 0.32 |

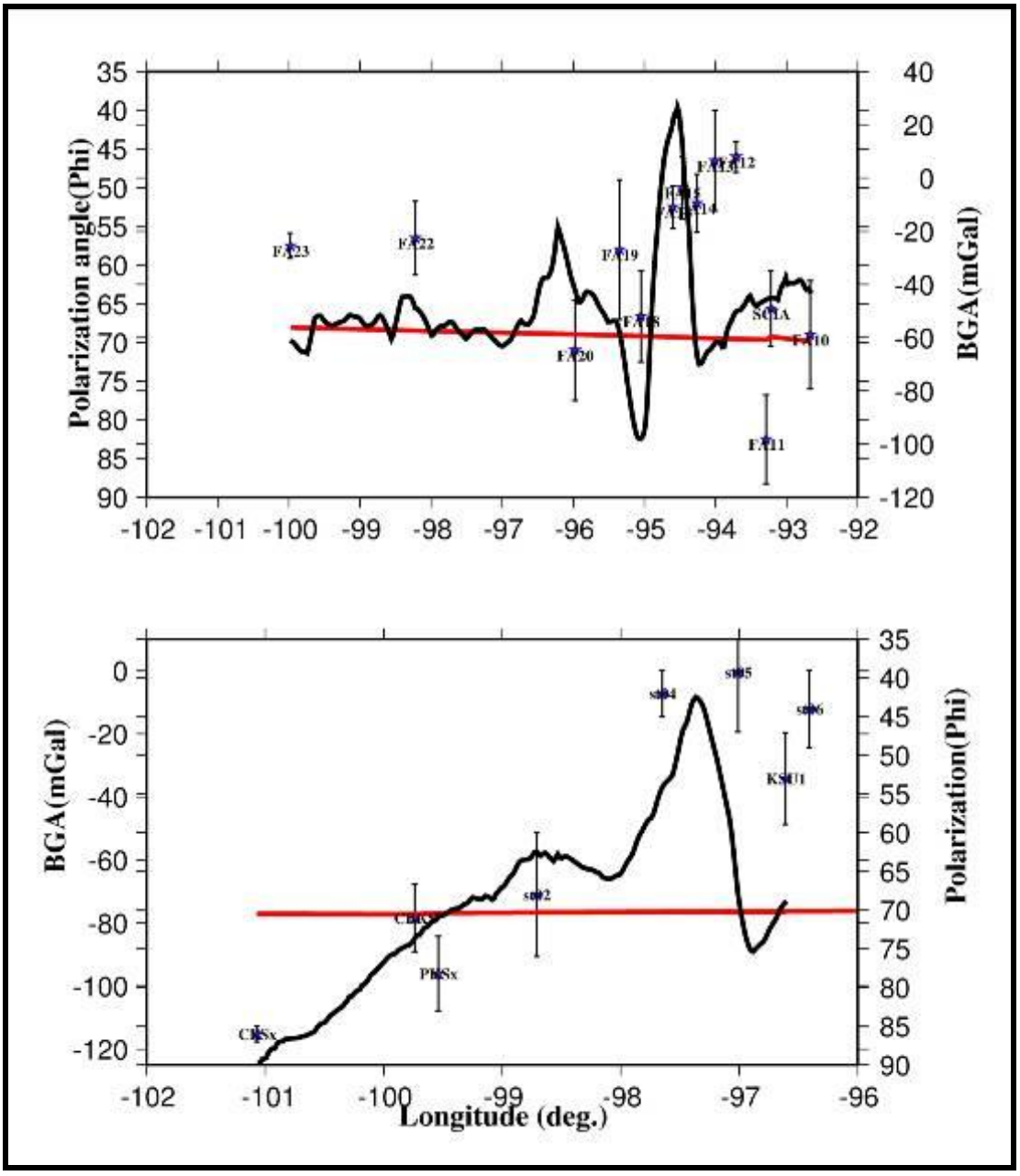


Figure 3.3: FLED (upper plot) and Kansas array (lower plot) showing the APM (red line) direction and the calculated polarization direction plotted against station longitude. Stations within the MCR rift show a deviation of about 25° from North American APM. Similar interpretation applies to station st05 from the Kansas profile.

## 3.8. DISCUSSION

The dominant NE-SW fast directions observed at stations off the MCR axis may reflect simple asthenospheric flow related to present-day absolute plate motion (APM) of the North America craton. The HS3-NUVEL1A model (Gripp and Gordon, 2002) predicts a slow plate velocity of 33mm/year with a rough NE–SW direction. On the other hand, this NE–SW dominant layer could be interpreted as 'frozen-in' anisotropy in the lithosphere, related to the most relevant orogenic process in the area. Splitting parameters obtained at stations located within the rift axis show fast directions that are different by $20^{o}$ from the APM.

**3.8.1 Origin of Seismic Anisotropy.** Continental regions show splitting patterns that appear closely related to surficial geologic features, suggesting a lithosphere origin. This type of anisotropy is related to fabric that was generated by the most recent significant tectonic event (e.g., Silver, 1996; Barruol et al., 1997) or that lithospheric and sublithospheric deformation is coherent. Other regions exhibit patterns of seismic anisotropy that are more closely related to the local direction of absolute plate motion (APM) in the hotspot reference frame (e.g., Vinnik et al., 1989, 1992), suggesting that seismic anisotropy exists primarily in the sublithospheric mantle and is generated by fabric resulting from mantle flow. Observations of seismic anisotropy have led to the conclusion that the observed anisotropy on continental settings is a combination of both

lithospheric and sublithospheric fabric (Savage and Silver 1993; Fouch et al., 2000). Patterns of anisotropy are a result of preferential alignment of minerals in the crust and/or mantle, or the preferential alignment of inclusions of fluid or melt, or some combination of these mechanisms. Anisotropy in the study area can be explained by pre-existing fossil anisotropy frozen in the lithosphere or APM related mantle flow. The absolute plate motion of North American plate is approximately 30 mm/yr in a direction N249$^{o}$E (HS3-NUVEL1A model of Gripp and Gordon (2002).

**3.8.2 Fossilized Anisotropy in the Lithosphere.** The fast directions for the North American plate within the MCR show fast directions that are parallel to the rift axis. The average value of Φ for stations within the rift is 50$^{o}$. This value deviates from APM direction by ≈20$^{o}$ but coincides with strike of the Keweenawan rift in the Iowa Horst. This characteristic is an indication that the mantle retains the history of Achaean deformational structures

**3.8.3 Simple Asthenospheric Flow and Anisotropy.** Lattice preferred orientations of the fast [100] 'a' axes of olivine probably develop in the asthenosphere because of dislocation-creep deformation associated with simple shear at the base of the plate (Savage 1999, Nicolas, 1989; Zhang and Karato, 1995). These orientations are roughly horizontal and in the direction of shear. Consequently, simple asthenospheric flow due to the passive shearing of the asthenosphere by the moving plate has been invoked to interpret Φ parallel to

absolute plate motion (APM) (Silver and Chan, 1991; Vinnik et al., 1992). These versions of the asthenospheric flow hypothesis assume there is no significant topography along the lithosphere/asthenosphere boundary. Our resulting fast directions show some degree of alignment with APM direction for stations that are NW of the MCR on 2.7 Ga Superior province and East of the MCR on the Eastern Granite Rhyolite province, and therefore simple asthenospheric flow hypothesis can be invoked to explain the observed splitting patterns. Fast directions on the Central plains show an E-W polarization direction. These data are consistent with the asthenospheric flow hypothesis if the plate is moving with respect to the underlying mantle, creating simple shear at the base of the rift. The relative motion between the lithosphere and the underlying mantle makes the asthenosphere to flow around and/or beneath continental root. Fouch et al. (2000) interpreted Φ as due to asthenospheric flow around the continental keel. In most regions of gentle topographical gradients, Φ is parallel to APM (Gripp and Gordon, 2002). In regions where the topographic gradients are large, Φ tends to be parallel to the topographic contours of the Moho topography, which are assumed to reflect the same variations in basal lithospheric topography.

## 3.9. CONCLUSION

Seismic anisotropy beneath the FLED and Kansas array at several permanent stations in the MCR and adjacent areas was investigated using shear wave splitting analysis of teleseismic SKS, PKS and SKS phases. The results show considerable variations in the splitting times (δt 0.4– 1.35 s) and differing polarization direction for the on-rift and off-rift stations. Off rift stations have

polarization directions nearly parallel to the AMP whereas stations within the rift demonstrate a deviation of Φ from the APM. Our splitting measurements within the MCR are explained by vertical fossil magmatic dikes along the rift axis. The expexted rift orthogonal anisotropic fabric that was caused by small scale mantle convection was erased by large scale mantle convention.

# 4. CRUSTAL THICKNESS, POISSON'S RATIO AND MOHO SHARPNESS BENEATH THE NEW MADRID SEISMIC ZONE FROM RECEIVER FUNCTION STUDIES

## 4.1 ABSTRACT

Receiver functions from numerous teleseismic earthquakes recorded at 26 broadband seismic stations within the NMSZ were analyzed to map crustal thickness, Poisson's ratio and Moho sharpness within and around the NMSZ. The time domain deconvolution method was used to compute the individual receiver functions and receiver function stacks. The receiver functions were then stacked using the slant stacking approach to estimate Moho depths and Vp/Vs for each station. The errors in the slant stacking were estimated using a bootstrap re-sampling technique. A bootstrap re-sampling approach was used to estimate errors in the grid search results. The average crustal thickness of the stations within the Mississippi embayment is 33.4±0.28 km. The crust thins to about 25.5±1.09 km at OXF and thickens to about 43.3±0.12 km at PLAL. In the Mazatazal Belt, the crustal thickness varies from 30.2±0.14 to 53.1±0.29 km. There is a dramatic change in crustal thickness between the cratonic stations and stations within the Mississippi embayment. Our results from the Mazatzal belt are comparable to other Proterozoic and Archean shields that include reasonably well determined Moho depths. The average crustal thickness for all shield stations is 39 km, while the average for stations on Proterozoic shields is 40 km, and that for Achean shields is 38 km. A dramatic change in crustal thickness from stations within the Mississippi embayment over a very short distance is observed.

## 4.2. INTRODUCTION

The crustal structure of Middle Proterozoic crust within the New Madrid Seismic Zone (NMSZ) (Figure 4.1) is investigated by using receiver functions to determine the extent of crustal modification by rifting processes. Our understanding of the deep continental crust has improved dramatically over the last decade as a result of detailed seismological studies and numerous studies of lower crustal rocks (Rudnick and Mountain, 1995). However, determination of crustal composition remains a difficult task This is due to (1) the large compositional differences between granulites that occur in terrains, in which felsic rocks dominate, and those that are carried as small fragments to the Earth's surface in rapidly ascending magmas (xenoliths, which are dominated by mafic rocks), (2) the very heterogeneous nature of the lower crust as observed in granulite terrains, and (3) the difficulty in determining rock type(s) from average seismic velocities derived from refraction studies.

The receiver function method has been used widely in order to understand crustal evolution based on $V_p/V_s$ ratio ($\Phi$) and crustal thickness (H) (Baikal Rift by Gao et al., 2004, Arabian plate by Al-Damegh et al. (2005), Afar rift by Dugda et al., 2005). Detailed determination of $\Phi$, H and Moho sharpness (R) have not been done in the NMSZ. Earlier geophysical investigations of in NMSZ have indicated a crustal thickness of about 32km, probably caused by crustal thinning (Van Schmus and Hinze, 1985). The crust in the NMSZ is inferred to have undergone extension mainly in the Cretaceous and to a less extent by a number of Cenozoic episodes (Van Schmus and Hinze, 1985, 1989).

South of the Mazatzal belt lies the Mississippi embayment which has a sedimentary thickness of ≈5 km, including at least 4–5 km of Cenozoic sediments (Van Schmus and Hinze, 1985). There is some evidence from seismic data of crustal thinning beneath the NMSZ (Bexfield et al., 2006), and high heat flows are observed in the NMSZ area (about 60mW/m$^2$).

The Mississippi embayment has been studied with reflection and refraction surveys (Braile et. al., 1989). Sediment thickness within the NMSZ from well-log data (Dorman and Smalley, 1994), interpretation of seismic reflection profiles (Mooney et al., 1983; Andrews et al., 1985) and travel-time differences between the direct and converted waves generated at the base of the sedimentary section (Hough, 1990; Chen et al., 1996) have resulted in thickness that varies from 405 m to 860 m within the Mississippi by linear interpolation. Street et al (1995) obtained the maximum sedimentary thickness of 640 m and 767 m from 11 of the strong motion stations along a north-south axis in the NMSZ using P and SH wave seismic reflection and refraction techniques. Receiver function analysis of data from CCM (Langston. 1994) indicates a crust of 40 km thick characterized by smooth-velocity gradients down to the Moho. Data from the MOMA array was used to investigate crustal thickness and isostasy in the northern Appalachians (Li et al., 2003). Some of the stations from the MOMA array will be incorporated in this study to provide further insights on Poisson's ratio and Moho sharpness in the Proterozoic craton, a region where very few refraction studies exist.

Previous geophysical studies have contributed significantly to our understanding on crustal structure; however, there are still geophysical

parameters that need to be addressed in order to fully understand the crustal evolution of the NMSZ. This study will provide new insights on the crustal thickness (H), Poisson's ratio and quantify the sharpness of Moho by stacking teleseismic P-to-S converted waves (PmS) and their multiples (PPmS and PSmS).

## 4.3. GEOLOGIC SETTING

The NMSZ within the Mississippi embayment is a failed Precambrian rift underlying the southern end of the Illinois basin extending from southern Illinois and western Kentucky southwestward to central Arkansas (Ervin and McGinnis, 1975; Braile et al., 1989). Reelfoot rift, a southwest-trending aulocogen of late Precambrian-early Paleozoic origin (Ervin and McGinnis, 1975; Braile et al., 1982) lays beneath the Mississippi embayment. Reactivation of the Reelfoot rift is believed to be responsible for the current seismicity. The 62 drill holes on the Illinois basin have penetrated crystalline rocks which are interpreted to be Precambrian in age (Buschbach and Kolata, 1991; Rudman and Rupp, 1993).

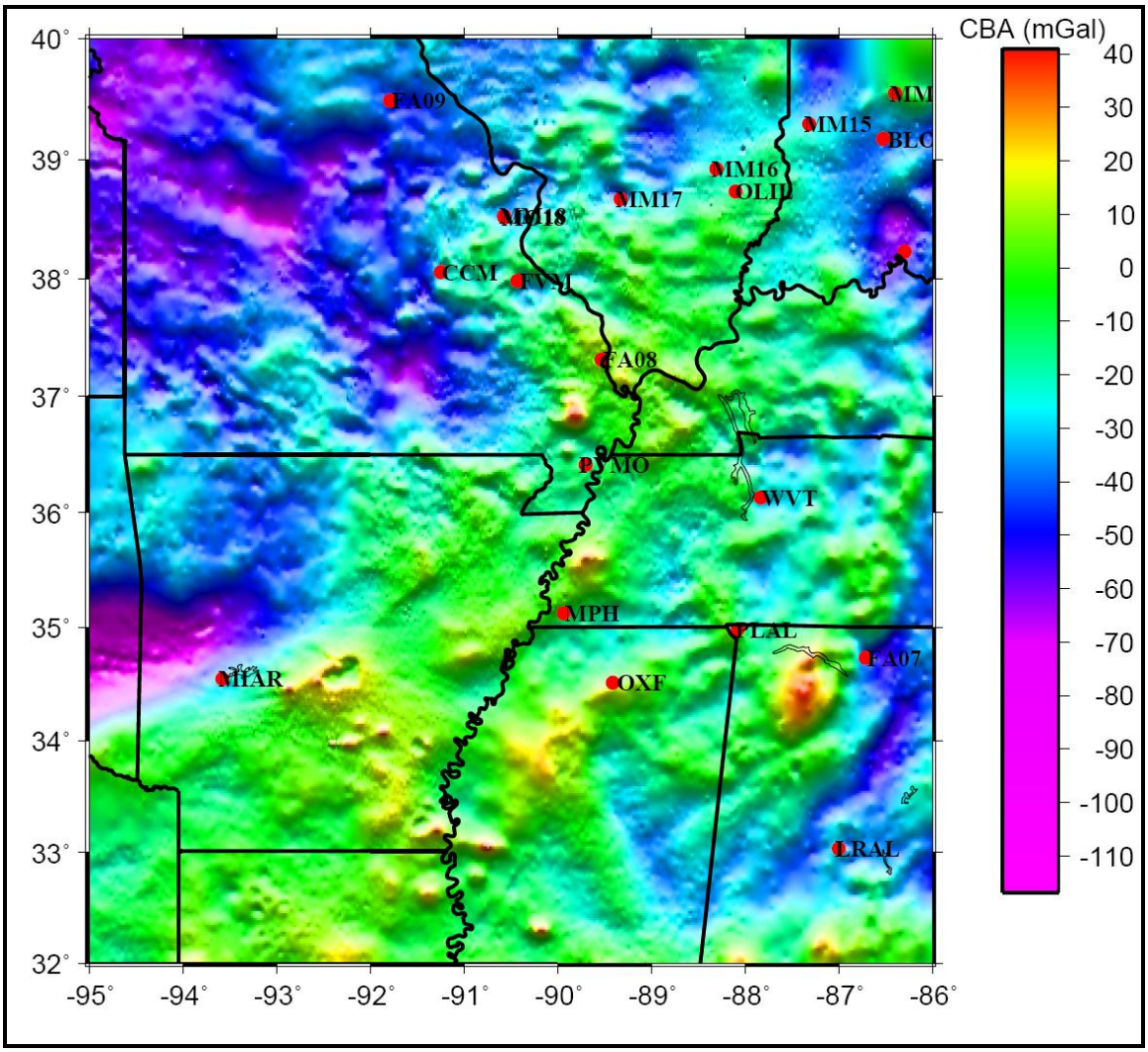


Figure 4.1: Complete Bouguer anomaly of the NMSZ showing seismic stations used for receiver function studies. The red dots represent the location of broadband stations (Gravity data was obtained from PACES: Pan-American Center for Earth and Environmental Studies).

Two distinct regions of deformation are known to overlap, trending from southwest to northeast in the NMSZ (Bexfield et al., 2006). Deep seated Paleozoic normal faults (Kolata and Nelson, 1991) propagate from the northeast. The faults were initiated during the Cambrian with the formation of the Reelfoot rift and have been mapped extensively where exposed in southeastern Illinois. The faults were contractionally reactivated during the late Paleozoic and were

again reactivated as normal faults in Mesozoic time (Kolata and Nelson, 1991). A final recurrence of faulting occurred in the late Tertiary and Pleistocene (Nelson et al., 1999). The second trend of deformation propagates from the southwest associated with contemporary seismicity in the northeast-striking NMSZ (Chiu et al., 1992).

The major terrains (Figure 4.1) in the study area includes the extensive Northern Rhyolite terrain (1.69–1.78 Ga), the Mazatazal belt (1.61-1.68 Ga) and the granite–rhyolite terrane (1.48–1.45 Ga). The tectonic blocks are interpreted to have been assembled during two main periods of convergent tectonism: 1.74 to 1.70 Ga (Yavapai orogeny) and 1.65 to 1.63 Ga (Mazatzal orogeny) (Van Schmus at al., 2007). The Yavapai-Mazatzal province is metamorphosed to greenschist or amphibolite facies. The tectonic units of the Yavapai province are made up of supracrustal rocks of the 1.79 to 1.70 Ga. Yavapai Supergroup contain mafic to intermediate volcanic rocks, volcaniclastic, and sedimentary rocks (Eisele and Isachsen, 2001). These are intruded by calc-alkaline batholiths of 1.75 to 1.69 Ga.

## 4.4. $V_p/V_s$ RATIO AND ITS IMPLICATIONS

Poisson's ratio depends on the temperature and pressure and provides tighter constraints on crustal composition than either the P or S wave velocity alone (Christensen, 1996). Laboratory measurements have shown that Poisson's ratio decreases by 0.2% at temperatures in the range of $0^o$ to $400^o$ for $CO_2SiO_4$ olivine and increases by 0.8% to 1.1% for other varieties of olivine. Quartzite show a significant decrease in $\Phi$ in the $200^o$ to $500^o$ temperature range associated with quartz $\alpha$-$\beta$ phase transition (Christensen, 1996). Progressive metamorphism

accompanied by systematic changes in plagioclase also contribute to the increase in Poisson's ratio. Granite rocks have low Φ of 1.71 because of high amounts of $SiO_4$. The transition between granite to gabbro is accompanied by decrease in $SiO_4$ and increase in plagioclase content. Mafic and ultramafic intrusions contain gabbro and peridotite or dunite which has originated from magmatic differentiation. A gradual change from gabbro to olivine rich gabbro and dunite lowers Poisson's ratio to approximately 0.26 (Christensen, 1996).

Several receiver function-based studies have been conducted using PmS-P and PPmS-P differential travel times (Clarke and Silver, 1991). Zandt and Ammon (1995) made measurements of Φ and observed that Precambrian shields have a mean Φ of (1.84 ± 0.06), Archaean-early Proterozoic platforms have an average Φ of (1.75), late Proterozoic have a Φ of 1.78, early Proterozoic have a Φ of 1.76, Mid-late Proterozoic have an average Φ of 1.81, and Palaeozoic have an average Φ of 1.73. Cenozoic and Mesozoic crust have the lowest Φ of (1.73 ± 0.09) (Musacchio et al., 1997), suggesting a possible relationship between Φ and age of the crust (increase in Φ suggesting an older crust). Such a relationship is not observed in Southern Africa (Nair et al., 2006).

Studies of the relation between P and S wave velocities using seismic refraction data by Musacchio et al. (1997) revealed that the crust in the Grenville and Appalachian provinces exhibits increasing Φ with depth from 1.64 to 1.84. The high Φ is an indication of a crust with an average mafic composition. Dugda et al. (2005) observed Φ values of 1.78 to 2.9 in the Afar region and the Main Ethiopian Rift. The high values of Φ were attributed to magma intrusion beneath the crust.

## 4.5. QUANTIFICATION OF MOHO SHARPNESS

Moho discontinuity is equated with the petrological crust/mantle boundary. From the geophysical point of view, the Moho is defined as the interface where the compressional wave velocity sharply increases from normal crustal velocities <7 km/s to typical mantle velocities >7.6 km/s. Mantle rocks are related to olivine dominated systems and the crust mantle boundary is considered as a transition zone where felsic or mafic rocks grade in to peridotite. Therefore the petrologic Moho is characterized by a compositional change whereas the geophysical Moho marks a prominent change of elastic and density properties (Scheuber et al., 1999). The sharpness of the Moho is related to the thickness of the crust/mantle boundary. A sharp Moho produces strong PmS and its multiples and a perturbed Moho produces weak PmS and its multiples. The apparent sharpness of the Moho beneath a station is quantified by taking the ratio (R) between the stacking amplitude corresponding to the optimal pair of (H,Φ) and the mean amplitude of the direct P wave on the radial components (Nair et al., 2006).

The amplitude of the converted phase can be affected by lateral variation in Moho depths (Nair et al., 2006). The observed crustal thickness (Figure 4.1) suggests that the Moho in the study area is fairly discontinuous or disturbed, and thus variation in Moho depth is likely to affect the amplitude of the converted phases. Velocity heterogeneities in the crust beneath the area surrounding a station can also affect the PmS amplitudes. The crustal volume traversed by the rays can results to incoherent stacking (Nair et al., 2006) and consequently

reduction in the stacked amplitude of the converted phases. The influence of the topography of velocity interfaces in the crust (Nair et al., 2006) could also affect the amplitude of the converted phases.

## 4.6. DATA

Teleseismic waveforms from 17 permanent and 8 portable stations recorded from 1989 to January 2008 were utilized in this study. Temporary network stations include 5 stations from Missouri to Massachusetts (MOMA) array (MM14 to MM18) and three stations from Florida to Edmonton (FLED) array (FA07 to FA09). Permanent stations used in this study consist of the following: BLO, CCM, FVM, MIAR, LRAL, MPH, OLIL, OXF, PLAL, PVMO, SIUC, UALR, USIN, UTMT, WCI and WVT. The data was obtained from the IRIS data management center. Events used in this study are shown in Figure 4.2. All analyzed phases have steeply dipping incidence angles and sample the upper mantle almost directly beneath the station, providing very good lateral resolution.

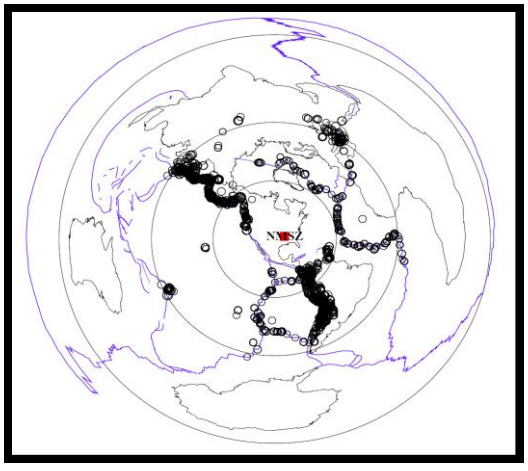

Figure 4.2: Locations of high quality events used for receiver function analysis.

## 4.7. METHOD

**4.7.1 Determination of Vp/Vs and H.** Converted PmS phases originating from the Moho has been widely used for studying the crustal structure for several decades (e.g., Langston, 1979; Owens et al., 1984). Receiver functions are calculated by deconvolving the vertical component from the radial and tangential components and are used to isolate and identify PmS converted phases (Al-Damegh et al 2005). A Gaussian low pass filter with a corner frequency of 0.5 Hz was applied to all receiver functions. For this study, the H- Φ stacking technique (H = Moho depth and $\Phi = V_p/V_s$ = velocity ratio of $V_p$ and $V_s$) of Zhu and Kanamori (2000) was employed. A series of candidate depths Hi in the range from 20 to 70 km in increments of 0.1 km and candidate Φj from 1.65 to 2.0 in increments of 0.0025 are used. For each (Hi, Φi) the moveout of PmS, PPmS and PSmS, were calculated using the method of Dueker and Sheehan, (1993) and Nair et al. (2006).

The method provides a robust estimate of crustal thickness and Poisson's ratio. Previous studies have shown that there is a strong tradeoff between depth (H) and velocity ratio ($V_p/V_s$). The ambiguity introduced by the trade off were reduced by incorporated the later arriving crustal reverberations PPmS and PSmS in a stacking procedure whereby the stacking itself transforms the time–domain receiver functions directly to objective function values in H–Φ parameter space (Ammon et al., 1990; Zhu and Kanamori, 2000). The time delay between the first arriving direct wave and the associated converted phases is a function of depth and velocity structure of the medium (Al-Damegh et al., 2005; Nair et al., 2006; Gao et al., 2004). Events used in this study come from distances of $30^0$–

100° and have magnitudes greater than 5.5. A time-domain iterative deconvolution method (Ligorria and Ammon, 1999) was used for computing the receiver functions and to evaluate their quality.

The uncertainty in mean crustal velocity was incorporated into error estimates for H and Φ by specifying a normal distribution of $V_p$ values so that 95% of the values selected fell between 5.9 and 6.5 km $s^{-1}$, with a mean value of 6.2 km $s^{-1}$, which is the mean crustal velocity in the NMSZ area. Once values for $V_p$ and the weights were selected, the bootstrap algorithm of Efron and Tibshirani (1991) was used together with the H–Φ stacking, to estimate H and Φ with statistical error bounds (Nair et al., 2006). The receiver functions at each of the stations are then stacked using the 'slant stack approach' shown below:

$$A(Hi,\phi j)=\sum_{k=1}^{n} w1S_k\left(t_1^{(i,j)}\right)+w2S_k(t_2^{(i,j)})+w3S_k\left(t_3^{(i,j)}\right) \qquad (1)$$

where w1, w2, w3 are weights, $S_k(t)$ are the receiver function amplitude values at the predicted arrival times t1, t2, and t3 of the Ps, PpPs, and PsPs + PpSs phases for the jth receiver function, and n is the number of receiver functions used (Zhu and Kanamori, 2000)

The H-Φ method requires weighting factors w1, w2, and w3 to be selected, and a value for Vp. More weight is given to the phase that is most easily picked. Given a range of plausible values for Vp (6.3 to 6.8 km/s), crustal thickness can vary by almost 4 km while the Vp/Vs ratio can change by 0.02. Thus, when estimating errors for the H-Φ method, the uncertainty in mean crustal velocity, as well as the sensitivity of our results to variations in weights (w1, w2, w3), must be considered (Dugda et al., 2005). The uncertainty in mean crustal velocity is

incorporated into error estimates for H and Φ by specifying a normal distribution of $V_p$ values so that 95% of the values selected fall between 6.2 and 6.8 km/s, with a mean value of 6.5 km/s. The procedure of selecting Vp and weights from the distribution described above and then performing the H- Φ stacking with bootstrapping was repeated 10 times. After each time, new average values of H and Φ and their uncertainties were computed. The error estimates in H range from 1.2 km to 5.4 km and the average is 2.9 km. The error estimates for Φ range from 0.03 to 0.2 and the average is 0.12.

**4.7.2 Estimating of Moho Sharpness.** Beneath the Kaapvaal craton in Southern Africa, Nguuri et al. (2001) found that the stacked amplitude of PmS in areas with thick crust is smaller than that in areas with thin crust. They proposed that the Moho beneath thick crust areas was disturbed by Proterozoic events and is thus less sharp. A sharp Moho produces strong PmS and its multiples. To quantify the apparent sharpness of the Moho beneath a station, the ratio amplitude R, which is the ratio between the stacking amplitude corresponding to the optimal pair of (H, Φ) and the mean amplitude of the direct P wave on the radial components is computed.

## 4.8. H- Φ STACKING RESULTS

Observations of H, R, and Φ were obtained at most of the 25 stations (Table 4.1, Figures 4.7a, 4.8 and 4.9). The receiver functions were categorized in four groups based on the quality of the H- Φ plots. Those in category 'A' display a clearly defined single peak in the H- Φ plots, and therefore both H and Φ are

determined with high confidence. Category B stations show clear PmS but not PPmS or PSmS. Thus an optimal pair of (H, Φ) cannot be determined. For these stations, an estimate of the crustal thickness (Hn) was obtained by using a global average Φ of 1.73. Category C involves stations in which none of the three Moho phases used in the study can be clearly observed, and therefore neither H nor Φ can be determined. Examples of H- Φ stacking results are shown in Figures 4.3, 4.4 and 4.5.

A larger departure of the real Φ beneath a station from 1.73 results in greater error in the estimated thickness (Hn). For these stations, the resulting maximum stacking amplitude (R) provides unrealistic Moho depth values. For the entire study area, the resulting Φ values range from 1.752 to 1.90, with a mean of 1.84, and the crustal thickness ranges from 25.1 km to 53.1 km, with a mean of 44.18 km. The R values have a mean of 0.122 with a range of 0.034-0.348. The study area is divided in three zones (Zone 1: stations within the Mississippi embayment, Zone 2: Stations on the Craton and Zone 3: stations of the orogenic belts)

**Table 4.1: Observations of Crustal thickness (H,Hn), Vp/Vs(Φ) and Moho sharpness (R)**

| **station** | long, deg, | lat, deg, | H, km | Φ | $H_n$, km | ΔH | ΔΦ | $\Delta H_n$ | R | ΔR | $N^{rfs}$ | Q |
|---|---|---|---|---|---|---|---|---|---|---|---|---|
| Zone 1 | | | | | | | | | | | | |
| MPHx | -89.932 | 35.123 | 31.3 | 1.974 | 43.8 | 0.1 | 0.005 | 0.16 | 0.319 | 0.007 | 170 | A |
| PVMO | -89.7 | 36.414 | 31.2 | 1.742 | 31.5 | 0.13 | 0.008 | 0.12 | 0.274 | 0.006 | 161 | A |
| WVTx | -87.83 | 36.13 | 36.9 | 1.995 | 52.5 | 0.14 | 0.001 | 1.43 | 0.086 | 0.003 | 312 | B |
| OXFx | -89.409 | 34.512 | 25.5 | 1.769 | 26.8 | 1.09 | 0.033 | 0.25 | 0.18 | 0.006 | 221 | A |
| PLAL | -88.075 | 34.982 | 46.3 | 1.982 | 37.3 | 0.12 | 0.006 | 4.36 | 0.038 | 0.003 | 223 | A |
| UTMT | -88.864 | 36.342 | 29 | 1.749 | 29.5 | 0.15 | 0.004 | 0.07 | 0.348 | 0.011 | 130 | A |

**Table 4.1: Observations of Crustal thickness (H,Hn), Vp/Vs(Φ) and Moho Sharpness (R) (cont.)**

| station | long, deg, | lat, deg, | H, km | Φ | $H_n$, km | ΔH | ΔΦ | $\Delta H_n$ | R | ΔR | $N^{rfs}$ | Q |
|---|---|---|---|---|---|---|---|---|---|---|---|---|
| Zone 2 | | | | | | | | | | | | |
| BLOx | -86.522 | 39.172 | 51.1 | 1.767 | 52.2 | 0.15 | 0.005 | 0.15 | 0.077 | 0.005 | 187 | A |
| CCMx | -91.245 | 38.056 | 47.4 | 1.788 | 49.2 | 0.14 | 0.003 | 0.17 | 0.078 | 0.002 | 690 | A |
| SLMx | -90.236 | 38.636 | 46.3 | 1.926 | 59.8 | 0.2 | 0.002 | 0.01 | 0.071 | 0.002 | 337 | B |
| FVMx | -90.426 | 37.984 | 46.8 | 1.945 | 53.2 | 0.35 | 0.007 | 8.49 | 0.034 | 0.002 | 210 | A |
| SIUC | -89.217 | 37.715 | 52.4 | 1.741 | 52.7 | 1.38 | 0.016 | 0.24 | 0.046 | 0.002 | 420 | A |
| USIN | -87.666 | 37.965 | 50.1 | 1.856 | 58.7 | 0.21 | 0.002 | 0.29 | 0.084 | 0.004 | 207 | A |
| OLIL | -88.099 | 38.734 | 51.2 | 1.752 | 52.3 | 0.42 | 0.006 | 0.24 | 0.141 | 0.006 | 112 | A |
| FA09 | -91.786 | 39.489 | 46 | 1.802 | 50.2 | 4.72 | 0.079 | 0.25 | 0.094 | 0.028 | 15 | B |
| MM14 | -86.395 | 39.549 | 50 | 1.74 | 50.2 | 1.24 | 0.056 | 0.24 | 0.154 | 0.012 | 29 | A |
| MM15 | -87.313 | 39.295 | 49.9 | 1.878 | 59.8 | 0.76 | 0.016 | 0.05 | 0.157 | 0.023 | 13 | A |
| MM16 | -88.305 | 38.922 | 49 | 1.81 | 51.7 | 0.31 | 0.013 | 1.41 | 0.096 | 0.011 | 44 | A |
| MM17 | -89.326 | 38.669 | 50.3 | 1.869 | 59.1 | 2.2 | 0.037 | 1.59 | 0.084 | 0.008 | 50 | A |
| MM18 | -90.569 | 38.529 | 49.8 | 1.877 | 58.6 | 1.8 | 0.025 | 1.61 | 0.054 | 0.007 | 43 | A |
| MO18 | -90.564 | 38.514 | 43.8 | 1.955 | 57.8 | 2.65 | 0.05 | 0.46 | 0.094 | 0.011 | 11 | A |
| WCIx | -86.294 | 38.229 | 53.1 | 1.744 | 53.8 | 0.29 | 0.006 | 0.16 | 0.083 | 0.005 | 127 | A |
| UALR | -92.344 | 34.775 | 30.2 | 1.935 | 38.6 | 0.14 | 0.008 | 0.24 | 0.138 | 0.007 | 173 | A |
| Zone 3 | | | | | | | | | | | | |
| FA07 | -86.71 | 34.731 | 51.8 | 1.789 | 53.6 | 0.52 | 0.015 | 0.33 | 0.088 | 0.01 | 40 | B |
| LRAL | -86.998 | 33.035 | 42.7 | 1.851 | 46.9 | 2.66 | 0.048 | 1.2 | 0.085 | 0.017 | 34 | A |
| MIAR | -93.576 | 34.545 | 42.6 | 1.915 | 53.9 | 0.44 | 0.012 | 0.43 | 0.148 | 0.005 | 183 | A |

$N^{rfs}$ is the number of receiver function used for calculating H and $V_p/V_s$
R is the ratio amplitude of the Direct P and its converted phase
Q is the category of quality of H- Φ plots

### 4.8.1 Stations within the Mississippi Embayment (Zone 1).

Stations within the Mississippi embayment are underlain by up to ≈5 km of sediments (see Figures 4.7a and 4.8). These sediment deposits are unconsolidated or poorly consolidated, with age ranging from late Cretaceous to present, and uncomformably overlay Paleozoic carbonate and clastic rocks (Andrews et al., 1985). The direct P-wave arrives at 1 s to

2 s with PmS phases arriving at 3 s to 6 s. The P phase for most of the stations within the Mississippi embayment manifest apparent offsets from zero time due to the effects of thick sedimentary layers. Such lags are apparent at MPH, UTMT, PVMO and OXF located over the anomalous feature. For most stations, PmS phases arrive at roughly 3-7 s and the Moho reverberations PPmS arrive from 16 to 28 s. There is a strong similarity between the PmS phases and Moho reverberations from adjacent stations, e.g. UTMT and PVMO. The crustal thickness beneath these stations ranges from 29±0.15 km (UTMT) to 46.3±0.12 km at PLAL (Figure 4.7a). The values of Φ range from 1.749 at UTMT to 1.995 at WVT. The R values range from 0.038 (PLAL) to 0.38 (UTMT). Both H and Φ are spatially consistent, as indicated by the small STD (Table 4.1). Examples of crustal thickness and Vp/Vs obtained from H-Φ plots for station UTMT (Figure 4.3).

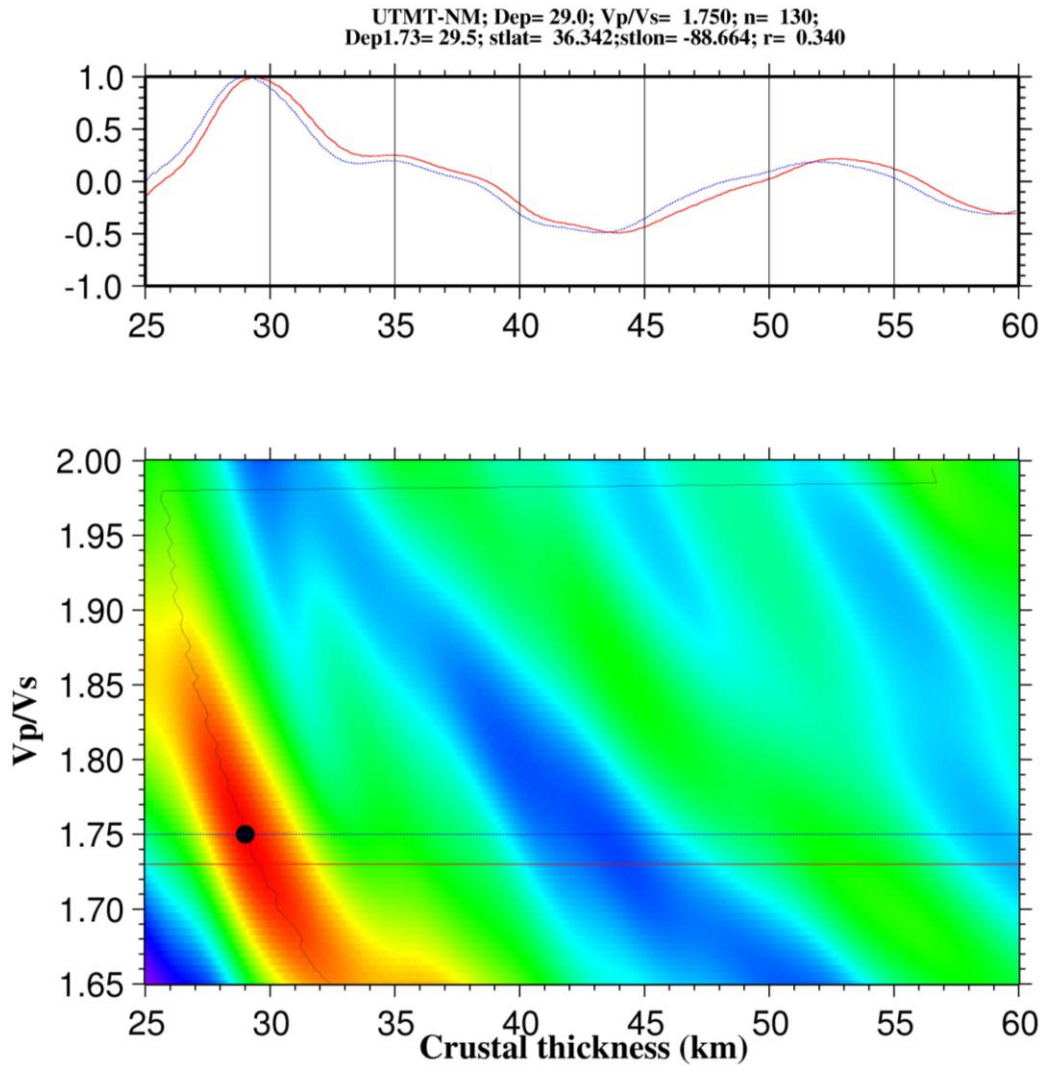


Figure 4.3: H-Φ plots for station UTMT. The red line shows the stacking amplitude for Φ=1.73. The blue line was obtained by using the optimal Φ. The resulting thickness, Φ, and the crustal thickness when Φ=1.73 (denoted as Depth1.73) are shown on the top panels.

**4.8.2 Stations on the Craton (Zone 2).** Receiver functions studies at stations on the Mazatzal Belt (1.61-1.68 Ga), were previously performed by Li et al. (2002). Stations within this group show well defined crustal thickness. P to S conversions at the Moho show strong amplitudes

due to the large velocity contrast across the Moho and are clearly visible even on individual receiver functions. Figure 4.6 shows the crustal receiver function stacks over a time window at -4 to 48 s for CCM, BLO, MIAR and UTMT. The strong phases at 0 s with large amplitudes are direct P wave arrivals. Certain P phases manifest apparent offsets from zero time due to the effects of thick sedimentary layers. Such lags are observed at MM16 to MM17 and BLO that are located in the Illinois basin.

The receiver function at UALR displays a significantly earlier PmS phase and Moho reverberations than those at other stations, suggesting a much shallower Moho. The phases at roughly 7 s on the stacks for MM17 seem too late for Moho conversions, and they may include interference between PmS and reverberations from discontinuities in the shallow crust which is shown by a strong PcS phase on stacked receiver function. The Moho reverberations at MM17 are similar to reverberations at adjacent stations. The crustal thickness beneath the Proterozoic NMSZ at WCI is among the thickest (53.1km), with values of Φ (1.744) and low values of R (0.083) measurements (Figures 4.8 and 4.9). Station CCM was previously studied by Langston (1994) and obtained a crustal thickness of about 40 km but this study shows a much thicker crust of about 47.4 km from inverting 690 good receiver functions (Table 4.1). Examples of crustal thickness and Vp/Vs obtained from H-Φ plots for station BLO (Figure 4.4).

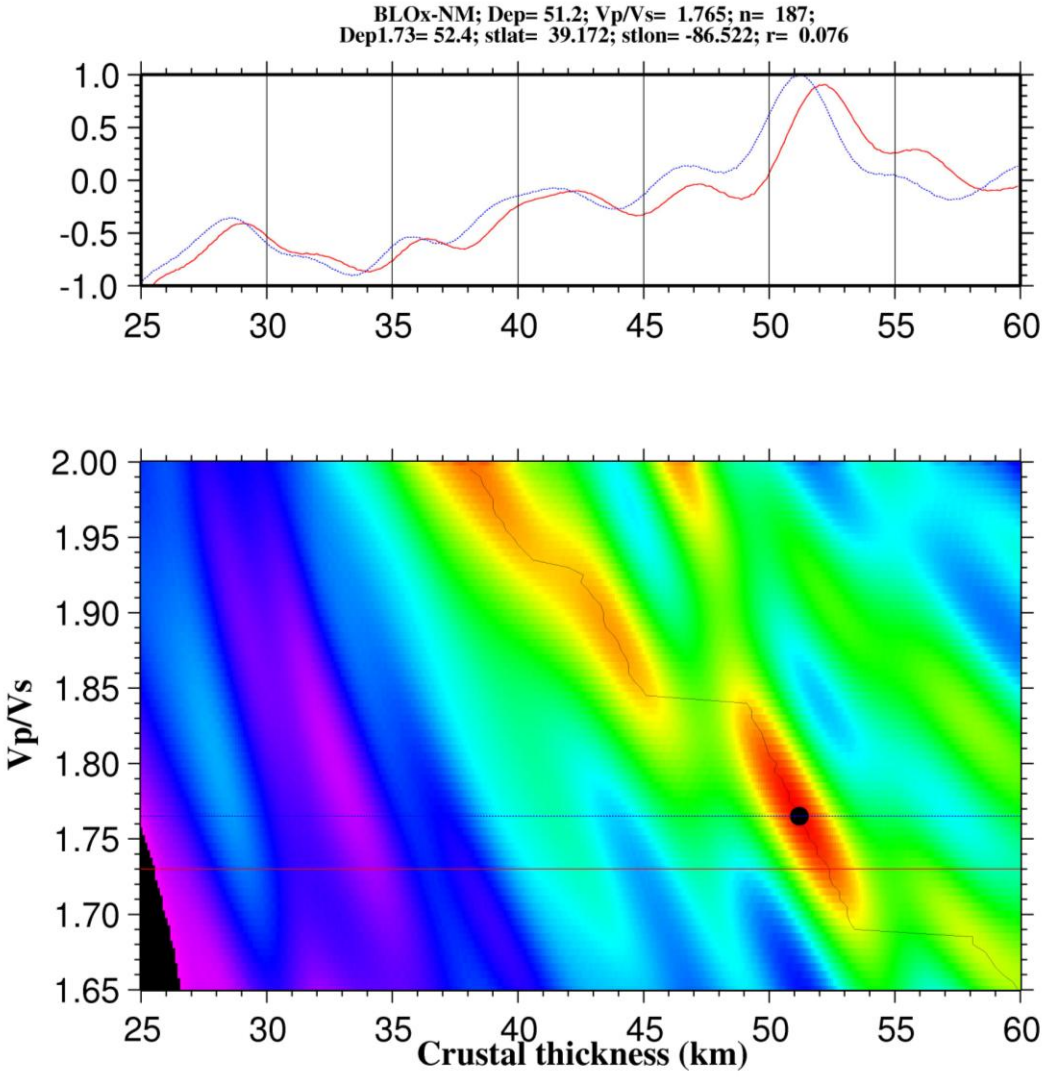


Figure 4.4: H-Φ plots for station BLO. The red line shows the stacking amplitude for Φ=1.73. The blue line was obtained by using the optimal Φ. The resulting thickness, Φ, and the crustal thickness when Φ=1.73 (denoted as Depth1.73) are shown on the top panels.

**4.8.3 Orogenic Belts Stations (Zone 3).** Stations in this category are characterized by clear PmS arrival with the direct P-wave at an offset of <1 s. These stations show a well pronounced PcS phase due sub-crustal interferences. The Moho reverberations arrive between 16 and 28 s. These stations are characterized by a thick crust (42-52 km) and Φ values between 1.789 and 1.915.

The R values (Figure 4.9) observed at these stations are lower than those observed at stations within the Mississippi embayment. The averaged H (Figure 4.7a), Vp/Vs (Figure 4.8) and R values (Figure 4.9) are shown in Table 4.1. The large contrast in crustal thickness (H) and Moho sharpness (R) between the MIAR and LRAL stations suggests that the crust has different characteristics. Examples of crustal thickness and Vp/Vs obtained from H-Φ plots for stationFA07 (Figure 4.5).

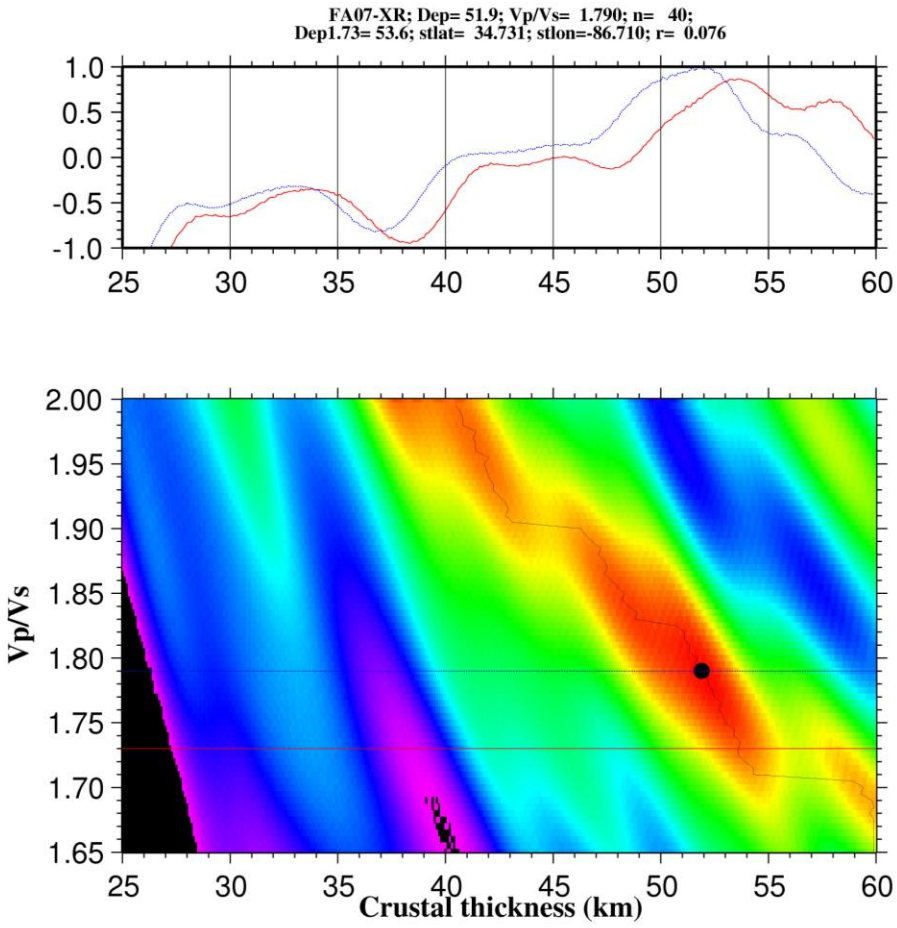


Figure 4.5: H-Φ plots for FA07. The red line shows the stacking amplitude for Φ=1.73. The blue line was obtained by using the optimal Φ. The resulting thickness, Φ, and the crustal thickness when Φ=1.73 (denoted as Depth1.73) are shown on the top panels.

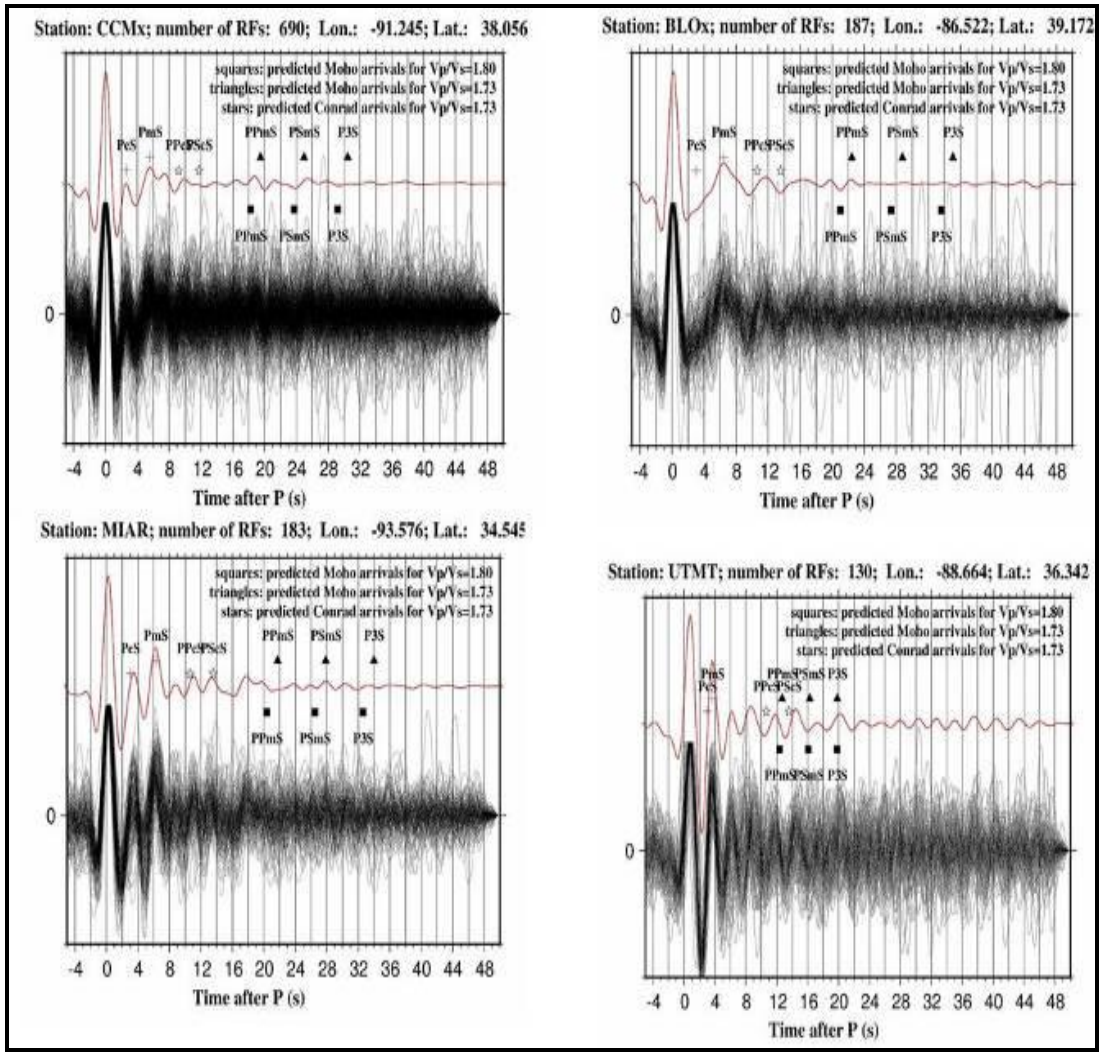


**Figure 4.6:** Stacked receiver functions in time domain for station CCM, BLO, MIAR and UTMT. The PmS phase is well pronounced for all the stations with MIAR showing a strong PcS phase suggesting a subcrustal interface before the Moho. The single trace at the top of the individual receiver functions is the result of simple time domain summation of individual traces. Triangles are theoretical arrival times for PPmS and PSmS calculated using equations (2) and (3) by taking p=5.0s/deg, $V_p$=6.5 km/s and Φ=1.73.The time difference between the PmS and the direct arrival is approximately 5sec (~40km of crustal thickness).

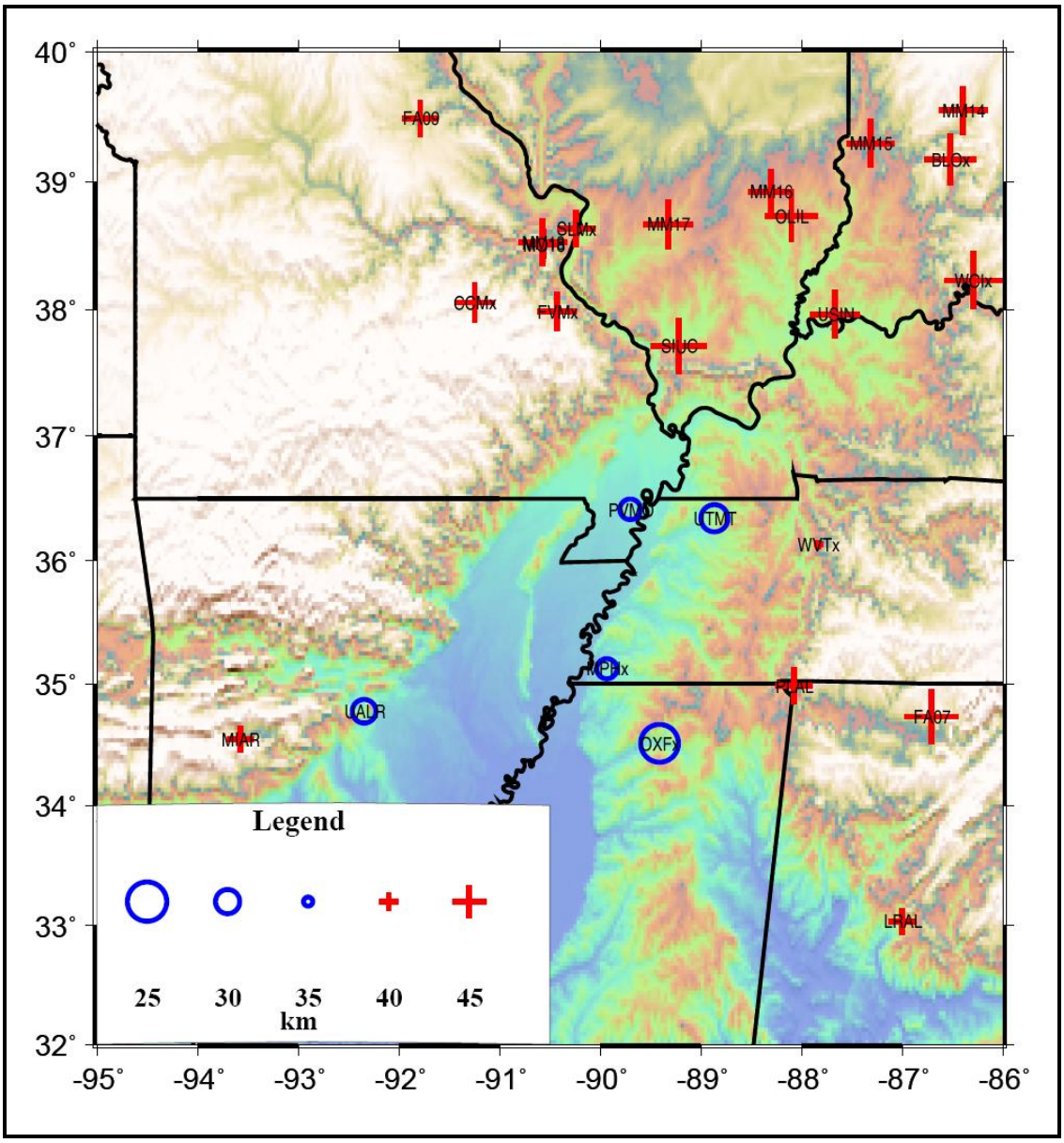


Figure 4.7a: Resulting crustal thickness (H). Open circles represent stations with a smaller thickness and pluses represents stations with a larger thickness.

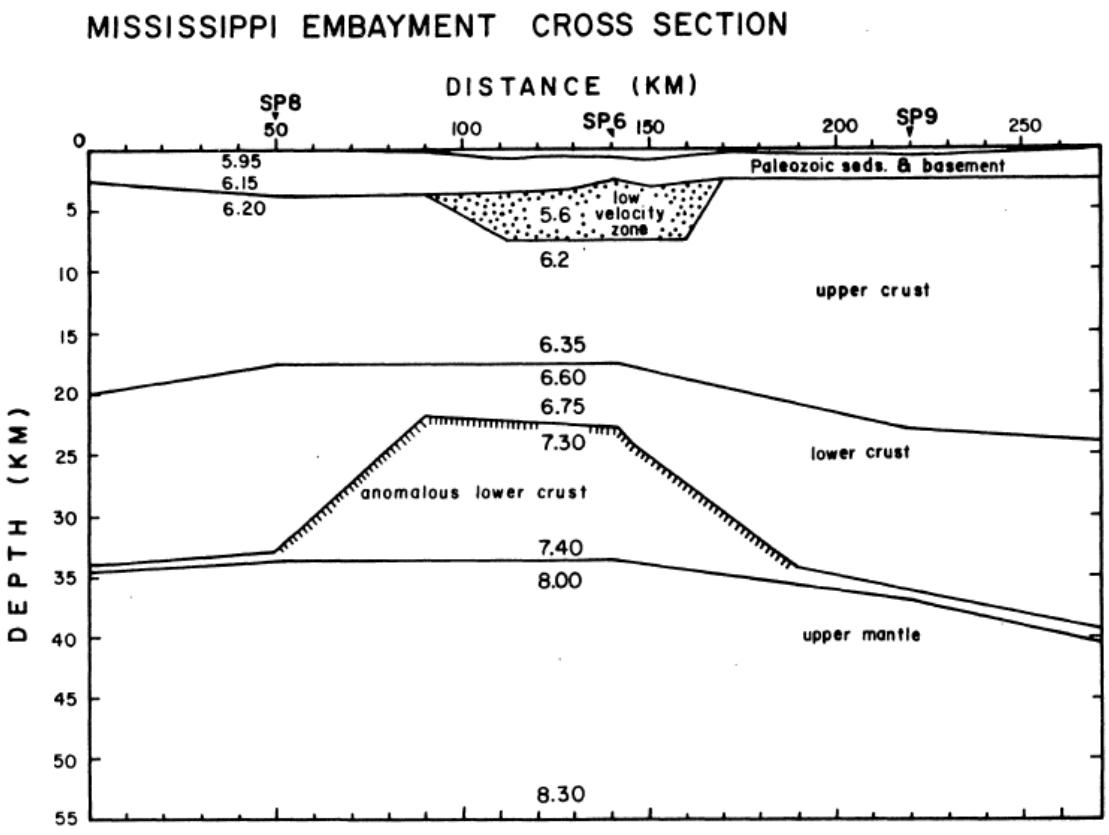


Figure 4.7b: Preliminary crustal cross-section across Mississippi Embayment based on an interpretation of the USGS seismic refraction profile S.P. 8-6-9 (Peters et al., 1981).

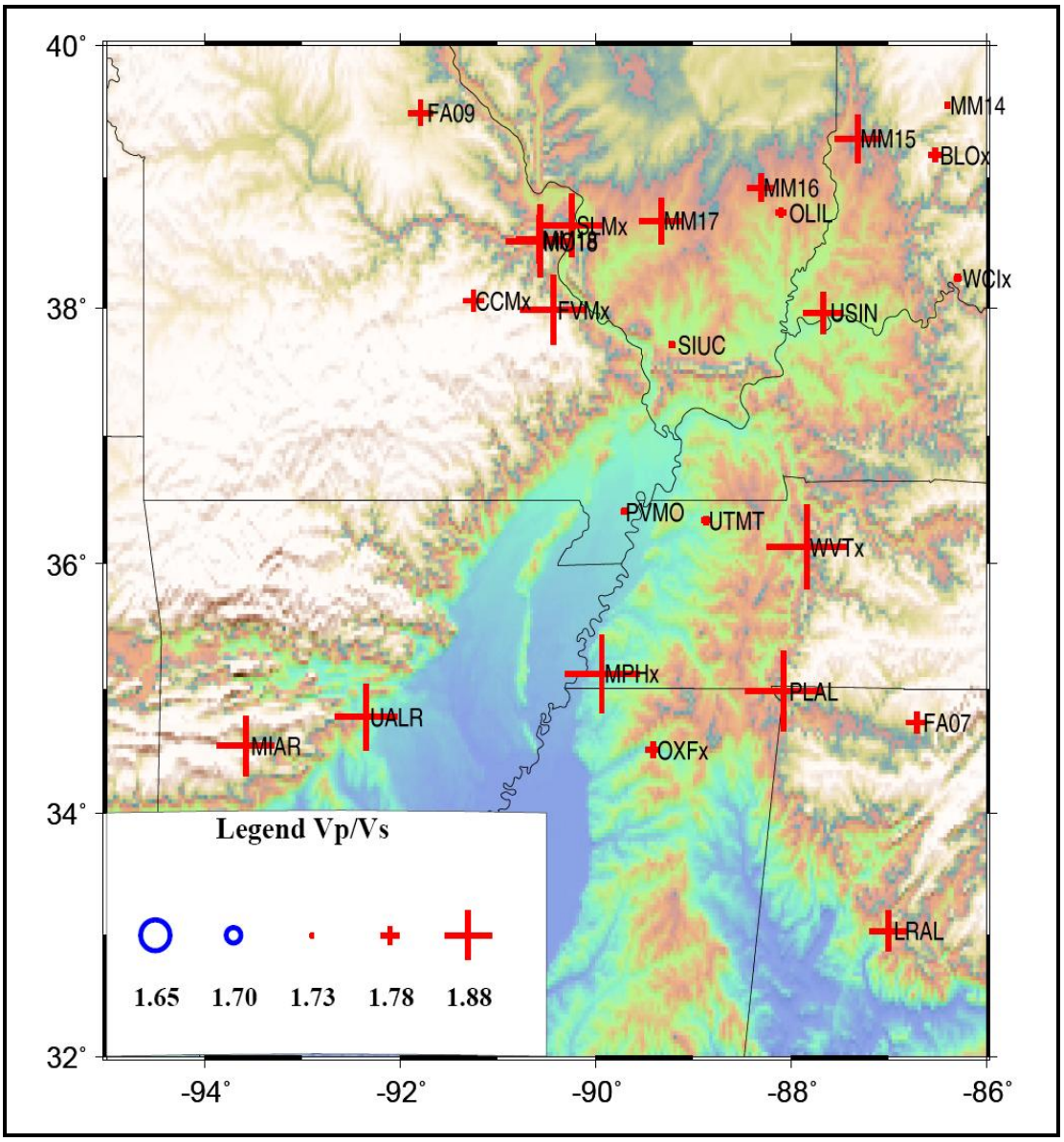


Figure 4.8: Resulting crustal Vp/Vs (Φ) for all stations in the study area.

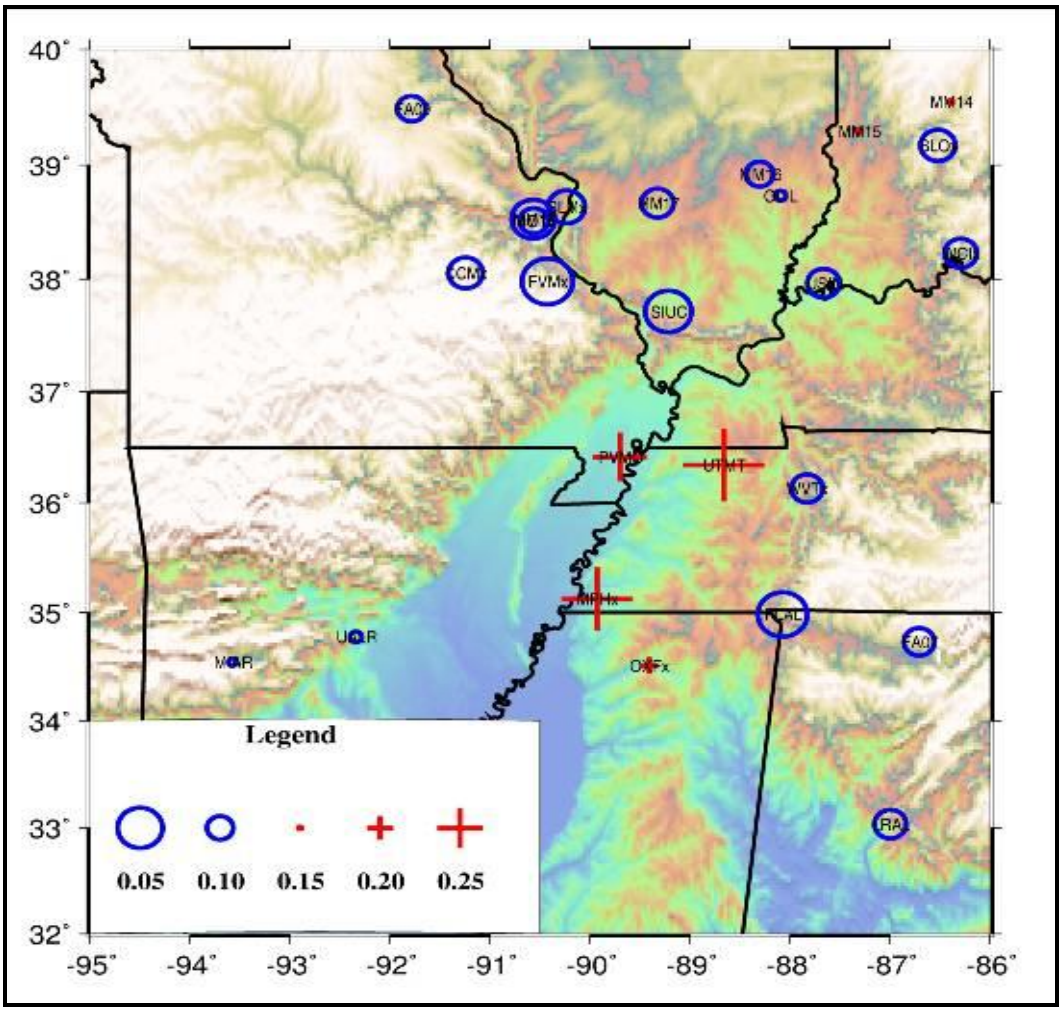


Figure 4.9: Resulting ratio (R) of the stacking amplitude corresponding to the optimal pair of (H,Φ) over that of direct P-wave on the radial component. R is calculated for all the stations**.**

## 4.9. DISCUSSION

**4.9.1 Spatial Distribution of Φ.** The results presented in this study are perhaps the most precise quantitative seismic measurements of crustal properties ever obtained for NMSZ area. The Vp/Vs distribution is remarkably coherent throughout the Mazatzal belt and orogenic belts with lower values observed at BLO and OLIL. Stations within the Mississippi embayment have variable Vp/Vs with lower values at PVMO and UTMT. Seismic stations on the Ouachita Orogen (station MIAR) – Appalachian (stations FA07 and LRAL) show values of Φ that

are similar to the cratons. The observed Φ values have no obvious relationship with either crustal thickness or the age of the surface rocks. The regions of thicker crust (Mazatzal belt and orogenic belt stations) show a wide range of Φ values. The thinnest crust in the Mississippi embayment (at UTMT and PVMO) possesses the smallest Φ. There is no obvious age relationship to Φ, as there is no significant difference in Φ between on-craton and off-craton regions.

The most prominent characteristic of the data set is that the highest values for Φ are found on cratonic stations. Zandt and Ammon (1995) suggest increasing Φ with age. Our results are clearly consistent with this observation. Zandt and Ammon (1995) obtained an average value of 1.81 ± 0.04 for shields and platforms, while Chevrot and van der Hilst (2000) obtained an average value of 1.76 ±0.01. The mean Φ value (1.84) obtained in this study suggest that mafic layer successfully accounts for both the thickness and $V_p/V_s$ ratio variations between NMSZ region and the rest of the study area.

**4.9.2 Composition of the NMSZ and Vp/Vs ratio.** Petrological studies suggest that the upper continental crust is felsic (Christensen and Mooney, 1995). The mineralogy is the most important factor influencing Vp/Vs or Poisson's ratio with the abundance of quartz and plagioclase feldspars having a dominant effect on common rocks. Granitic rocks have a Poisson's ratio of 0.24 while intermediate composition rocks (e.g. diorite) have values around 0.27 and mafic rocks (e.g. gabbro) about 0.30 (Christensen, 1996). Based on the classification of Ferris et al. (2006), rocks with a Φ of 1.76 or smaller are considered felsic, between 1.76 and 1.81 as intermediate, and larger than 1.81 as

mafic. This classification was used with our estimate of Φ to constrain the crustal composition of NMSZ. Proterozoic crust has been found to have $V_p/V_s$ ratio of 1.78±0.06 (Nair et al., 2006). The observed high values of Φ (1.82) of the Mazatzal belt are a result of crustal modification by tectonic activity. The variability in Moho depth beneath the stations reflects differences in the amount of crustal modification. The high Vp/Vs ratio within the Mazatzal belt indicates the presence of mafic crust. Our average value of 1.84 is thus significantly higher and corresponds to a low $SiO_2$ content.

**4.9.3 Moho Sharpness beneath the NMSZ.** The sharpness and the topographic relief on the Moho are quantitatively constrained to a high level of accuracy. These findings provide critical constraints on the mechanisms of crustal formation and evolution in NMSZ and the surrounding area. Additional insights that emerge from this study as to the structure and morphology of the Moho beneath the seismic stations is that within stations on the craton, the Moho is perturbed and well preserved for stations within the Mississippi embayment. There is a dramatic change in Moho quality between station within the Mississippi embayment and station off the rift.

The observed sharpness and flatness of the Moho have fundamental implications for crustal formation and evolution in the Archean crust. Although details of crustal aggregation are still unclear, models typically involve extensive collisional accretion of island arcs and micro-continental blocks to form nuclear continental masses. Such accretionary processes may be expected to produce a complicated mosaic of varying Moho structures and diverse crustal lithologies.

On the other hand, relatively flat Moho structures have been found to be preserved over areas of significant extent in some Phanerozoic accretionary terranes in western Canada (Cook, 1995), so it remains possible that the Moho structures observed today are simply those preserved from the time of crustal formation. An alternative and more plausible explanation of our observations is that the North American crust was assembled by accretionary tectonics, but that the flat and perturbed Moho was achieved in a later stage of crustal evolution. This explanation implicitly requires that a large volume of the crust has been re-worked on a regional scale since its formation.

## 4.10. CONCLUSION

The Mazatzal belt within the North American craton is characterized by high values of Φ, suggesting a mafic bulk crustal composition. The largest Φ values are associated spatially with the North American craton, and are most likely due to the intrusion of gabbro into the crust. The addition of basaltic material successfully explains the thicker crust, in terms of higher Φ, as well as the diffuse character of the Moho in this area. We suggest that mafic addition is a dominant process in the modification of crustal composition. Collisional zones have values of Φ that are not significantly different from surrounding regions.

# 5. CRUSTAL THICKNESS, POISSON'S RATIO, AND MOHO SHARPNESS BENEATH THE MIDCONTINENT RIFT

## 5.1 ABSTRACT

The Mesoproterozoic Midcontinent rift (MCR) in the central US is an approximately 2000 km long, 100 km wide structure from Kansas to Michigan. During the 20-40 million years of rifting, a thick (up to 20 km) layer of basaltic lava was deposited in the rift valleys. Quantifying the effects of the rifting and associated volcanic eruptions on the structure and composition of the crust and mantle beneath the MCR is important for the understanding of the evolution of continental lithosphere. In this study, measurements of crustal thickness (H), crustal mean $V_p/V_s$ (which is directly related to Poisson's ratio), and the sharpness of the Moho (R) are determined at about 20 portable and permanent stations in Iowa, Kansas, and South Dakota by stacking P-to-S converted waves (PmS) and their multiples (PPmS and PSmS). Under the assumption that the crustal mean velocity in the study area is the same as the IASP91 earth model, a significantly thickened crust beneath the MCR, from about 42 km to about 46 km is observed. The crustal $V_p/V_s$ increases from about 1.80 off rift to as large as 1.95 within the rift, which corresponds to an increase of Poisson's ratio from 0.28 to 0.32, suggesting a more mafic crust beneath the MCR. The R measurements are spatially variable and are relatively small in the vicinity of the MCR indicating the disturbance of the original sharp Moho by the rifting and magmatic intrusion and volcanic eruption.

## 5.2. INTRODUCTION

Receiver function methods have been used in different parts of the world ( Baikal Rift by Gao et al., 2004, Arabian plate by Al-Damegh et al., 2005, Afar rift by Dugda et al., 2005) to understand crustal evolution based on Poisson's ratio, $V_p/V_s$ ratio and crustal thickness. Receiver function studies have not been done in the MCR but earlier geophysical investigations of the MCR have indicated a crustal thickening beneath the rift,, assumed to be caused by the presence of magmatic under-plating (Cannon et al., 2001), above a modified lower crust (Van Schmus and Hinze, 1989), or a basaltic dome in the lower crust causing flexure of the upper crustal layers (Nyquist and Wang, 1988).

Previous seismic studies by the Consortium for Continental Reflection Profiling (CORCORP) across the MCR in the 1970s showed fault bounded basins characterized by volcanic rocks overlain by thick clastic sedimentary rock units (Behrendt et al., 1988). Another seismic reflection survey conducted in 1986 by Great Lakes International Multi-disciplinary Program on Crustal Evolution (GLIMPCE) in the Great Lakes provided images of the rift to sub-Moho depths. Moho reflections have been found to occur at 36-42 km at Lake Huron and Lake Michigan. A zone of reflections beneath the MCR was interpreted as evidence of magmatic underplating associated with the rifting 1100 Ma based on the character of the seismic reflections and suggests a dipping Moho, shallower at the north and deepens towards the center of the basin. The base of these reflections is interpreted as corresponding to Moho with velocities of ~8.1 km/s reported at 55-56 km depth (Steinhart and Smith, 1966; Halls, 1982).

High gravity anomalies are observed along the rift axes with positive anomalies occurring over the volcanic rocks and negative anomalies over sedimentary basins. The central gravity high within the MCR is interpreted as a horst consisting of mafic volcanic rocks. Interpretation of gravity data suggests that the average crustal thickness in the central Midcontinent is about 40 km (Carmichael and Black, 1986). Previous researchers suggested magmatic under-plating based on the observations of seismic reflection velocities but did not quantitatively address the Poisson's ratio or quality of Moho beneath the rift.

This study will provide new insights into the crustal structure by determining the crustal thickness and Poisson's ratio and quantify the sharpness of Moho by stacking teleseismic P-to-S converted waves and their multiples. Gravity modeling is also used to provide additional constraints on the crustal thickness.

## 5.3 GEOLOGIC SETTING

The 1.1 Ga Midcontinent Rift system of North America extends for more than 2000 km northeasterly from Kansas through the Lake Superior region and then southeasterly through lower Michigan (Figure 5.1). The rift is traceable by pronounced magnetic and gravity anomalies (Hinze et al., 1982; Van Schmus and Hinze, 1985). The rift has been postulated to be the result of a mantle plume, based on the enormous volume of dominantly tholeiitic composition igneous rocks and the short sub-aerial eruption interval (Paces and Bell, 1989; Hutchinson et al., 1990; Nicholson and Shirey, 1990).

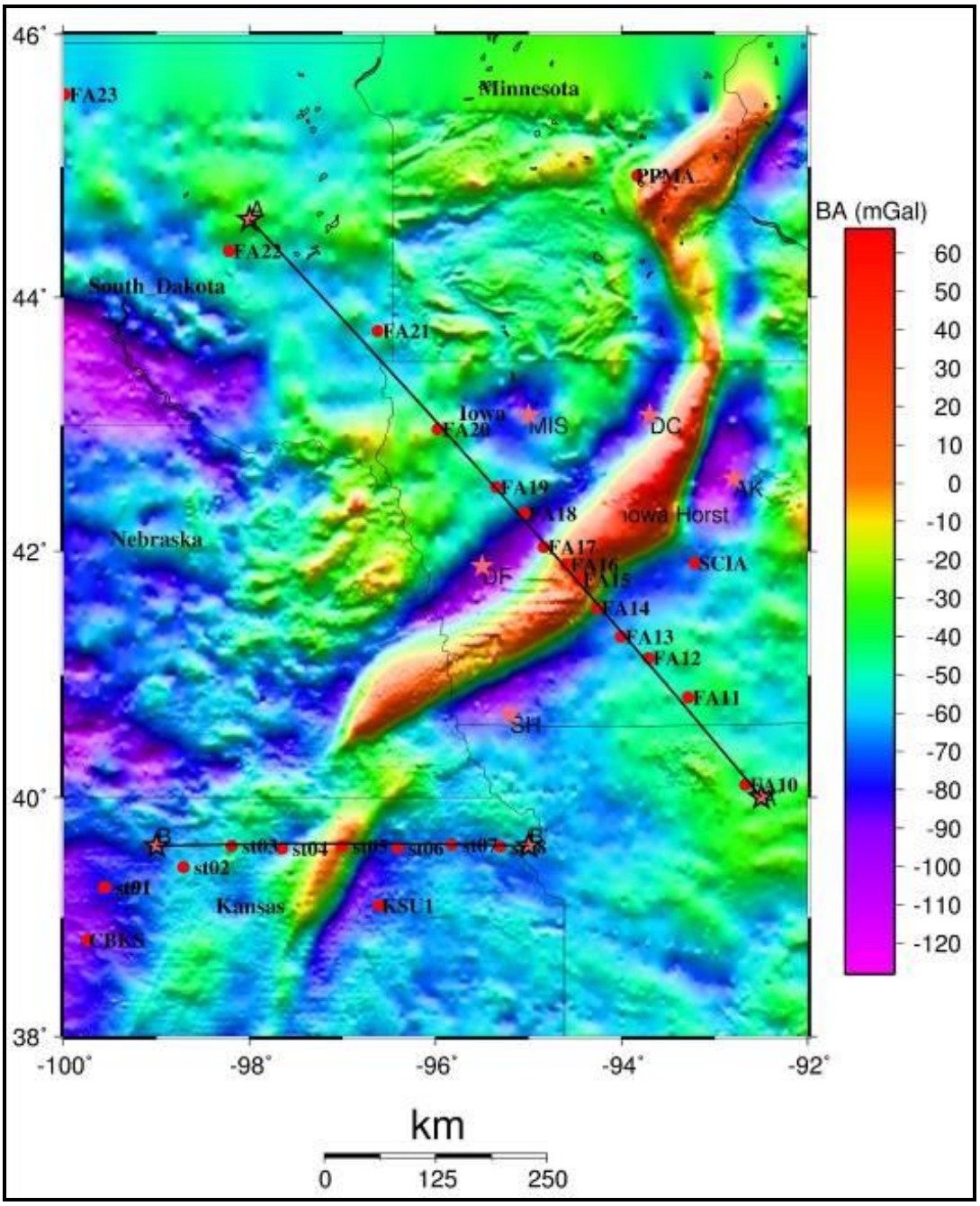


**Figure 5.1:** Bouguer anomaly of the MCR showing FLED and Kansas profiles used for receiver function studies. The red dots represent the location of temporary broadband stations. Gravity data was obtained from PACES: Pan-American Center for Earth and Environmental Studies. Structural components of the Midcontinent Rift and related features: DF: Defiance Basin, DC: Duncan Basin, MIS: Manson Impact Structure, SH: Shenandoah Basin, AK: Ankeny Basin.

The gravity anomaly cuts across Precambrian basement terranes of different age, structure, and composition in the North America craton that existed prior to 1.2 Gyr ago (Van Schmus and Hinze, 1985). Lake Superior basin occurs in the Archean Superior Province of the Canadian Shield and constituted the northern part of the Mid-continent rift. Rocks in the Superior Province have remained stable since 2.62 Gyr ago. The southern gneiss-migmatite terrane formed 2.6-3.6 Gyr ago was subjected to extensive deformation during Early Proterozoic (Van Schmus, 1989). The rift system has a changing regional trend associated with the differences in the two Achean terranes (Klasner et al., 1982).

The southeastern and southwestern segments are found south of the Lake Superior and occur for the most part in early Proterozoic crust, although the northern part of the MCR segment occurs in the Archean gneiss-migmatite terrane (Van Schmus and Hinze, 1985). The Proterozoic crustal basement rocks on south-western branch of the MCR formed 1300-1900 Myr ago and consist of 1600-1900-Myr-old new crust which probably formed as orogenic continental margin assemblages (Van Schmus and Bickford, 1981) and 1300-1500-Myr-old anorogenic plutonic and volcanic rocks that formed by re-melting of the older Proterozoic crust (Thomas et al., 1984; Nelson and DePaolo, 1985; Anderson, 1983). Orientations of various segments of the rift system are believed to be controlled by structures within the Early Proterozoic basement (Klasner et al., 1982). However, knowledge of structures in the basement is very limited, and other factors could be dominant. Lithologic units in the Midcontinent rift system are exposed only in the Lake Superior region and comprise the Keweenawan rocks (Morey and Green, 1982). Subsurface samples indicate extensive igneous

activity and sedimentation along the Midcontinent rift system at about 1100 Myr ago. The proximity in time and space of the Grenville Province and the Midcontinent rift system has led to suggestions that the two are genetically related (Van Schmus, 1989).

## 5.4. DATA

Data used in this study was requested from IRIS Data Management Center and consists of teleseismic recordings from 25 broadband stations in the MCR and adjacent areas (Figure 5.1). The two profiles used in this study traverse different terrains of different ages. The FA10-FA14 stations are located in the Mazatzal belt (1.61 to 1.68 Ga) and stations FA15 to FA17 are within the 1.1Ga Keweenawan province. Stations FA18 to FA23 are situated in the 1.69 to 1.78Ga Northern Rhyolite terrain (Carmichael and Black, 1986). The data used in this study spans from 2001 to 2006 was acquired from events with epicentral distances between $30^{o}$ and $100^{o}$.

The seismograms were band pass filtered between frequency range of 0.05 Hz and 1.5 Hz and were converted in to radial receiver functions using the technique developed by Ammon et al. (1990). Visual inspection was carried out and those that show a clear P wave arrival was used in receiver function analysis (see Table 5.1). A total of 743 radial functions from 25 stations were chosen. Receiver functions were then grouped into one degree bins according to their depth corrected epicentral distances and those in the same bins are then stacked in time domain. The positive PmS and PPmS and the negative PSmS phases can

be observed clearly. A reliable determination of Φ depends on clear PPmS and PSmS arrivals, which are found at some stations.

The gravity data used in this study was obtained from PACES: Pan-American Center for Earth and Environmental Studies (http://paces.geo.utep.edu/grav_database/grav_db_getstart.shtml). The gravity data was used to produce the Bouguer anomaly map shown on Figure 5.1, after applying a series of corrections including drift corrections, free air correction, latitude correction, terrain correction and Tidal corrections (Telford et al. 1980). Gravity data provides insights on variation of subsurface density of material and hence it will be a useful tool in revealing the MCR which is buried by sediments in the study area. Gravity 2.5D models were made by using a GM-SYS package. GM-SYS is a 2.75 – dimensional gravity and magnetic modelling package used to generate anomalies caused by density or magnetic contrasts. GM-SYS is an interactive gravity and magnetic profile modeling program that enables users to create a geologic model of the subsurface and compare the model's gravity and magnetic response to observed gravity and magnetic measurements. The densities of geologic features were assigned as shown in figure 5.3a.

## 5.5. RESULTS

### 5.5.1. Crustal Models from the H-Φ Stacking Method.

Observations of Φ were obtained at most of the 25 stations (Table 5.1 and Figure 5.2). The receiver functions were categorized in to three groups based on the quality of the H-Φ plots. Those in category 'A' display a clearly defined single

peak in the H-Φ plots, and therefore both H and Φ can be determined with high confidence. Category 'B' stations show clear PmS but not PPmS or PSmS. Thus an optimal pair of (H, Φ) cannot be determined. For these stations, an estimate of the crustal thickness (Hn) was obtained by using a global average Φ of 1.73. Category 'C' involves stations in which none of the three Moho phases used in the study can be clearly observed, and therefore neither H nor Φ can be determined. This category was not included in the calculation of either H or Φ. Most of receiver functions show a well defined peak on the H-Φ plot and therefore both H and Φ can be determined with high confidence (Figure 5.2). Obviously, a larger departure of the real Φ beneath a station from 1.73 results in greater error in the estimated thickness ($H_n$).

Most of the stations show well pronounced PmS phases whereas station FA12 does not show three Moho phases and therefore neither H nor Φ can be determined. For these stations, the resulting maximum stacking amplitude (R) provides unrealistic Moho amplitudes values. For the entire study area, the resulting Φ values (Figure 5.3) range from 1.775 to 1.90, with a mean of 1.84, and the crustal thickness ranges from 40 to 53 km, with a mean of 41 km (Figure 5.4). The R values have a mean of 0.12 with a range of 0.05–0.32.

**5.5.2 Special Cases.** For some stations, receiver functions obtained using data from two different back azimuths gave different results. For station st05, events coming from the south east sample the crust under the MCR and give a Moho depth of 45 km and Poisson's ratio of 0.32. Events coming from the

north-east sample the crust under the MCR rift axis, producing a complicated receiver function with no obvious PmS or PSmS phases.

**Table 5.1.Observarions of Crustal thickness (H, $H_n$), $V_p/V_s$ (Φ) and R)**

| station | long, deg, | lat, deg, | H, km | Φ | $H_n$, km | ΔH | ΔΦ | $\Delta H_n$ | R | ΔR | $N^{rfs}$ | Q |
|---|---|---|---|---|---|---|---|---|---|---|---|---|
| **CBKS** | -99.737 | 38.814 | 43.7 | 1.819 | 49.0 | 0.15 | 0.003 | 0.08 | 0.133 | 0.005 | 209 | A |
| **ECSD** | -96.600 | 43.730 | 43.8 | 1.854 | 49.8 | 1.87 | 0.030 | 1.55 | 0.228 | 0.004 | 2 | A |
| **FA10** | -92.670 | 40.104 | 48.2 | 1.787 | 49.5 | 0.54 | 0.020 | 0.22 | 0.119 | 0.034 | 9 | A |
| **FA11** | -93.287 | 40.819 | 36.1 | 1.985 | 49.1 | 1.41 | 0.032 | 0.28 | 0.105 | 0.016 | 23 | B |
| **FA12** | -93.711 | 41.139 | 40.1 | 1.849 | 44.8 | 0.12 | 0.008 | 0.00 | 0.142 | 0.027 | 13 | C |
| **FA13** | -94.008 | 41.313 | 45.5 | 1.781 | 46.7 | 0.22 | 0.004 | 0.18 | 0.182 | 0.012 | 24 | A |
| **FA14** | -94.264 | 41.545 | 46.3 | 1.775 | 47.5 | 0.22 | 0.002 | 0.22 | 0.226 | 0.013 | 19 | A |
| **FA15** | -94.465 | 41.772 | 44.3 | 1.888 | 54.4 | 2.89 | 0.084 | 2.14 | 0.100 | 0.002 | 41 | B |
| **FA16** | -94.598 | 41.893 | 53.4 | 1.738 | 53.6 | 0.43 | 0.016 | 0.00 | 0.134 | 0.013 | 27 | B |
| **FA17** | -94.838 | 42.035 | 42.5 | 1.902 | 48.6 | 0.16 | 0.007 | 9.78 | 0.138 | 0.011 | 47 | A |
| **FA18** | -95.049 | 42.302 | 42.1 | 1.809 | 45.8 | 0.28 | 0.009 | 2.39 | 0.214 | 0.007 | 27 | A |
| **FA19** | -95.349 | 42.512 | 42.4 | 1.816 | 45.7 | 1.15 | 0.020 | 0.70 | 0.135 | 0.008 | 29 | B |
| **FA20** | -95.977 | 42.970 | 42.6 | 1.866 | 50.0 | 0.24 | 0.007 | 0.87 | 0.197 | 0.019 | 31 | A |
| **FA21** | -96.624 | 43.738 | 47.2 | 1.803 | 51.0 | 0.55 | 0.010 | 0.58 | 0.111 | 0.012 | 37 | B |
| **FA23** | -99.984 | 45.550 | 40.5 | 1.829 | 44.9 | 0.14 | 0.004 | 3.32 | 0.295 | 0.014 | 17 | A |
| **KSU1** | -96.609 | 39.101 | 48.3 | 1.707 | 47.7 | 0.00 | 0.004 | 0.07 | 0.124 | 0.025 | 70 | A |
| **PKS** | -99.541 | 39.257 | 40.5 | 1.848 | 44.8 | 4.31 | 0.064 | 0.35 | 0.192 | 0.014 | 14 | A |
| **SCIA** | -93.215 | 41.907 | 46.6 | 1.785 | 49.5 | 0.33 | 0.015 | 1.75 | 0.249 | 0.017 | 12 | A |
| **st02** | -98.710 | 39.421 | 41.7 | 1.758 | 42.3 | 1.13 | 0.032 | 0.28 | 0.175 | 0.015 | 6 | B |
| **st03** | -98.193 | 39.599 | 33.8 | 1.955 | 42.7 | 0.43 | 0.005 | 1.19 | 0.387 | 0.101 | 2 | B |
| **st04** | -97.652 | 39.578 | 33.6 | 1.956 | 53.9 | 0.90 | 0.006 | 8.78 | 0.334 | 0.061 | 2 | A |
| **st05** | -97.006 | 39.597 | 46.4 | 1.901 | 56.1 | 0.00 | 0.011 | 0.85 | 0.072 | 0.002 | 31 | A |
| **st06** | -96.406 | 39.582 | 42.9 | 1.776 | 44.0 | 0.25 | 0.009 | 0.42 | 0.097 | 0.017 | 8 | A |
| **st07** | -95.827 | 39.608 | 43.8 | 1.800 | 46.7 | 1.13 | 0.023 | 1.18 | 0.212 | 0.029 | 5 | A |
| **st08** | -95.305 | 39.592 | 42.7 | 1.778 | 44.8 | 1.32 | 0.029 | 0.32 | 0.198 | 0.011 | 14 | A |
| **st91** | -99.549 | 39.254 | 36.2 | 1.980 | 49.3 | 0.15 | 0.014 | 0.47 | 0.168 | 0.018 | 16 | B |

$N^{rfs}$ is the number of receiver function used for calculating H and $V_p/V_s$
R is the ratio amplitude of the Direct P and its converted phase
Q is the category of quality of H- Φ plots

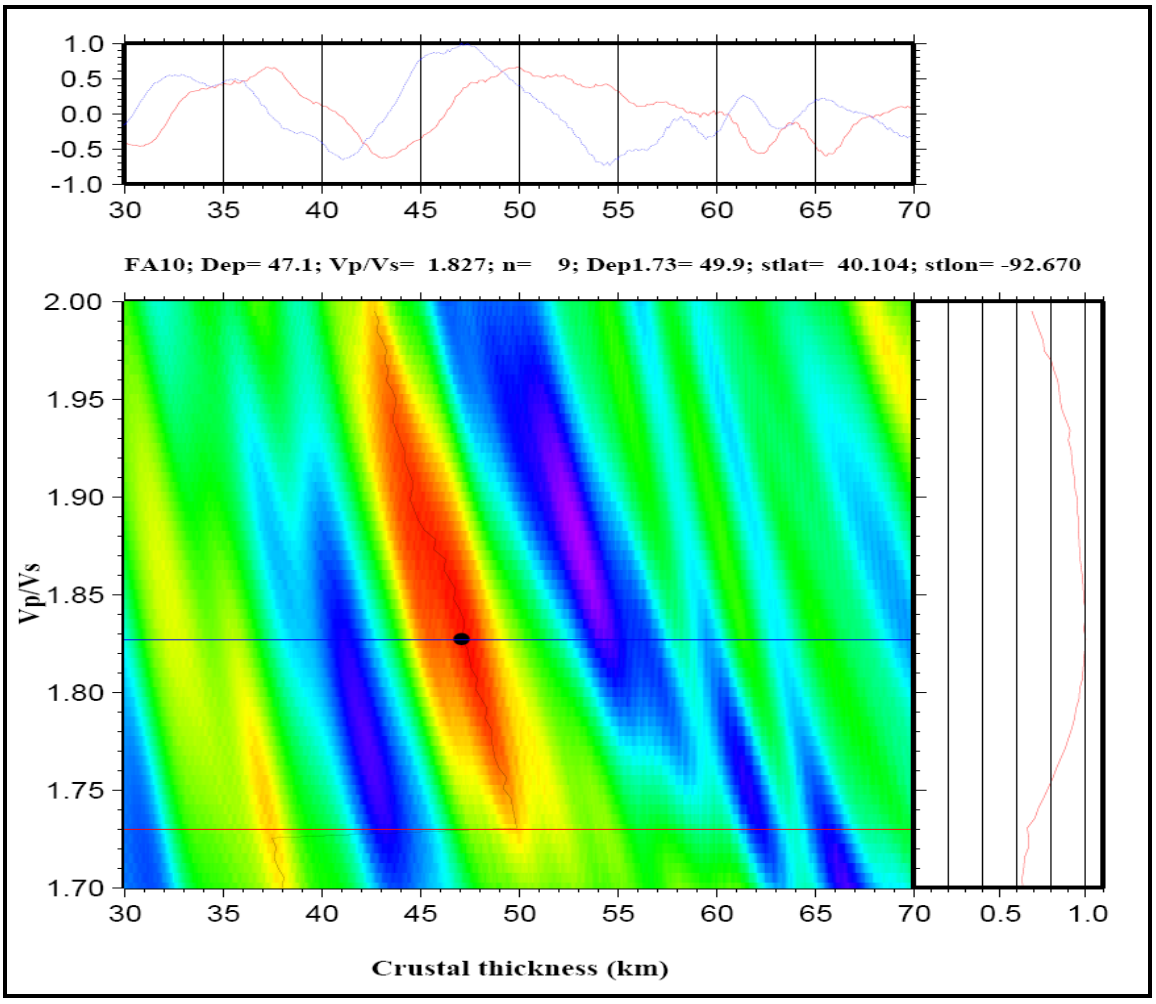


Figure 5.2: H- Φ stacking and bootstrap results for station FA10. The red line shows the stacking amplitudes for Φ =1.73. The blue line was produced by using the optimal Φ. The resulting crustal thickness, Φ and the crustal thickness when Φ =1.73 is assumed (denoted as Dep 1.73) are shown on the top panels.

For FA15, receiver functions from events sampling the crust to the east and south of the station yield similar Moho depth estimates of 45.2 km, but different Poisson's ratios. For station st02 and st03, it was difficult to identify the PmS and PSmS phases, although the Moho PmS phase was clear. Some stations show clear PSmS phases but it was difficult to identify the PPmS reverberation.

The ambiguity in estimating crustal thickness was resolved by incorporating crustal thicknesses from the gravity model shown in Figures 5.8a and 5.8b.

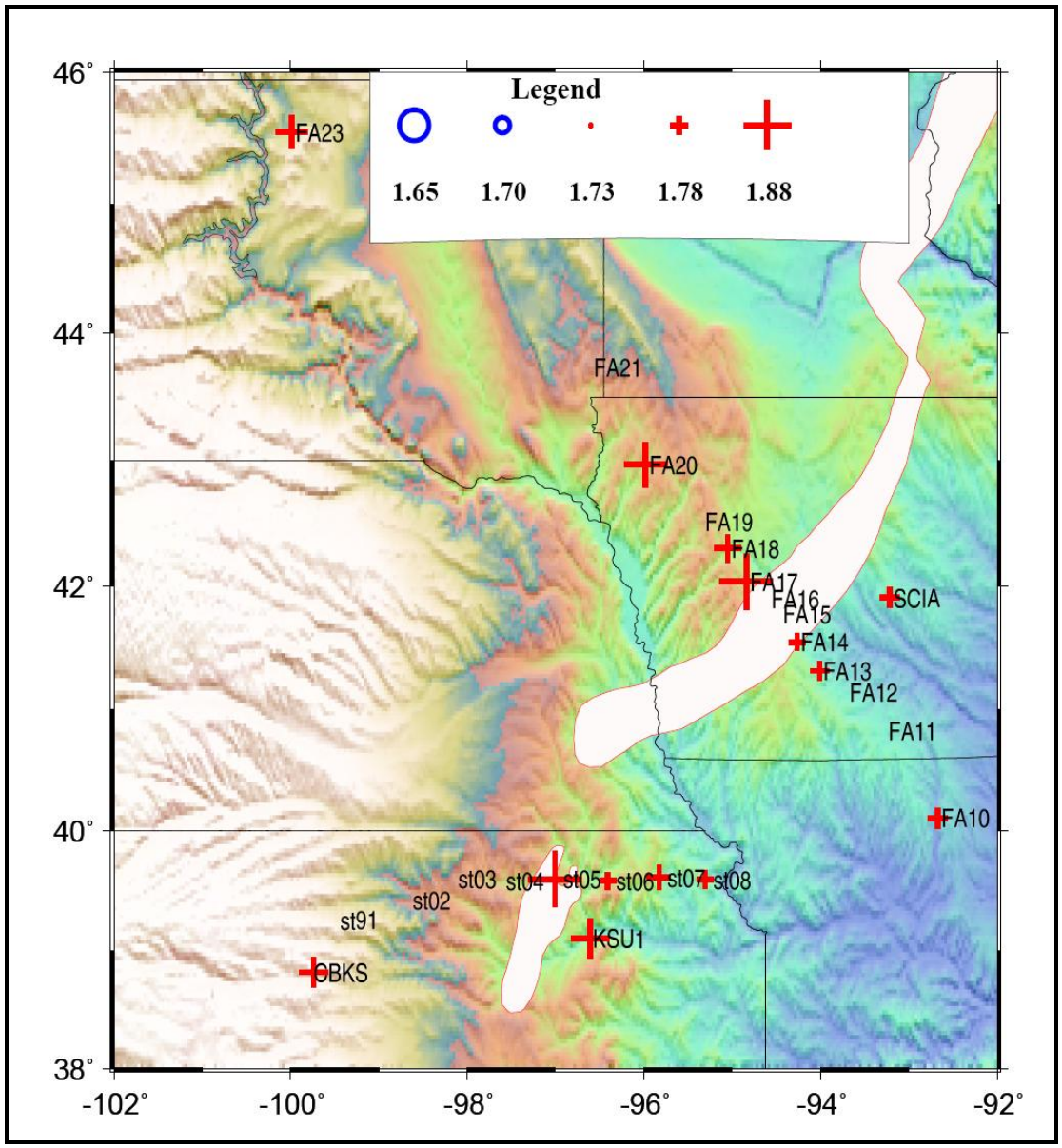


Figure 5.3: $V_p/V_s$ ratio of the two profiles crossing the Midcontinent rift. High values are observed within the rift (FA14, FA17 and st05). The Φ values range from 1.85 to 1.90 which are typical values for mafic crustal composition. Only category A values are used for this Figure.

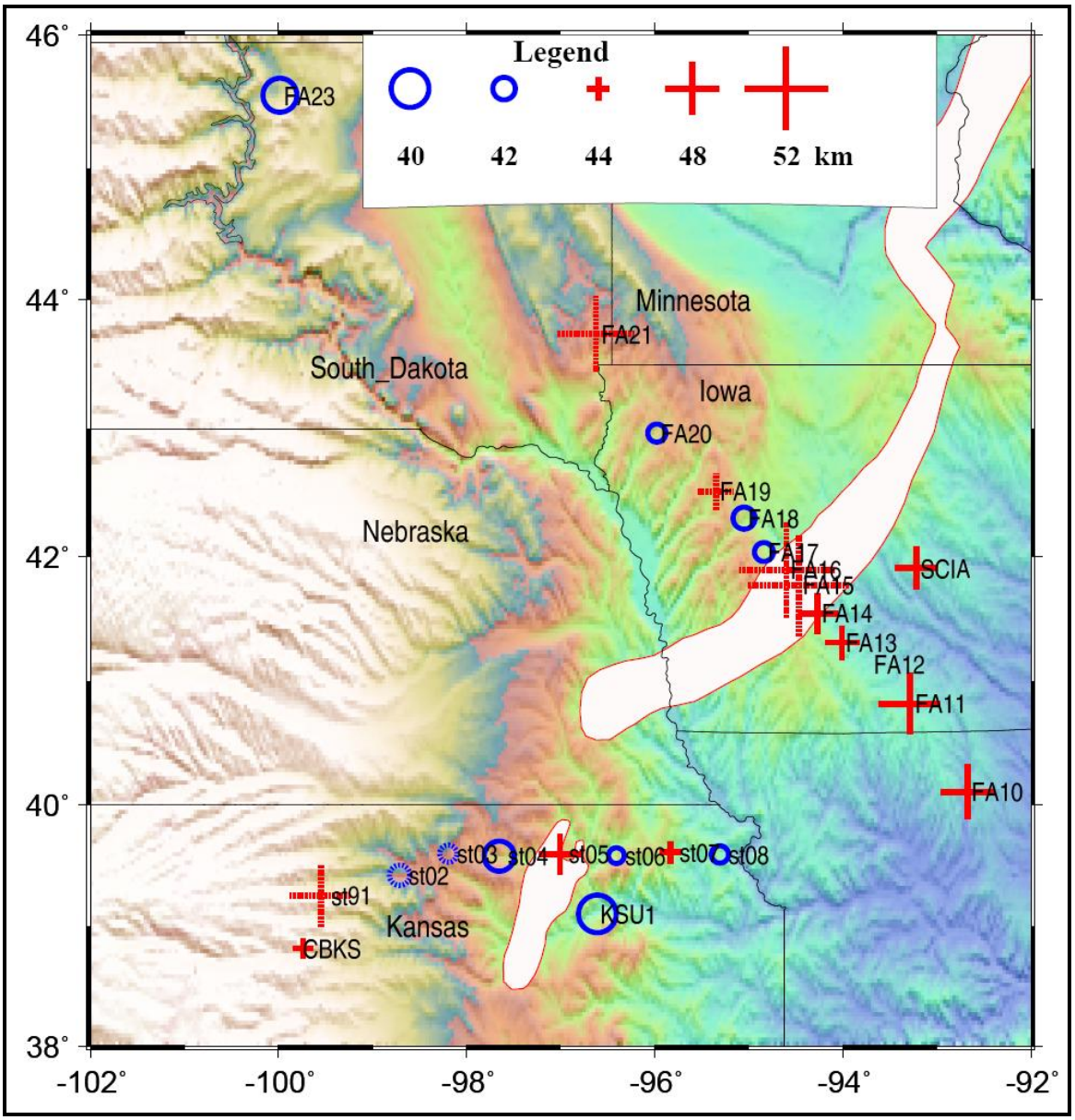


Figure 5.4: Receiver function results show varying crustal thickness across the Midcontinent rift. Over thickened crust is observed beneath stations within the rift (FA14 to FA17 and st05). Solid circles and crosses represent category A results and dashed circles and crosses represent category B results.

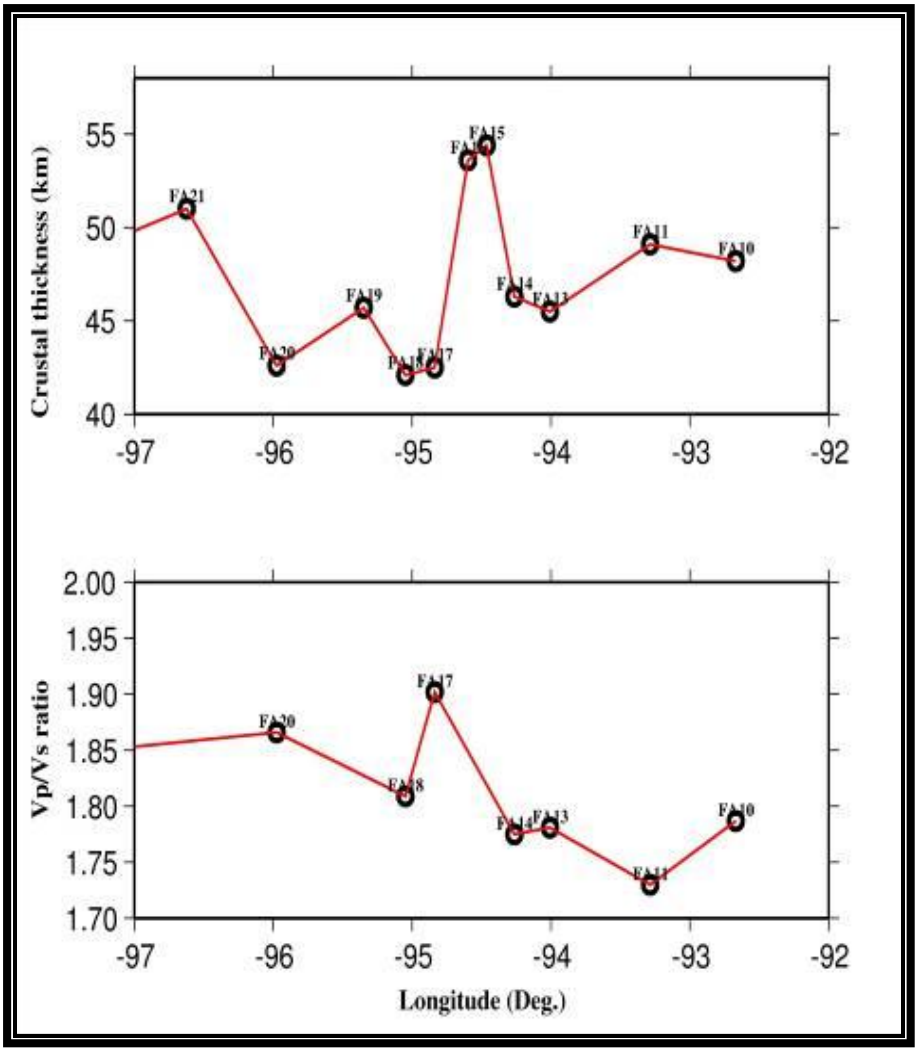


Figure 5.5: Transects showing the variation of (a) crustal thickness and (b) Φ across the MCR.

**5.5.3 Moho sharpness (R).** Some of the PcS amplitudes are unusually large at some stations (e.g. FA11, FA14, FA22, st02, st04, st05 and st08), approaching or exceeding the direct PmS wave amplitude in some instances (see Figure 5.7), which might be indicative of the presence of multiple, interfering arrivals. The amplitude ratio (R) for this stations ranges from 0.075 to 0.226 (see Table 5.1) with st04 showing highest amplitude value of R=0.336. An alternative interpretation of high PcS amplitude could be due to the actual complexity in the Moho with lower R values representing a disturbed Moho. The

amplitude ratio shows varying Moho signatures across the Midcontinent rift. The quality of the Moho (based on the calculated R values) varies from station to station without a clear pattern but low R values are observed in stations st05, st02, FA11 to FA12, FA16 and FA17. The Moho seems to be segmented probably as a result of extension that occurred million yrs ago.

By stacking PmS receiver functions from all the stations (e.g. Figure 5.7), it was observed that stacked amplitude of PmS in areas with thick crust, is smaller than that in areas with thin crust. Similar perturbation of Moho was observed in other area like the Bushveld Complex and Limpopo province (Nair et al., 2006). It was proposed that the Moho beneath such areas is disturbed by Proterozoic events and thus less sharp.

**5.5.4. Receiver Function Stacking Results**. The approach applied in this study makes use of a simple stack of receiver functions and the arrival times of the PmS and PPmS phases. An example of a simple receiver function stack is given in Figure 5.7. For most stations, the PmS and PPmS phases were easily picked on the receiver functions, but the PSmS phase was not (Figure 5.3). However, for station st05, the PSmS phase was more clearly identifiable than the PPmS phase, and in that case the later arriving phase was picked for the computation of H and Poisson's ratio. The receiver functions display a clear arrival in the time window of 3.5–6 s, which is considered as PmS, and at least one of the multiples near the vicinity of the predicted arrival times (calculated using $\Phi = 1.73$; see Figure 5.7 ).

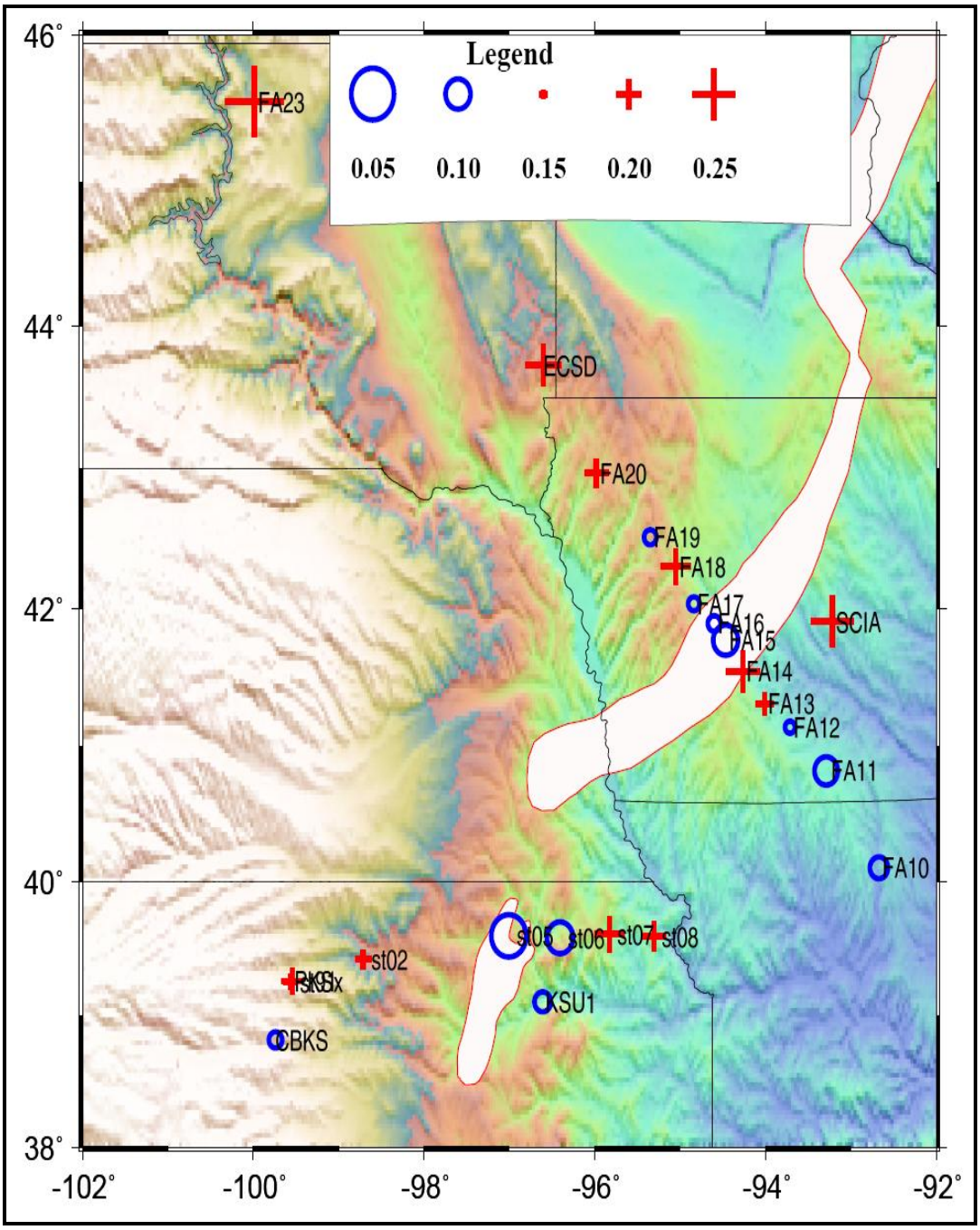


Figure 5.6: Amplitude ratio (R) calculated from stacking amplitude corresponding to the optimal pair of (H, Φ) over that of direct P wave and the radial component.

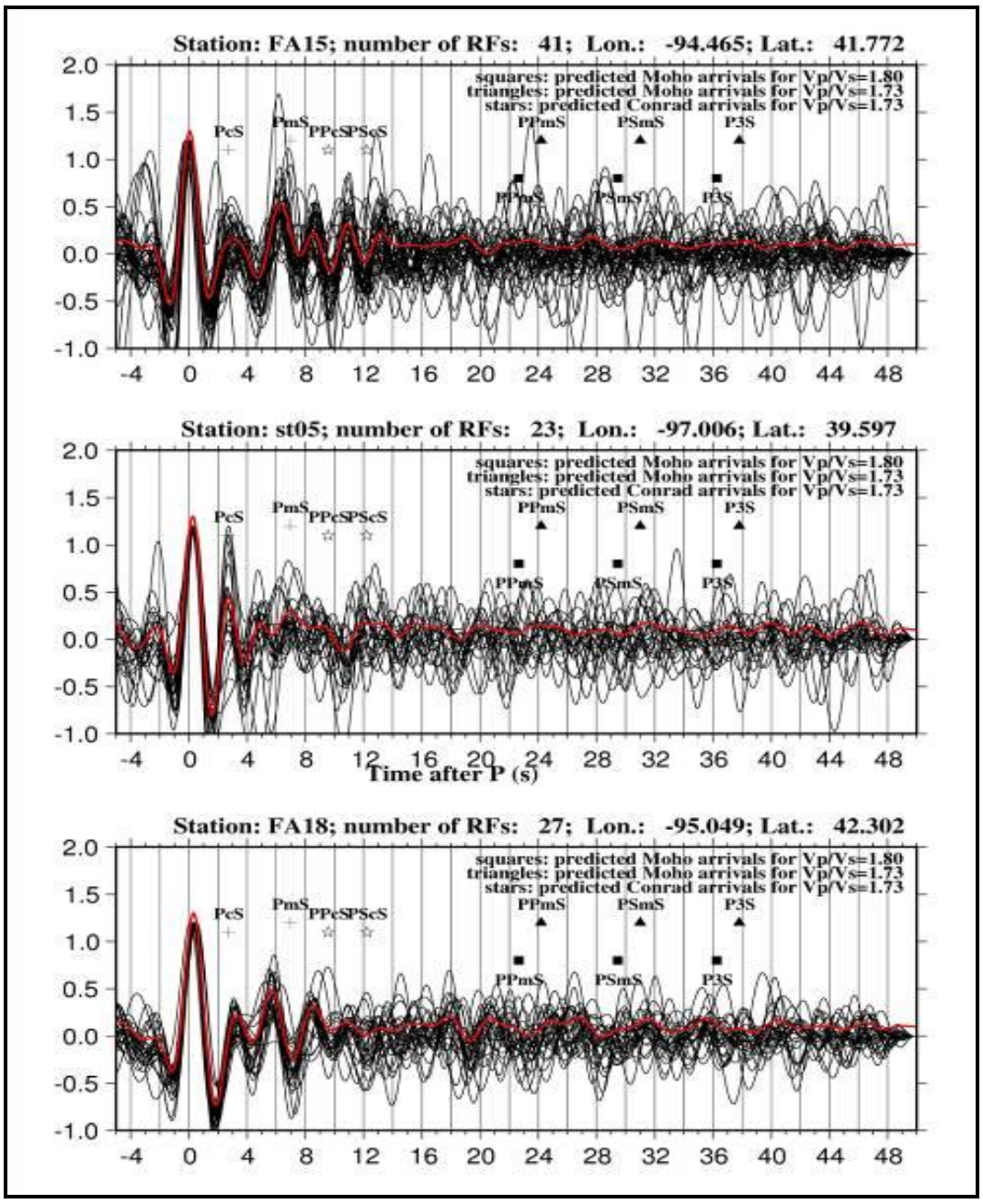


Figure 5.7**:** Example receiver functions st05, FA15 and FA18. The red trace from each station is the result of simple time domain summation (without move-out correction) of the individual traces. Triangles are theoretical arrival times for PPmS and PSmS calculated using equations (2) and (3) of Nair et al., (2006) by taking p = 5.0 s/deg, Vp = 6.5 km/s, and Φ = 1.73.

## 5.6. DISCUSSION

### 5.6.1 Vp/Vs ratio and Moho Sharpness beneath the MCR.

Our study shows relatively high the values of Φ (greater than 1.75) along both profiles (Figure 5.1). Stations within the rift have Φ values up to 1.8, which is indicative of magmatic underplating or volcanic intrusions beneath the rift and represents the addition of a mafic component. The low values of Φ (Table 5.1) elsewhere and their apparent age independence place important constraints on models for crustal formation and evolution. The Moho depths appear to be variable across the profiles. Between FA09 and FA13, the Moho appears to be at a relatively constant depth. From FA14 through FA17, the Moho depths increase towards the center of the Midcontinent Rift, indicating that the Moho is deepening and agreeing with previous studies showing crustal thickening beneath the rift (Hinze et al., 1992).

**5.6.2 Composition of the MCR and Vp/Vs Ratio.** Previous petrological studies suggest that the upper continental crust is felsic (Christensen and Mooney, 1995). The mineralogy is the most important factor influencing Vp/Vs or Poisson's ratio with the abundance of quartz and plagioclase feldspars having a dominant effect on common rocks. Granitic rocks have a Poisson's ratio of 0.24 while intermediate composition rocks (e.g. diorite) have values around 0.27 and mafic rocks (e.g. gabbro) about 0.30 (Christensen, 1996). Based on the classification of Ferris et al. (2006), rocks with a Φ of 1.76 or smaller are considered felsic, between 1.76 and 1.81 as intermediate, and larger than 1.81 as mafic. This classification was used with our estimate of Φ to constrain the crustal

composition of MCR. Proterozoic crust has been found to have $V_p/V_s$ ratio of 1.78±0.06 (Nair et al., 2006). Thus high Vp/Vs ratio within the MCR (stations: st05, FA14 to FA17) indicate the presence of mafic crust. Our average value of 1.82 is thus significantly higher and corresponds to a low $SiO_2$ content in the Keweenawan group.

**5.6.3 Influence of the Grenville Orogeny.** The rift transects the Grenville Front, a complex geologic boundary of approximately the same age as the MCR and was interpreted as a suture zone resulting from plate collision (e.g. Donaldson and Irving, 1972; Dewey and Burke, 1973) However, the junction or contact between these two major structures is hidden beneath thick Paleozoic sedimentary rocks and the nature of this contact is obscure (Green, 1982). The compressional forces from the Grenville orogeny are believed to have stopped the development of the rift in Proterozoic North America to the east of the Midcontinent region. The combination of high-grade metamorphism, reworked continental crust, compressional structures, and abundant crustal material strongly suggests that the Grenville Province represents a continental collision (Van Schmus, 1989). Much of the igneous and metamorphic activity of the Grenville event occurred 1150-900 Myr ago, with an earlier peak of activity 1100± 50 Myr ago and a second peak of activity 950±50 Myr ago (e.g. Baer, 1981). The proximity in time and space of the Grenville Province and the midcontinent rift system has led to suggestions that the two are genetically related. It is possible that extensional forces behind a continental collisional zone (Green, 1982; Van Schmus, 1991) may have contributed significantly to the development of the rift.

It is reasonable to conclude that the high Φ and H values observed in the vicinity of the MCR are due to basalt intruding the crust from the mantle below. Thus a mafic layer successfully accounts for both the thickness and $V_P/V_S$ ratio variations in the MCR region. Several authors have pointed out that the development of the MCR occurred at a time during which rifting was prevalent throughout the world (Stewart, 1976; Sawkins, 1976; Halls, 1978), and thus it may be related to a major extensional stress field that developed at this time in continental lithosphere, perhaps as a result of widespread plate movement and breakup.

**5.6.4 Gravity Modeling.** Thiel (1956) showed that the central positive gravity anomaly is associated with Keweenawan basalt deposited in an elongate depression, and that the flanking minima correlate with prisms of clastic rocks that thin away from the central gravity high (see Figure 5.1). Gravity studies played a critical role in the early delineation of the MCR (Thiel, 1956; Hinze, 1963). These methods readily detect the associated large physical property contrasts (Klasner et al., 1982; Hinze et al., 1982). Gravity data along the broadband seismic profiles show intense gravity anomalies over the length of the rift as positive gravity anomalies where the volcanic rocks are prominent and negative and featureless anomalies over sedimentary basins. The gravity anomaly rises to over 60 mGal in Minnesota with adjacent marginal minima that are less than 80 mGal below the regional level in Iowa. Gravity modeling results (Figures 5.8 and 5.9) show mafic intrusions in the sub-rift continental crust and thickening of the crust. Our gravity modeling results are consistent results from

Hinze et al. (1982). The crustal thickness determined from receiver function studies (this study) along the profiles shown in Figure 5.1 shows an over-thickening of the crust along the rift. Over-thickening of the crust has been observed across the western Lake Superior from gravity 2-D models constrained with seismic data (Hinze and Allen, 1982.

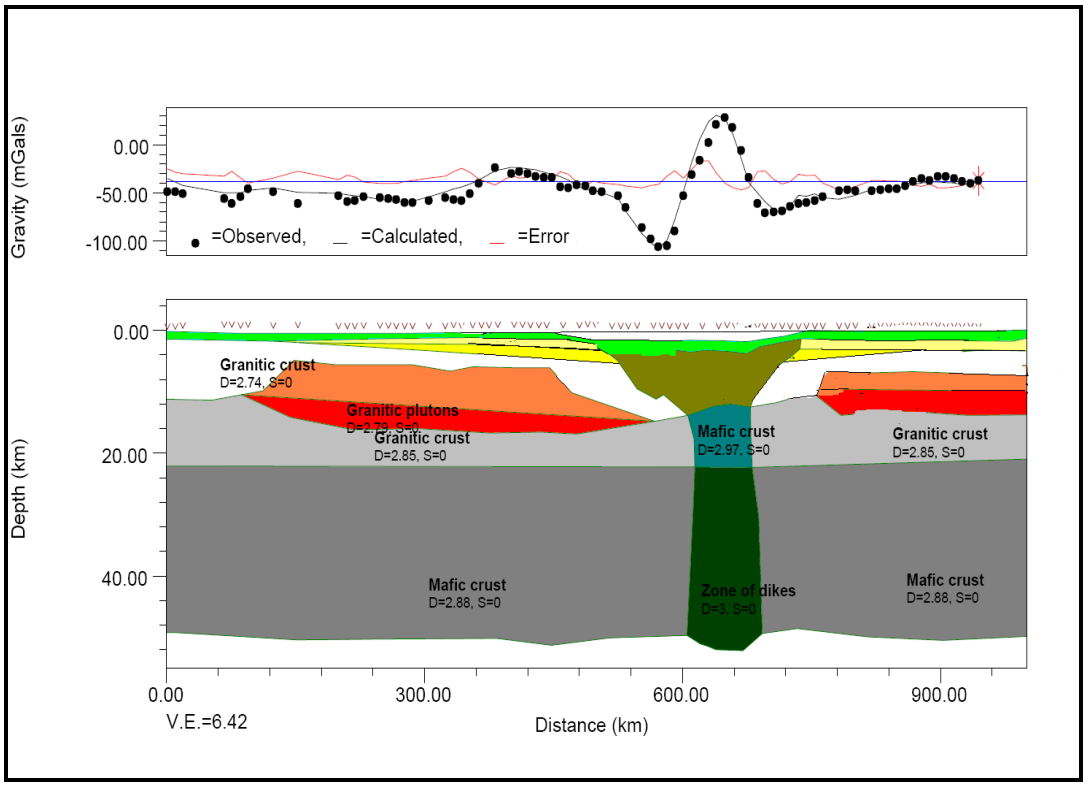


Figure 5.8: Gravity 2D model extracted along the FLED array. Depth to the Moho is constrained by Moho depth calculations from receiver functions. Blue represent Paleozoic sediments underlain by Keweenawan basalts with a density of 2.9 g/ccm within the rift axis, yellow (Upper Red clastic), white (granitic crust) light orange (Granitic Plutons) and red (Granitic Plutons) represent volcanic intrusions densities of 2.4, 2.7, 2.67, 2.74 and 2.79 g/ccm respectively.

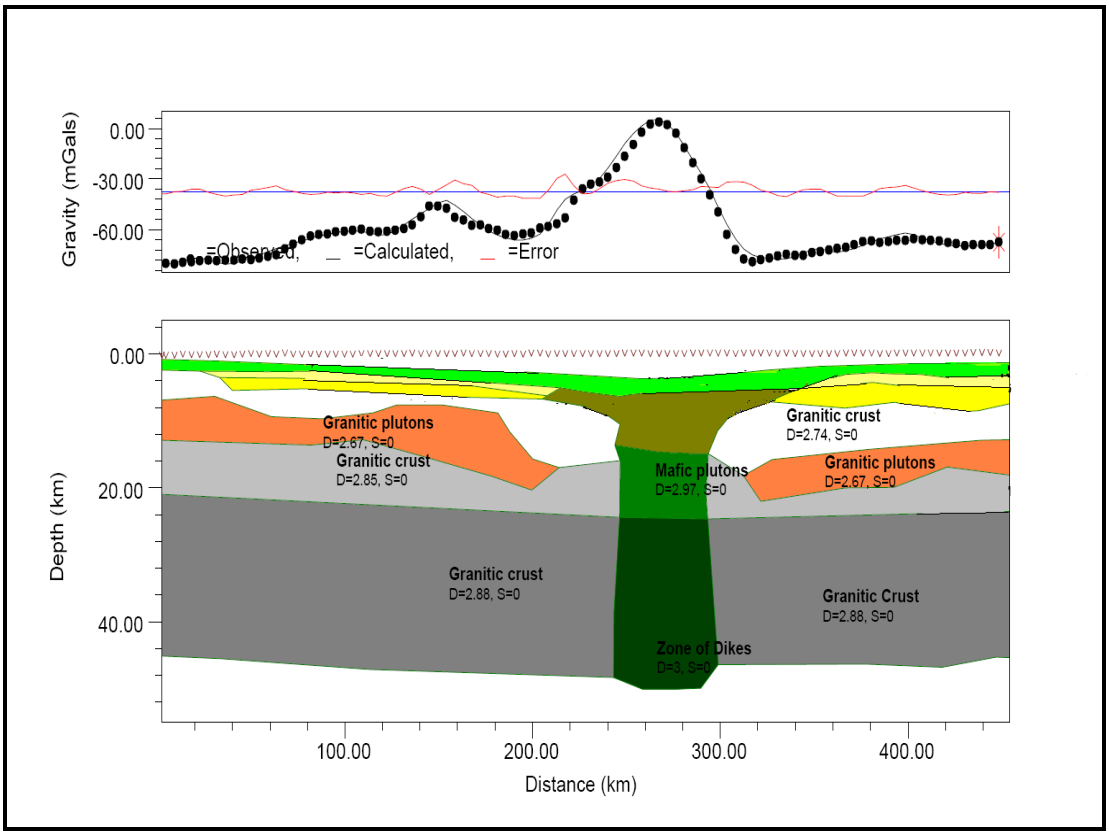


Figure 5.9: Gravity 2D model extracted along the Kansas array. Blue represent Paleozoic sediments underlain by Keweenawan basalts with a density of 2.9 g/ccm within the rift, yellow (Upper Red clastic), white (granitic crust) light orange (Granitic Plutons) and red (Granitic Plutons) represent volcanic intrusions densities of 2.4, 2.7, 2.67, 2.74 and 2.79 g/ccm respectively.

## 5.7. CONCLUSIONS

Moho depth was found to vary between 40 km and 53.6 km along the FLED array. The Moho is at its shallowest at either end of the array and thickens significantly beneath the Appalachians (station FA10), the Midcontinent Rift (station FA14, FA15, FA16, FA17), and the Williston Basin (FA23). The Poisson's ratio values vary from 0.26 to 0.305 in the vicinity of the rift, probably as a result of varying sediment deposition and erosion processes after cessation of rifting. Lower values of R within the rift further suggest the Moho is disturbed as a result of dike intrusion or magmatic underplating whereas on the rift flanks the

amplitude ratio (R) is well pronounced, suggesting less disturbed Moho. The MCR in Kansas array shows slightly lower H (~ 46km), R (0.1 to 0.15) and elevated Φ (~1.80) values. On either side of the rift the crustal thickness ranges from 42 to 49km and Poisson's ratios vary from 0.24 to 0.28, which indicate that the crustal composition is mafic due to the addition of basaltic material in the crust.

## 5.8. ACKNOWLEDGEMENTS

The teleseismic data used was obtained from Incorporated Research Institutions for Seismology (IRIS). The Diagrams in this paper were generated by Generic Mapping Tool (GMT version 4.2) a free software by Wessel and Smith (1991). I also thank Dr S. Gao for allowing use his Fortran77 program.

# 6. CONCLUSIONS AND RECOMMENDATIONS

Shear wave splitting observations in the NMSZ and the surrounding area show a complex pattern of anisotropy across the region, suggesting a complicated combination of causes. This also implies that the depth extent of Reelfoot fault system is confined to the upper part of the brittle-ductile transition. A two layer anisotropy model can explain the observations at some of the stations. The results from MCR show considerable variations in the splitting times (δt 0.4–1.35 s) and differing polarization direction for stations within the on-rift and off-rift stations. Off rift stations have polarization directions that are nearly parallel to AMP whereas stations within the rift can be explained by fossil rift parallel magmatic dykes. The gravity profiles across the rift show that the gravity high in MCR coincides with the rift-parallel fast directions

The largest Vp/Vs ratio values are associated spatially with the MCR and are most likely due to the intrusion of basalt into the crust. The addition of basaltic material successfully explains the thicker crust, higher Φ, as well as the diffuse character of the Moho in this area. Mafic addition is assumed to be a dominant process in the modification of crustal composition. Moho depth along the FLED array varies between 40 km and 53.6 km. The Moho is at its shallowest at either end of the array and thickens significantly beneath the Appalachians (station FA10), the Midcontinent Rift (station FA14, FA15, FA16, FA17), and Williston Basin (FA23). The Poisson's ratio values vary from 0.26 to 0.305 in the vicinity of the MCR.

The Mazatzal belt in the NMSZ is characterized by high values of Φ, suggesting a mafic crust. The largest Φ values are associated spatially with the North American craton, and are most likely due to the intrusion of basaltic material into the crust. Mafic addition from past tectonic events is the dominant process in the modification of crustal composition. Collisional zones have values of Φ that are not significantly different from surrounding regions. Φ values observed within the Mississippi embayment are highly variable.

Although this study has shed some light on the tectonic structure of the NMSZ and MCR, more work is need to investigated the possibility of existence of double layer anisotropy beneath the Midcontinent Rift system. The incoming USArray will provide a great opportunity to significantly improve our understanding about the structure and evolution of the MCR and NMSZ, and consequently test the results presented in this dissertation.

# BIBLIOGRAPHY

Al-Damegh, K., E. Sandvol, and M. Barazangi (2005). Crustal structure of the Arabian plate: New constraints from the analysis of teleseismic receiver functions, Earth and Planet. Sci. Lett., 231, 177-196.

Andrews, M. C., W. D. Mooney, and R. P. Meyer (1985). The relocation of microearthquakes in the northern Mississippi embayment, J. Geophys. Res. 90, 10223-10236.

Ammon, C. J., G. E. Randall, and G. Zandt (1990). On the non-uniqueness of receiver function inversions, J. Geophys. Res., 95, 15,303– 15,318.

Anderson, R. R. (1997). Keweenawan Supergroup clastic rocks in the Midcontinent Rift of Iowa, Geol. Society of America, Special paper 312.

Anderson, R. N., and R. M. Mckay (1989). Strategic and critical minerals in the Midcontinent region, United states U.S. Geological survey bulletin.

Anderson, J. L. (1983). Proterozoic anorogenic granite plutonism of North America, Geol. Soc. Am. Mem., 161 : 133-54.

Babuska, V., and M. Cara (1991). Seismic Anisotropy in the Earth, Kluwer Academic Publishers.

Baer, A. J. (1981). A Grenvillian model of Proterozoic plate tectonics. In Precambrian Plate Tectonics, ed. A. Kr6ner, 353-85. Amsterdam: Elsevier

Barruol, G., and W. B. Ismail (2001). Upper mantle anisotropy beneath the African IRIS and Geoscope stations, Geophys. J. Int., 146, 549–561.

Barruol, G., and D. Mainprice (1993). A quantitative evaluation of the contribution of crustal rocks to the shear wave splitting of teleseismic SKS waves, Phys. Earth planet. Inter., 78, 281–300.

Barruol, G., P. G. Silver, and A. Vauchez (1997). Seismic anisotropy in the eastern US: Deep structure of a complex continental plate, J. Geophys. Res., 102, 8329-8348.

Barruol, G., and A. Souriau (1995). Anisotropy beneath the Pyrenees range from teleseismic shear wave splitting, Geophys, Res. Lett., 22, 493-496.

Behrendt, J.C., D. R. Hutchinson, M. Lee, C. R. Thornber, A. Trtihu, W. Cannon and A. Green (1990). GLIMPCE seismic reflection evidence of deep-crustal and upper-mantle intrusions and magmatic underplating associated with the Midcontinent Rift system of North America.

Behrendt, J. C., A. G. Green, W. F. Cannon, D. R. Hutchinson, M. W. Lee, B. Milkereit, W. F. Agena, and C. Spencer (1988). Crustal structure of the Midcontinent rift system: Results from GLIMPCE deep seismic reflection profiles, Geology, 16: 81-85.

Bexfield, C.E., J. H. McBride, A. J. M. Pugin, D. Ravat, S. Biswas, W. J. Nelson, T. H. Larson, S. L. Sargent, M. A. Fillerup, B. E. Tingey, L. Wald, M. L. Northcott, J. V. South, M. S. Okure, and M. R. Chandler (2006). Integration of P- and SH-wave high-resolution seismic reflection and micro-gravity techniques to improve interpretation of shallow subsurface structure: New Madrid seismic zone, Tectonophysics 420, 5–21.

Bhattacharji, S., and H. Koide (1987). Theoretical and experimental studies of mantle upwelling, penetrative magmatism, and development of rifts in continental and oceanic crusts, Tectonophysics, 143, 13–30.

Braile, L. W., (1989). Crustal structure of the continental interior, in Geophysical framework of the continental United States, edited by L. C. Pakiser and W. D. Mooney, Memoirs of the Geol. Soc. of America, 172, 285-315, Boulder, Colo.

Braile, L. W., G. R. Keller, W. J. Hinze, and E. G. Lidiak (1982). An ancient rift complex and its relation to contemporary seismicity in the New Madrid seismic zone, Tectonics 1, 225–237.

Braile, L. W., W. J., Hinze, G. R., Keller, E. G., Lidiak, and J. L., Sexton (1986). Tectonic Development of the New Madrid Rift Complex, Mississippi Embayment, North America, Tectonophysics, 131, p. 1-21.

Buck, W. R. (2006). The role of magma in the development of the Afro-Arabian Rift System: From: YIRGU, G., Ebinger, C. J. and Maguire, P. K. H. (eds) 2006. The Afar Volcanic Province within the East African Rift System. Geol. Soc., Lon., Special Publications, 259, 43–54.

Burke, K. and J.F. Dewey (1973). Plume-generated triple junctions: key indicators in applying plate tectonics to old rocks, J. Geology, 81: 406-433.

Buschbach, T.C. and D.R. Kolata (1991). Regional setting of the Illinois Basin, American Association of Petroleum Geologists, Memoir 51, 29-55.

Cannon, W. F., D. L. Daniels, S. W. Nicholson, J. Phillips, L. G. Woodruff, Val W. Chandler, G. B. Morey, T. Boerboom, K. R. Wirth, and M. G. Mudrey Jr. (2001). New map reveals origin and geology of North American Mid-continent Rift, EOS, 82, 97-101.

Cannon, W.F. (1992). The Midcontinent Rift in the Lake Superior region with emphasis on its geodynamic evolution. In: P.A. Ziegler (Editor), Geodynamics of Rifting, Volume II. Case History Studies on Rifts: North and South America and Africa, Tectonophysics, 213: 41-48.

Cannon, W.F., and J.W. Hinze (1992). Speculations on the origin of the North American Midcontinent rift, Tectonophysics, 213, 49-55.

Carmichael, R. S., and R. A. Black (1986). Analysis and use of MAGSAT satellite magnetic data for interpretation of crustal structure and character in the U.S. mid-continent, Phys. Earth and Planet. Int., 44, 333-347.

Chen, K. C., J. M. Chiu, and Y. T. Yang (1996). Shear-wave velocity of the sedimentary Basin in the upper Mississippi Embayment using S _to P converted waves, Bull. Seis. Soc. Am., 86, 848-856.

Chevrot, S., and R. D. van der Hilst (2000). The Poisson ratio of the Australian crust: Geological and geophysical implications, Earth Planet. Sci. Lett., 183, 121–132.

Chiu, J. M., A. C. Johnston, and Y. T. Yang (1992). Imaging the active faults of the central New Madrid seismic zone using PANDA array data, Seismol. Res. Lett., 63, 375-393.

Clarke, T. J., and P. G. Silver (1991). A procedure for the systematic interpretation of body wave seismograms: Application to Moho depth and crustal properties, Geophys. J. Int., 104, 41– 72.

Christensen, N. I. (1984). The magnitude, symmetry, and origin of upper mantle anisotropy based on fabric analysis of ultramafic tectonites, Geophys. J. R. Astron. Soc., 76, 89 – 111.

Christensen, N. I. (1996). Poisson's ratio and crustal seismology, J. Geophys. Res., 101, 3139– 3156.

Christensen, N. I., and W. D. Mooney (1995). Seismic velocity structure and composition of the continental crust: A global view, J. Geophys. Res., 100, 9761–9788.

Clarke, T. J., and P. G. Silver (1991). A procedure for the systematic interpretation of body wave seismograms: Application to Moho depth and crustal properties, Geophys. J. Int., 104, 41– 72.

Clarke, T. J., and P. G. Silver (1993). Estimation of crustal Poisson's ratio from broad band teleseismic data, Geophys. Res. Lett., 20, 241–244.

Clitheroe, G., and R. van der Hilst (1998). Complex anisotropy in the Australian lithosphere from shear-wave splitting in broad-band SKS records, in Structure and Evolution of the Australian Continent, Geodyn. Ser., edited by J. Braun et al., vol. 26, pp. 73 – 78, AGU, Washington D. C.

Cook, F.A. (1995). The reflection Moho beneath the southern Canadian Cordillera, Can. J. Earth Sci. 32, 1520-1530

Cox, R. T., and R. B. Van Arsdale (1997). Hotspot origin of the Mississippi embayment and its possible impact on contemporary seismicity, Eng. Geol. 46, 5–12.

Crampin, S. (1994). The fracture criticality of crustal rocks, Geophys. J. Int., 118, 428–438.

Crampin, S., and S. Peacock (2005). A review of shear-wave splitting in the compliant crack-critical anisotropic Earth, Wave Motion 41, 59–77.

Crampin, S. (2003). The New Geophysics: shear-wave splitting provides a window into the crack-critical rock mass, Leading Edge 22, 536–549.

Denison, R. E., R.B. Koepnick, W.H. Burke, E.A. Hetherington, and A. Fletcher (1994). Construction of the Mississippian, Pennsylvanian and Permian seawater 87Sr/86Sr curve, Chem. Geol. 112:145–167.

Denison, R. E., E. G. Lidiak, M. E. Bickford and E. B. Kisvarsanyi (1984). Geology and geochronology Precambrian rocks of the central interior region of the United States: U.S. Geol. Surv. Profess. Paper 1241-C, 20.

Dueker K.G., and A.F. Sheehan (1993). Mantle discontinuity structure beneath Colorado Rocky Mountains and High Plains, J. Geophys. Res., 103, 7153-7169.

Dugda, M. T., A. A. Nyblade, J. Julia, C. A. Langston, C. J. Ammon, and S. Simuya (2005). Crustal structure on Ethiopia and Kenya from Receiver function analysis: Implications for rift development in eastern Africa, Journal of Geophysical Research, 11-, B01303, doi 10.1029/2004JB003065.

Donaldson, J.A., and E. Irving (1972). Grenville Front and rifting of the Canadian Shield, Nature (London). Phys. Sci., 237: 139- 140.

Dorman, J., and R. Smalley (1994). Low-frequency seismic surface waves in the Upper Mississippi Embayment, Seism. Res. Lett., 65(2):137-148.

Eisele, J., and C. Isachsen (2001). Crustal growth in southern arizona: U-Pb Geochronologic and sm-nd isotopic evidence for Addition of the paleoproterozoic cochise block to the Mazatzal province, Americ. J. of Sci., 301, 773–797.

Efron, B., and R. Tibshirani (1986). Bootstrap methods for standard errors, confidence intervals, and other measures of statistical accuracy, Stat. Sci., 1, 54– 77.

Efron, B., and R. Tibshirani (1991). Bootstrap methods for standard errors, confidence intervals, and other measures of statistical accuracy, Stat. Sci., 1, 54– 77.

Ervin, C. P., and L. D. McGinnis (1975). Reelfoot rift-Reactivated precursor to the Mississippi Embayment, Geol. Soc. Am. Bull. 86, 1287-1295.

Ewenet M. G., S. L. Klemperer, A. A. Nyblade, K. T. Walker, and K. M. Keranen (2004). Shear--wave splitting in Ethiopia: Precambrian mantle anisotropy locally modified by Neogene rifting, GRL, 31, L18602, doi:10.1029/2004GL020471.

Ferris, A., G. A. Abers, B. Zelt, B. Taylor, and S. Roecker (2006). Crustal structure across the transition from rifting to spreading: the Woodlark rift system of Papua New Guinea, Geophys. J. Int., 166, 622–634 doi: 10.1111/j.1365-246X.2006.02970.x.

Fischer, K., S. Rondenay, E. Syracuse, C. McCarthy, C. A. Rychert, L. Doermann, M. Salas, M. Welsh, M. Wysession, G. Aleqabi, P. Shore, J. F. Lawrence, B. Shiro, M. Pyle, G. Euler, and T. Mayeau (2006). Investigating Crust and Mantle Structure with the Florida-to-Edmonton Broadband Array, Surface of the Earth: North America, Iris 5-Year Proposal.

Forte A. M., J. X. Mitrovica, R. Moucha, N. A. Simmons, and S. P. Grand (2007). Descent of the ancient Farallon slab drives localized mantle flow below the New Madrid seismic zone, Geophys. Res. Let. 34, L04308, doi:10.1029/2006GL027895.

Fouch, M. J., K. M. Fischer, E. M. Parmentier, M. E. Wysession, and T. J. Clarke (2000). Shear wave splitting, continental keels, and patterns of mantle flow, J. Geophys. Res. 105, 6255-6275.

Franklin, J. M., W. H. McIlwaine, H. K. Poulsen, and, R. K. Wanless (1980). Stratigraphy and depositional setting of the Sibley Group, Thunder Bay district, Ontario, Canada, Can. J. Earth Sci. 17 : 633-5

Gao, S., K. H. Liu, R. J. Stern, G. R. Keller, J. P. Hogan, J. Pulliam, and E. Y. Anthony (2008). Characteristics of mantle fabrics beneath the South-central Unites states: Constraints from shear-wave splitting parameters, Geosphere, 4, doi: 10.1130/GES00159.1, 411-417.

Gao, S. S., K. H. Liu, and C. Chen (2004). Significant crustal thinning beneath the Baikal rift zone: New constraints from receiver function analysis, Geophysical Research Letters, 31, L20610, doi:10.1029/2004GL020813.

Gao, S., P. M. Davis, P. D. Slack, A. W. Rigor, Y. A. Zorin, V.V. Mordvinova, V.M. Kozhevnikov and N.A. Logatchev (1997). SKS splitting beneath continental rift zones, J. Geophys. Res. 102, 22781-22795.

Gao, S., P. M. Davis, H. Liu, P. Slack, Y. A. Zorin, N. A. Logatchev, M. Kogan, P. Burkholder, and R.P. Meyer (1994). Asymmetric upwarp of the Asthenosphere beneath the Baikal Rift zone, Siberia, J. of Geophys. Res., 99**:** 15,319-15,330.

Gledhill, K., and G. Stuart (1996). Seismic anisotropy in the fore-arc region of the Hikurangi subduction zone, New Zealand, Phys. Earth Planet. Int., 95, 211-225.

Green, J. C. (1982). Geochemical Evidence for the nature and development of the middle proterozoic (Keweenanwan) mid-continent rift of North America, Tectonophysics, 94, 313-437.

Gripp, A. E., and R. G. Gordon (2002). Young tracks of hotspots and current plate velocities, Geophys. J. Int. 150, 321–361.

Halls, H. C. (1982). Crustal thickness in the Lake Superior region. In: R.J. Wold and W.J. Hinze (Editors), Geology and Tectonics of the Lake Superior Basin, Geol. Sot. Am., Mem., 156: 239-243.

Hinze, W. J. (1963). Regional gravity and magnetic anomaly maps of the Southern Peninsula of Michigan. Michigan Geol. Surv. Rep. Invest., 1, 26.

Hinze, W. J., L. W. Braile, and V. W. Chandler (1990). A geophysical profile of the southern margin of the Midcontinent Rift System in western Lake Superior, Tectonics, 9: 303-310.

Hinze, W. J., Wold, R. J., and N. W. Cara (1982). Gravity and magnetic anomaly studies of Lake Superior, In: R.J. Wold and W.J. Hinze (Editors), Geology and Tectonics of the Lake Superior Basin, Geol. Sot. Am. Mem., 156: 203-222.

Hinze, W. J. (1963). Regional gravity and magnetic anomaly maps of the Southern Peninsula of Michigan, Michigan Geol. Surv. Rep. Invest., 1, 26 pp.

Holm, D. K., R. Anderson, T. J. Boerboomc, W. F. Cannond, V. Chandler, M. Jirsa, J. Miller, D. A. Schneider, K. J. Schulz, W. R. Van Schmus (2007). Reinterpretation of Paleoproterozoic accretionary boundaries of the north-central United States based on a new aeromagnetic-geologic compilation, Precambrian Research 157, 71–79.

Hough, S. E. (1990). Constraining sediment thickness in the San Francisco Bay area using observed resonances and Ps conversions, Geophys. Res. Lett., 17, 1469-1472.

Kaminski, E., and N. M. Ribe (2002). Timescales for the evolution of seismic anisotropy in mantle flow, Geophys, 3, 1051, doi:10.1029/2001GC000222.

Karato, S. (1987). Seismic anisotropy due to lattice preferred orientation of minerals: kinematic or dynamic? In: Manghnani, M.H., Syono, S. (Eds.), High-Pressure Research in Mineral Physics, Geophys. Monogr. Ser., vol. 39. Am. Geophy. Union, Washington, DC, 455–471.

Karlstrom, K. E., and S. A. Bowring (1988). Early Proterozoic assembly of tectono-stratigraphic terranes in southwestern North America: Journal of Geology, v. 96, p. 561–576.

Kind, R., G. L. Kosarev, and N. V. Petersen (1995). Receiver function at the stations of the German Regional Seismic Network (GRSN), Geophys. J. Int., 121, 191-202.

Keller, G. R., G. Lidiak, W. J. Hinze, and L. W. Braile (1983). The role of rifting in the tectonic development of the Midcontinent, U.S.A, Tectonophysics, 94, 391-412.

Kendall, J. M. (1994). Teleseismic arrivals at a mid-ocean ridge: effects of mantle melt and anisotropy, Geophys. Res. Lett. 21, 301– 304.

Klasner, J.S., W. F. Cannon, and W. R. Van Schmus (1982). The pre-Keweenawan tectonic history of the north-central United States and central Canada and its influence on formation of the Midcontinent Rift. In: R.J. Wold and W.J. Hinze (Editors), Geology and Tectonics of the Lake Superior Basin. Geol. Sot. Am., Mem., 156: 27-46.

Klewin, K. W. and S. B. Shirey (1992). Igneous petrology and magmatic evolution of the Midcontinent rift system. In: P.A. Ziegler (Editor), Geodynamics of Rifting, Volume II. Case History Studies on Rifts: North and South America and Africa. Tectonophysics, 213: 33-40.

Kolata, D. R., and W. J. Nelson (1997). Role of the Reelfoot Rift-Rough Greek Graben in the evolution of the Illinois Basin, in Ojakangas, R.W., Dickas, A.B., and Green, J.C., eds., Middle Proterozoic to Cambrian rifting, central North America: Boulder, Colorado, Geological Society of America Special Paper 312, 287-298.

Kolata, D.R., and W.J. Nelson, 1991, Tectonic history of the Illinois Basin: American Association of Petroleum Geologists, Memoir 51, p. 263–285.

Langston, C. A. (1979). Structure under Mount Ranier, Washington, inferred from teleseismic body waves, J. Geophys. Res., 84, 4749-4762.

Langston, A. C. (1994). An integrated study of crustal Structure and Regional wave propagation for Southern Missiouri, Bull. Seis. Soc. Am., 84, 105-118.

Li, A., D. W. Forsyth, K. M. Fisher (2003). Shear velocity structure and azimuthal anisotropy beneath eastern North America from Rayleigh wave inversion, J. Geophys. Res. 108 (B8) (Art. No. 2362).

Ligorria, J. P., and C. Ammon (1999). Iterative deconvolution and receiver function estimation, Bull. Seismol. Soc. Am., 89, 1395–1400.

Liu, K. H., S. S. Gao, Y. Gao, and J. Wu (2008). Shear wave splitting and mantle flow associated with the deflected Pacific slab beneath northeast Asia, JGR, 113, B01305, doi:10.1029/2007JB005178.

Liu, L., and M. D. Zoback (1997). Lithospheric strength and intraplate seismicity in the New Madrid seismic zone, Tectonics, 16, 585 – 595.

Mainprice, D., G. Barruol, and W. Ben Ismail, and A. G. Union (2000). The seismic anisotropy of the earth's mantle : From single crystal to polycrystal, AGU, 117.

Mainprice, D., A. Tommasl, H. Couvy, P. Cordier, and D. J. Frost (2005). Pressure sensitivity of olivine slip systems and seismic anisotropy of Earth's upper mantle, Nature 433, 731–733.

Mainprice, D., and P. G. Silver (1993). Interpretation of SKS-waves using samples from the subcontinental lithosphere, Phys. Earth Planet. Inter., 78, 257– 280.

Marone M. and B. Romanowicz (2007). The depth distribution of azimuthal anisotropy in the continental upper mantle, Nature, 447.

McBride, J. H., W. J. Stephenson, and Guest Editors (2003). Contributions to neotectonics and seismic hazard from shallow geophysical imaging. Special Tectonophysics, 368, Issues 1–4, 1–227.

McNamara, D. E., and T. J. Owens (1994). Shear wave anisotropy beneath the Tibetan Plateau, J. Geophys. Res., 99, 13655-13665.

McNamara, D. E., T. J. Owens, P.G. Silver, and F.T. Wu (1994). Shear wave anisotropy beneath the Tibetan Plateau, Journal of Geophysical Research, v. 99, p. 13,655–13,665.

McWilliams, M. O., and D. J. Dunlop (1978). Grenville paleomagnetics and tectonics, Can. J. Earth Sci.. 15: 687-695.

Mickus, K. L., and G. R. Keller (1992). Lithospheric structure of South Central United States, Geology, 20, 335-338.

Mitchell, R. H., and R. G. Platt (1978). Mafic mineralogy of ferroaugite syenite from the Coldwell Alkaline Complex, Ontario, Canada. J. Petrol. 19:627-51

Mooney, W. D., M. C. Andrews, A. Ginzburg, D. A. Peters and R. M. Hamilton (1983). Crustal structure of the northern Mississippi embayment and a comparison with other continental rift zones, Tectonophysics, 94, 327-348, 1983.

Musacchio G., W. D. Mooney, J. H. Luetgert, and N. I. Cristensen (1997). Composition of the crust in the Grenville and Appalachian Provinces of North America inferred from Vp/Vs ratios, Journal of Geophysical Research, 102, B7, 15,225-15,241.

Nair, K. S., S. S. Gao, K. H. Liu, and P. G. Silver (2006). Southern African crustal evolution and composition from receiver function studies, Journal of geophysical research, 111, B02304, doi:10.1029/2005JB003802.

Nelson, B. K., and D. J. DePaolo (1985). Rapid production of continental crust 1.7 to 1.9 b.y. ago; Nd isotopic evidence from the basement of the North American Mid-continent, GSA Bulletin; 96, 6, 746-754.

Nelson, W. J., Denny, F. B., Follmer, L. R., Masters, J. M. (1999). Quaternary grabens in southernmost Illinois: deformation near an active intraplate seismic zone, Tectonophysics, 305, 381– 397.

Nguuri, T. K., J. Gore, D. E. James, S. J. Webb, and Kaapvaal Seismic Group (2001). Crustal structure beneath southern Africa and its implications for the formation and evolution of the Kaapvaal and Zimbabwe cratons, Geophys. Res. Lett., 28, 2501– 2504.

Nicolas, A., and N. I. Christensen (1987). Formation of anisotropy in upper mantle peridotites—a review. In: Fuchs, K., Froidevaux, C. (Eds.), Composition, Structure and Dynamics of the Lithophere- Asthenosphere System, Geodyn. Ser., vol. 16. AGU, Washington, DC, 111–123.

Nyquist, J. E., and H. F. Wang (1988). Flexural modeling of the Midcontinent Rift, J. Geophys. Res., 93, 8852-8868.

Orzalaybye, S., and M. K. Savage (1995). Shear-wave splitting beneath western United States in relation to plate tectonics, J. Geophys. Res. 100, 18,135-18,149

Owens, T. J., G. Zandt, and S. R. Taylor (1984). Seismic evidence for an ancient rift beneath the Cumberland Plateau, Tennessee: A detailed analysis of broadband teleseismic P waveforms, J. Geophys. Res., 89, 7783-7795.

Peters, D., W. Lutter, A. Ginzburg, A. Walter, and W. Mooney (1981). Deep structure of the Mississippi embayment from seismic refraction measurements. Lunar and Planetary Institute, 3303, 161.

Rowlands, H. J., D.C. Booth, and J. M. Chiu (1993). Shear-wave splitting from microearthquakes in the New Madrid seismic zone, Can. J. Expl. Geophys. 29, 352–362.

Rudman, A. J., and J. A. Rupp (1993). Geophysical properties of the basement rocks of Indiana, Indiana Geological Survey, Special Report no. 55, 16.

Rudnick, R. L., and D. M. Fountain (1995). Nature and Composition of the Continental Crust: A Lower Crustal Perspective, Reviews of Geophysics, 33, 3, 267-309.

Wessel, P., and W. H. F. Smith (1991). Free software helps map and display data, Eos Trans. AGU, 72, 441, 445-446.

Wysession, M. E., K. M. Fischer, P. J. Shore, and G. I. Aleqabi (2004). Waves across America: Using a seismic array from Florida to Alberta to examine the geology beneath the middle of North America, Abstracts of the 38th Annual Meeting of the North-Central Section of the Geological Society of America, St. Louis, MO, April.

Sandvol, E., and J. Ni (1997). Deep azimuthal seismic anisotropy in the southern Kurile and Japan subduction zones, J. Geophy. Rev., 102, 9911-9922.

Sandvol, E., J. Ni, S. Ozalaybey, and J. Schlue (1992). Shear-Wave Splitting in the Rio Grande Rift, Geophys. Res. Lett., 19, 2337-2340.

Savage, M. K., and A. F. Sheehan (2000). Seismic anisotropy and mantle flow from the Great Basin to the Great Plains, western United States, J. Geophys. Res., 105, 13,715–13,734.

Savage, M. K., and P. G. Silver (1993). Mantle deformation and tectonics: constraints from seismic anisotropy in the western United States, Phys. Earth Planet. Int. 78(3-4), 207-227.

Savage, M. K. (1999). Seismic anisotropy and mantle deformation: What have we learned from shear wave splitting?, Rev. Geophys., 37, 65-106.

Sawkins, F. J. (1976). Wide spread continental rifting: some considerations of timing and mechanism, Geology 4: 427-30

Scheuber, E., P. Giese, F. Schilling, M. Schmitz, and P. Wigger (1999). Crustal thickening in the Cental Andes and the different natures of the Moho discontinuity, J. South American Earth Sci., 12, 201-220.

Silver, P. G., and S. Kaneshima (1993). Constraints of mantle anisotropy beneath Precambrian North America from a transportable teleseismic experiment, Geophys. Res. Lett., 20, 1131-1134.

Silver, P. G., and W. W. Chan (1991). Shear-wave splitting and continental mantle deformation. J. Geophys. Res., 96, 16429-16454.

Silver, P. G. (1996). Seismic anisotropy beneath the continents, Probing the depths of geology, Ann. Rev. Earth planet. Sci., 24, 385–432.

Silver P. G., and M. K. Savage (1994). The interpretation of shear wave splitting parameters in the presence of two anisotropic layers, Geophys. J. Int., 119, 949-963.

Steinhart, J. S., and T. J. Smith (1966). The Earth beneath the Continents, Am. Geophys. Union, Geophys. Monogr., 10: 663 pp.

Stewart, J. H. (1976). Late Precambrian evolution of North America: plate tectonics implication. Geology 4, 11-15

Street, R., E. Woolery, Z. Wang, and J. Harris (1995). A short note on shear-wave velocities and other site conditions at selected strong-motion stations in the New-Madrid seismic zone, Seis. Res. Lett., 66, 56-63.

Thiel, E. C. (1956). Correlation of gravity anomalies with the Keweenawan geology of Wisconsin and Minnesota, Geol. Soc. Am. Bull. 67:1079-1100.

Thomas, J. J., R. D. Shuster, and M. E. Bickford (1984). A terrane of 1350-1400 m.y. old silicic volcanic and plutonic rocks in the buried Proterozoic of the midcontinent and in the Wet Mountains, Colorado. Geol. Soc. Am. Bull. 95:1150-57.

Tron, V., Brun, J. P. (1991). Experiments on oblique rifting in brittle-ductile systems. Tectonophysics 188, 71–84.

Van Arsdale, R., J. Purser, W. Stephenson and J. Odum (1998). Faulting along the southern margin of Reelfoot Lake, Tennessee, Bulletin of the Seismological Society of America, 88, 131-139.

Van Schmus, W. R., D. A. Schneider, D. K. Holm, S. Dodson, B. K. Nelson (2007). New insights into the southern margin of the Archean–Proterozoic boundary in the north-central United States based on U–Pb, Sm–Nd, and Ar–Ar geochronology, Precambrian Research 157,80–105.

Van Schmus, W. R., M. E. Bickford, and A. Turek (1996). Proterozoic geology of the east–central Midcontinent basement. In: van der Pluijm, B.A., Catacosinos, P.A. (Eds.), Basement and basins of eastern North America, Geol. Soc. Am. Spec. Pap., 308, 7– 32.

Van Schmus, W. R., and M. E. Bickford (1981). Proterozoic chronology and evolution of the Midcontinent region, North America. In Precambrian Plate Tectonics, ed. A. Kroner, 261-96. Amsterdam: Elsevier.

Van Schmus, W. R., and W. J. Hinze (1989). Midcontinent Rift system, The Geology of North America, vol. C-2, Precambrian: Conterminous United States, edited by R. D. Hatcher, Jr., W. A. Thomas, and G. W. Viele, pp. 292-303, Geological Society of America, Boulder, Colo.

Van Schmus, W. R., and W. J. Hinze (1985). The Midcontinent Rift System, Ann. Rev. Earth Planet. Sci., 13: 345-383.

Van Schmus, W. R., J. C. Green, and H. C. Halls (1982). Geochronology of Keweenawan rocks in the Lake Superior region, In: R.J. Wold and W.J. Hinze (Editors), Geology and Tectonics of the Lake Superior Basin. Geol. Sot. Am.. Mem.. 156: 165-172.

Van Schmus, W. R., and M. E. Bickford (1981). Proterozoic chronology and evolution of the Midcontinent region, North America. In Precambrian Plate Tectonics, ed. A. Kroner, 261-96. Amsterdam: Elsevier.

Vauchez, A., and G. Barruol (1996). Shear wave splitting in the Appalachians and the Pyrenees: Importance of the inherited tectonic fabric of the lithosphere, Phys. Earth Planet. Inter., 95, 127-138.

Vinnik, L. P., L. Makeyeva, A. Milev and A. Usenko (1992). Global patterns of azimuthal anisotropy and deformation in the continental mantle, Geophys. J. Int., 111, 433-447.

Vinnik, L. P., R. W. E. Green, and L. O. Nicolaysen (1996). Seismic constraints on dynamics of the mantle of the Kaapvaal craton, Phys. Earth Planet. Int. 95, 139-151.

Walker, K. T., A. A. Nyblade, S. L. Klemperer, G. H. R. Bokelmann, and T. J. Owens (2004). On the relationship between extension and anisotropy: Constraints from shear wave splitting across the East African Plateau, J. Geophys. Res. 109(#B18#), 8302, DOI:10.1029/2003JB002866.

Wilson, D, R. Aster, M. West, J. Ni, S. Grand, W. Gao, W. S. Baldridge, S. Semken, and P. Patel (2005). Lithospheric structure of the Rio Grande rift, Nature 433, 851-855.

Williams, L. A. J. (1982). Physical aspects of magmatism in continental rifts. In Continental and Oceanic Rifts, Am. Geophys. Union Geodyn. Set., ed. G. Palmason, 8 : 193-22

Withjack, M. O., and W. R. Jamison (1986). Deformation produced by oblique rifting, Tectonophysics, 126, 99–124.

Woolery, E. W., R. Street, Z. Wang, and J.B. Harris (1993). Near surface deformation in the New Madrid seismic zone as imaged by high-resolution SH-wave seismic methods, Geophys. Res. Let. 20, p. 1615-1618.

Wylegalla, K., G. Bock, J. Gossler, and W. Hanka, and the TOR Working Group (1999). Anisotropy across the Sorgenfrei-Tornquist Zone from shear wave splitting, Tectonophysics, 314, 335–350.

Zandt, G., S. C. Myers, and T. C. Wallace (1995). Crust and mantle structure across the Basin and Range– Colorado plateau boundary at 37$^{o}$N latitude and implications for Cenozoic extensional mechanism, J. Geophys. Res., 100, 10,529–10,548.

Zandt, G., and C. J. Ammon (1995). Continental-crust composition constrained by measurements of crustal Poisson's ratio, Nature, 374, 152–154.

Zhang, S.Q., and S.I. Karato (1995). Lattice preferred orientation of olivine aggregates deformed in simple shear, Nature 375, 774–777.

Zhang, N. F. (2006). The uncertainty associated with the weighted mean on measurement data, Metrologia, 43, 195-204.

Zheng, T. Y., L. Chen, L. Zhao, W. W. Xu, and R. X. Zhu (2006). Crust–mantle structure difference across the gravity gradient zone in North China Craton: seismic image of the thinned continental crust, Phys. Earth Planet. Int. 159, 43–58

Zhu, L. P., and H. Kanamori (2000). Moho depth variation in southern California from teleseismic receiver functions, J. Geophys. Res., 105, 2969– 2980.

Zoback, M. D., and M. Zoback (1980). State of stress in the conterminous United States, J. Geophys. Res., 85, 6113 – 6156.

# VITA

I Moikwathai Moidaki, was born on the 25th December 1974 in Bobonong Village situated in the eastern side of Botswana. I started primary school in 1982 at Bobonong Primary School and completed Cambridge certificate in 1993. In 1994, I did Pre-Entry Science (PESC) course at the University of Botswana (UB) and then completed BSc in Physics in 1999 at UB. I also completed MSc in Physics at the UB in 2001. I received my PhD in Geology and Geophysics from Missouri University of Science and Technology (MS&T) in 2009. During my stay at MS&T I became a member of several professional associations including; Society of Exploration Geophysics (SEG), American Association of Professional Geologists (AAPG), Geological Society of America (GSA), National Association of Black Geologists and Geophysicists (NABGG). I also served as a secretary SEG student chapter in 2006. My research interests involve studying the crustal structure using teleseismic shear wave splitting and receiver functions and also using potential field methods for mineral exploration.